D-MEM
PhD-UNIMI

Doctorate program
Milan
EXPERIMENTAL
MEDICINE

Università degli Studi di Milano

PhD Course in
Experimental Medicine

CYCLE XXXIV

PhD thesis

SOLVING THE PUZZLE OF PROTOCADHERIN-19 MOSAICISM TO UNDERSTAND THE PATHOPHYSIOLOGY OF DEVELOPMENTAL AND EPILEPTIC ENCEPHALOPATHY 9 (DEE9)

Candidate: **Dr. Sara MAZZOLENI**
Matr. R12364

Tutor: **Prof. Diego Maria Michele FORNASARI**

Supervisor: **Dr. Silvia BASSANI**

Director: **Prof. Nicoletta LANDSBERGER**

Academic Year 2021-2022

INDEX

ABSTRACT

Developmental and Epileptic Encephalopathy 9 (DEE9) is a severe neurological disorder characterized by clustered epilepsy, intellectual disability (ID) and autism spectrum disorder (ASD) (*Dibbens et al., 2008*). DEE9 is caused by mutations affecting the X – linked gene *PCDH19*, which encodes for a calcium – dependent cell – cell adhesion molecule, called protocadherin – 19 (PCDH19) (*Dibbens et al., 2008*). PCDH19 is mainly expressed in the Central Nervous System (CNS), where it is involved in cell – adhesion, neuronal migration, and circuit formation (*Cooper et al 2015*). Even though DEE9 is a X – linked disorder, the 90% of the patients are females (*Shibata et al., 2021).* This peculiarity was attributed to a cellular interference mechanism: due to random chromosome X inactivation, female patients have a mosaic expression of PCDH19 in the brain. This mosaicism is supposed to be responsible for a scrambled neuronal communication, promoting the onset of DEE9 features (*Dibbens et al., 2018*). The cellular interference hypothesis was supported by the identification of few DEE9 male patients with PCDH19 somatic mutations (*Niazi et al., 2019*). However, pathophysiological mechanisms behind DEE9 are still unclear and the generation of animal models could help in elucidating them.

In our laboratory, we generated a new conditional knock – out (cKO) mouse model for PCDH19, through the Cre – Lox P technology (*Pcdh19* floxed mouse). Two different approaches were used to deliver Cre recombinase: 1) crossbreeding of *Pcdh19* floxed mice with mice expressing Cre under the rat Synapsin – 1 promoter, to target specifically neurons; 2) intracerebroventricular (ICV) injection in *Pcdh19* floxed mice of an adeno – associated virus (AAV) expressing Cre fused to GFP. This last approach allowed to discriminate PCDH19 positive from PCDH19 negative neurons. Once evaluated *in vitro* specific Cre – mediated excision and absence of protein production by activation of the Nonsense Mediated Decay (NMD) system, we molecularly, functionally, and behaviorally characterized the new *Pcdh19* cKO mouse model. In cortical and hippocampal tissues, *Pcdh19* cKO female mice were characterized by a reduction in both PCDH19 mRNA and protein of ~40% compared to control female mice. Interestingly, also *Pcdh19* cKO male mice were mosaic for PCDH19 expression, most likely due to the low Cre expression under the relatively weak Synapsin – 1 promoter. Indeed, they displayed a mRNA and protein reduction of ~60% compared to their sex – related controls. So, both *Pcdh19* cKO female and male mice recapitulated PCDH19 brain mosaicism, considered DEE9 triggering feature. This allowed us to perform some of the analyses on both sexes, to identify a possible gender effect associated to DEE9. *Pcdh19* cKO female mice were characterized by synaptic defects in the hippocampal CA1 region. Indeed, they showed a reduced number of excitatory synapses with a reduced number of neurotransmitter vesicles and reduced post-synaptic density (PSD) thickness compared to control female mice. In association with synaptic structural defects, *Pcdh19* cKO female mice presented also impaired synaptic functionality. Indeed, *Pcdh19* cKO female mice were characterized by a reduced Long-Term Potentiation (LTP) and a reduced Paired Pulse Ratio (PPR) compared to their sex – matched control mice. These synaptic defects prompted us to investigate the behavioral features of *Pcdh19* cKO mice. Since DEE9 is characterized by ID and ASD, we investigated these two aspects. *Pcdh19* cKO female and male mice displayed an increased number and duration of self – grooming events, suggesting an ASD-like phenotype.

Moreover, *Pcdh19* cKO mice of both sexes showed impairment in learning and memory plasticity, evaluated through the Morris Water Maze (MWM) test. Interestingly, the Fear Conditioning Test reconfirmed hippocampal – related memory defects exclusively in female cKO, suggesting that the female sex could be more susceptible to *Pcdh19* loss. Concerning epilepsy, our *Pcdh19* cKO mouse model didn't show spontaneous seizures, as observed in the constitutive *Pcdh19* KO mouse models (*Pederick et al., 2016, Hoshina et al., 2021*). However, *Pcdh19* cKO mice displayed some hyperexcitability features at subclinical level. Indeed, PCDH19 negative neurons in the mosaic brain of *Pcdh19* floxed mice were characterized by a reduced rheobase and by a higher firing frequency compared to neighboring cells retaining PCDH19 expression. Moreover, *Pcdh19* cKO mice were characterized by an aberrant surface expression of the $GABA_A$Rs α1 subunit, underlying possible GABAergic defects.

To conclude, we generated a new *Pcdh19* cKO mouse model which was able to recapitulate *Pcdh19* brain mosaicism and features of ID and ASD, as in DEE9 pathology. Besides behavioral alterations, also functional and morphological synaptic defects in hippocampus were noticed. Finally, our mouse model provided clues of a GABAergic impairment and a possible gender – effect at the basis of DEE9 pathophysiology.

DISCLOSURE FOR RESEARCH INTEGRITY

I state that my PhD research was conducted following the European Code of Conduct for Research Integrity.
All my research procedures were conducted according to the principles of reliability, honesty, respect, and responsibility.
My tutor and my supervisor supervised my research all along the three years of my PhD formation and the experiments were carried out in an accurate and rigorous way.
The results, here presented, are transparent and reproducible.

Animals' care and all experimental procedures involving animals were performed in accordance with the CNR licensing and were approved by the Italian Ministry of Health. The 3R (Replacement, Reduction and Refinement) principles were applied whenever possible to avoid excessive animal suffering.

The thesis underwent plagiarism evaluation.

After accurate review, the supervisor and the tutor agreed with the submission of the thesis.

ABBREVIATIONS

- aa = aminoacids
- AAV = Adeno – Associated Virus
- ADNFLE = Autosomal Dominant Nocturnal Frontal Lobe Epilepsy
- AMPA = α-amino-3-hydroxy-5-methyl-4-isoxazolepropionate
- ASD = Autism Spectrum Disorder
- Bp = Base pair
- BZ = benzodiazepine
- CA1 = *Cornu ammonis* 1 (Hippocampal area)
- cKO = conditional Knock – Out
- CM = conserve motif
- CNS = Central Nervous System
- cPcdhs = clustered protocadherins
- Cre = Cre Recombinase
- CTF = C – Terminal Fragment
- DEE9 = Developmental and Epileptic Encephalopathy 9
- DG = Dental Gyrus (Hippocampal area)
- DGGCs = Dental Gyrus Granule Cells
- DIV = Days In Vitro
- E = Embrionic day
- EC = extracellular cadherin repeat
- ER = Endoplasmic Reticulum
- ER = Estrogen Receptor
- F = Familiar Object
- FLP = Flippase
- $GABA_AR$s = γ - aminobutyric acid type A
- GFP = Green Fluorescent Protein
- I = Discrimination Index (in NOR)
- ICC = ImmunoCytoChemistry
- ICV = IntraCerebroVentricular

- ID = Intellectual Disability
- iDG =immature Dental Gyrus
- IHC = ImmunoHistoChemistry
- LSD1 = Lysine – Specific Demethylase 1
- LTP = Long Term Potentiation
- MWM = Morris Water Maze
- N = Novel Object
- ncPcdhs = non clustered protocadherins
- NMD = Nonsense – mediated Decay
- NMDA = N – methyl – D – aspartate
- NONO = non-POU domain-containing octamer binding protein
- NOR = Novel Object Recognition
- P = Post Natal Day
- PCDH19 = protocadherin – 19
- Pcdhs = protocadherins
- PP1α = protein phosphatase – 1α
- PPR = Paired Pulse Ratio
- PSD = Post Synaptic Density
- RIPA = Radio Immunoprecipitation Assay
- RMP = Resting Membrane Potential
- RPM = Revolutions Per Minute;
- RT – PCR = Real Time PCR
- RT = Room Temperature
- SE = Status Epilepticus
- TEM = Transmission Electron Microscopy
- TLE = Temporal Lobe Epilepsy
- TM = Transmembrane domain
- W2 = tryptophane specific residue
- WAVE = WASP-family verprolin homologous protein
- WB = Western Blot
- WRC = WAVE Regulatory Complex

INTRODUCTION

1. DEVELOPMENTAL AND EPILEPTIC ENCEPHALOPATHY 9 (DEE9)

Developmental and Epileptic Encephalopathy 9 (DEE9, OMIM #300088) is a severe genetic neurodevelopmental disorder, mainly characterized by epilepsy, autism spectrum disorder (ASD) and intellectual disability (ID) (*Dibbens et al., 2008; Depienne et al., 2009*).

DEE9 was clinically described for the first time in the ’70 as a new form of convulsive disorder and mental retardation restricted to female patients (*Juberg and Hellman,1971*). However, only in the XXI century, it was possible to identify the causative locus, Xq22.1, (*Ryan et al., 1997*) and the causative gene, *PCDH19* (*Dibbens et al., 2008*) (Fig.1). Since the beginning, clinicians mainly focused the attention on female patients, considering DEE9 restricted to females (*Dibbens et al., 2008; Depienne et al., 2009*). However, after the identification of a male patient with a mosaic PCDH19 deletion (*Depienne et al., 2009*), new interest in male patients raised and different male patients with PCDH19 somatic mutations and affected by DEE9 were reported (*Terracciano et al., 2016; Thiffault et al., 2016; Perez et al., 2017; de Lange et al. 2017; Tan et al., 2018*), opening new insights into DEE9 features.

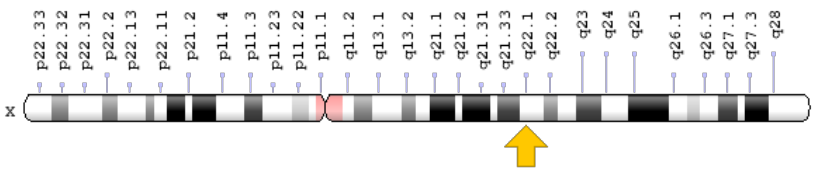

Figure 1 ***PCDH19 locus on the X chromosome*** *(www.ghr.nlm.nih.gov)*

1.1 CLINICAL FEATURES OF DEE9

From a clinical point of view, DEE9 resembles closely Dravet syndrome (OMIM# 607208), also known as Developmental and Epileptic Encephalopathy 6A (DEE6A). Dravet syndrome is due to mutations in the *SCN1A* gene, encoding for the α subunit of the sodium gated ion channel (*Dravet et al., 1978, Dravet et al., 1992)*. However, DEE9 patients differ from Dravet syndrome ones for the presence of fewer myoclonic and absence seizures, fewer episodes of status epilepticus, less photosensitivity and in general for a more favorable outcome (*Depienne et al., 2009*).

It is estimated that 1 in 10 girls suffering of seizures before the age of 5 may have DEE9 (*https://www.epilepsy.com*) (estimated prevalence in the population: 1:10.000 (*Niazi et al., 2018)*), making *PCDH19* the second most important gene involved in monogenic epilepsy, after *SCN1A* gene (*Depienne and LeGuern, 2012*).

DEE9 is characterized by seizures occurring in clusters (*Depienne et al., 2009*), with clusters frequency ranging from daily to yearly (*Smith et al., 2018*) and lasting from hours to days (*Smith et al., 2018; Kolc et al., 2020*). Most of the seizures are focal, but also generalized tonic – clonic seizures were reported (*Trivisano et al., 2018; Kolc et al., 2019).* In most cases, seizures are fever – sensitive (*Marini et al., 2012, Smith et al., 2018*) and they are refractory to treatments, so patients require cocktail of anti – epileptic drugs to control epilepsy (*Mazzoleni and Silvia, 2021*).
Mean seizures onset is around 10 months (*Breuillard et al., 2016; Trivisano et al., 2018*; *Kolc et al., 2020*) and during adolescence there is a reduction or remission of epilepsy (*Scheffer et al., 2008; Marini et al., 2010; Specchio et al.,*

2011). However, neuropsychiatric disorders, like schizophrenia, and intellectual disability persist or even get worst (*Cappelleti et al., 2015; Smith et al., 2018; Vlaskamp et al.,2018*), becoming the prominent symptoms in DEE9 patients.

DEE9 is characterized by a strong variability in the severity of the symptoms among patients, ranging from mild to severe, making difficult to forecast the patient possible outcome (Fig. 2) (*Kolc et al., 2020*).

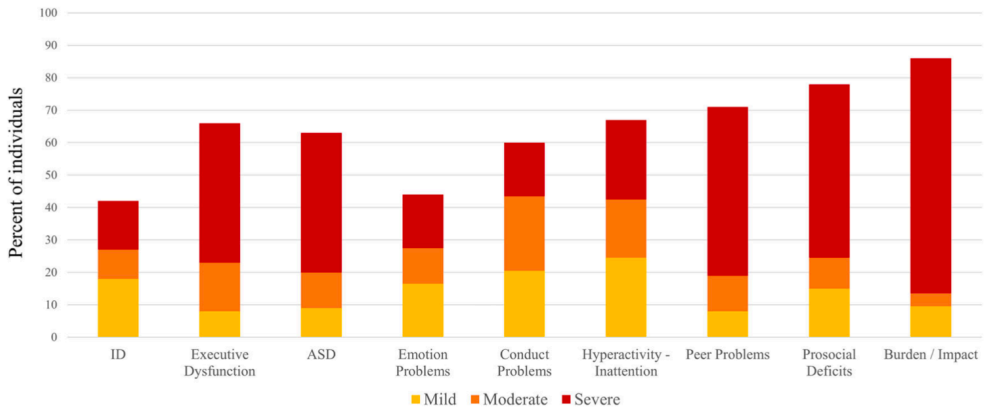

Figure 2 ***DEE9 comorbidities variability among a cohort of 112 affected patients.*** *The heatmap (yellow, orange and red) represents severity distribution for each comorbidity (Kolc et al.,2020)*

Moreover, an established genotype – phenotype correlation is still missing (*Smith et al., 2018; Trivisano et al., 2018; Kolc et al., 2020*). The only identified correlation is between seizures onset and ID severity and ASD. Indeed, if the seizures onset is before 12 months, patients are characterized by a more severe ID and by a higher probability to develop ASD (*Breuillard et al., 2016*; *Trivisano et al., 2018; Kolc et al., 2020; Shibata et al., 2021*).

Mean developmental regression occurs around the 12th month and the most affected areas are the motor, social and language ones (*Breuillard et al., 2016; Kolc et al., 2020*). Some patients are also characterized by sleep dysregulations, mainly insomnia (*Smith et al., 2018*) and by neuropsychiatric and behavioural defects, like obsessive – compulsive disorder and aggressive behaviour (*Smith et al., 2018; Kolc et al., 2020*).

Male carriers are not affected by epilepsy, although they seem to suffer from a more rigid personality and ID (*van Harssel et al., 2013; Scheffer et al., 2018*).

However, in 2009, it was discovered the first mosaic male patient affected by DEE9 (*Depienne et al., 2009*). To date, 12 mosaic male patients with somatic mutations in *PCDH19* were reported, and they display the typical features of DEE9 as female patients, including epilepsy (*Niazi et al., 2019*).

1.2 DEE9 GENETICS

DEE9 is caused by mutations affecting *PCDH19* gene, which is localized on the X chromosome (Xq22.1) and encodes for a member of the cadherin superfamily, called protocadherin – 19 (PCDH19) (*Dibbens et al., 2008*).

Up to now, more than 200 mutations have been reported affecting *PCDH19* (*Shibata et al., 2021*), of which 90% were present in female patients, while just 10% in mosaic male patients (*Niazi et al., 2019; Shibata et al., 2021*).

In most cases, *PCDH19* mutations are *de novo* mutations, followed by maternally and paternally inherited variants (*Niazi et al., 2019; Kolc et al., 2019*).
Concerning distribution, mutations mostly fall in exon 1, which encodes for the extracellular domain, the transmembrane domain and the initial portion of the intracellular domain (*Kolc et al., 2019*), and they are expected to affect protein adhesiveness and so cell – cell interaction (*Cooper et al., 2016*). Missense mutations are the most recurrent, followed by frameshift and nonsense variants (*Kolc et al., 2019*). Deletions can affect the whole gene or the first three exons, but they are observed sporadically (*Kolc et al., 2019*) (Fig.3).
Overall, mutations are considered to be loss of function for PCDH19, even though no demonstration has been provided yet (*Cooper et al., 2016*).

Moreover, 313 functional polymorphisms were discovered and considered to be more likely benign. However, it is not possible to exclude that these polymorphisms could cause the onset of DEE9 with low penetrance or with a variable expressivity (*Niazi et al., 2019*).

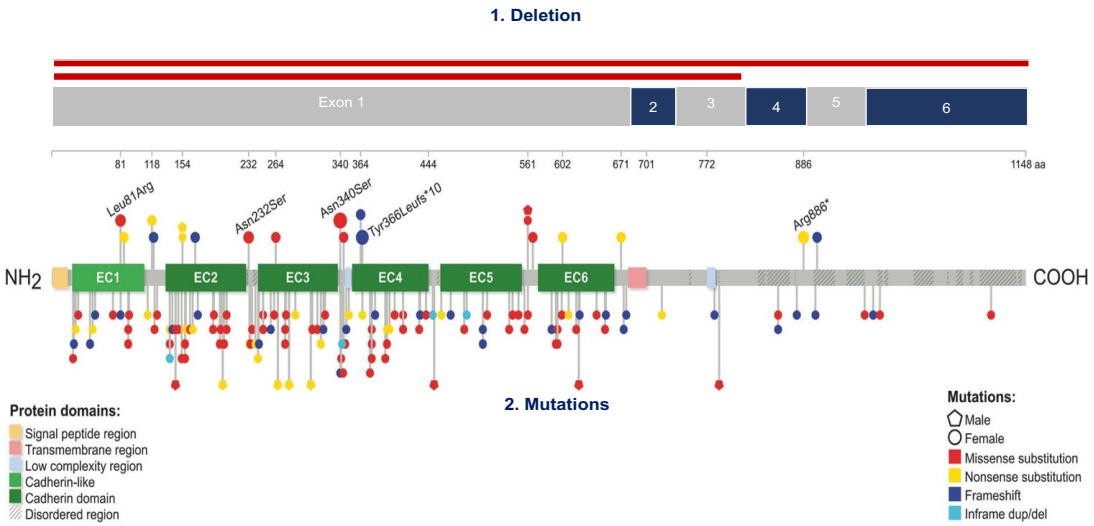

Figure 3 ***PCDH19 mutations distribution****. Lollipop size is exponentially proportional to the number of times the variants have been observed. The most recurrent variants are named above the respective lollipop (modified from Kolc et al.,2019)*

1.3 BEHIND DEE9 PATHOGENIC MECHANISMS

DEE9 is a peculiar X – linked disorder, since it affects mostly heterozygous female patients, sparing males (*Dibbens et al., 2008*). The identification of few DEE9 male patients with somatic mutations and a Klinefelter patient (XXY, 47 chromosomes) with PCDH19 mutation in one of his two PCDH19 copies (*Romasko et al., 2018*) helped to hypothesize a possible pathological mechanism behind this mechanism of inheritance. Indeed, *Dibbens (2018)* attributed to the cellular interference hypothesis the pathophysiological mechanism responsible for DEE9 (Fig. 4). According to this theory, hemizygous mutated males have a homogeneous population of cells which do not express PCDH19, and cells would still be able to interact properly. By contrast, mutated females, due to random chromosome X – inactivation, and somatic mosaic mutated males have a mosaic expression of PCDH19 with PCDH19 positive and PCDH19 negative cells. This mosaicism would scramble neuronal communication promoting the onset of DEE9 features (*Dibbens et al., 2008*).

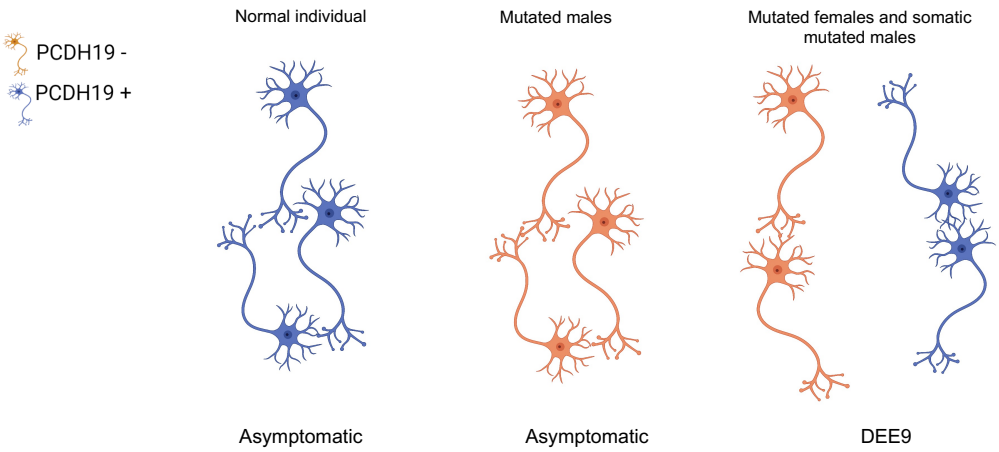

Figure 4 ***Cellular interference hypothesis*** *(adapted from Dibbens et al., 2008)*

The first molecular evidence of the cellular interference hypothesis was provided by *Hoshina (2021, discussed in Chapter 2.3 PCDH19*).

2. PROTOCADHERIN – 19 (PCDH19)

2.1 CADHERIN SUPERFAMILY

The cadherin superfamily consists of more than 100 members in vertebrates. Cadherins are divided into classical cadherins, desmosomal cadherins, protocadherins and other solitary members (*Takeichi, 2007*) (Fig 5). Their primary role is to promote cell – cell adhesion, a highly important process especially in the brain (*Takeichi, 2007*). Indeed, neuronal interaction and specific neuronal recognition promote a correct neuronal wiring (*Parrish et al., 2007*).

Besides cell adhesion, cadherins superfamily members are also involved in signal transduction, mechanotransduction and brain morphogenesis (*Leckband et al., 2011; Hirano and Takeichi., 2012*).

Cadherin superfamily members are transmembrane proteins and each family presents its own structural and functional diversity. However, they show some structural elements in common (*Takeichi, 2007*):

- *Extracellular domain*: it contains repetitive motifs, called extracellular cadherin repeats (EC), which can vary in number among members (from 1 to 34) and they present sequences involved in Ca^{2+} binding. The extracellular domain is responsible for cis – and trans – interaction;
- *Transmembrane* (TM) *domain*;
- *Intracellular domain*: it is the most variable region and it gives specificity to cadherins function. It mediates a cell signaling, according to the downstream pathway activated.

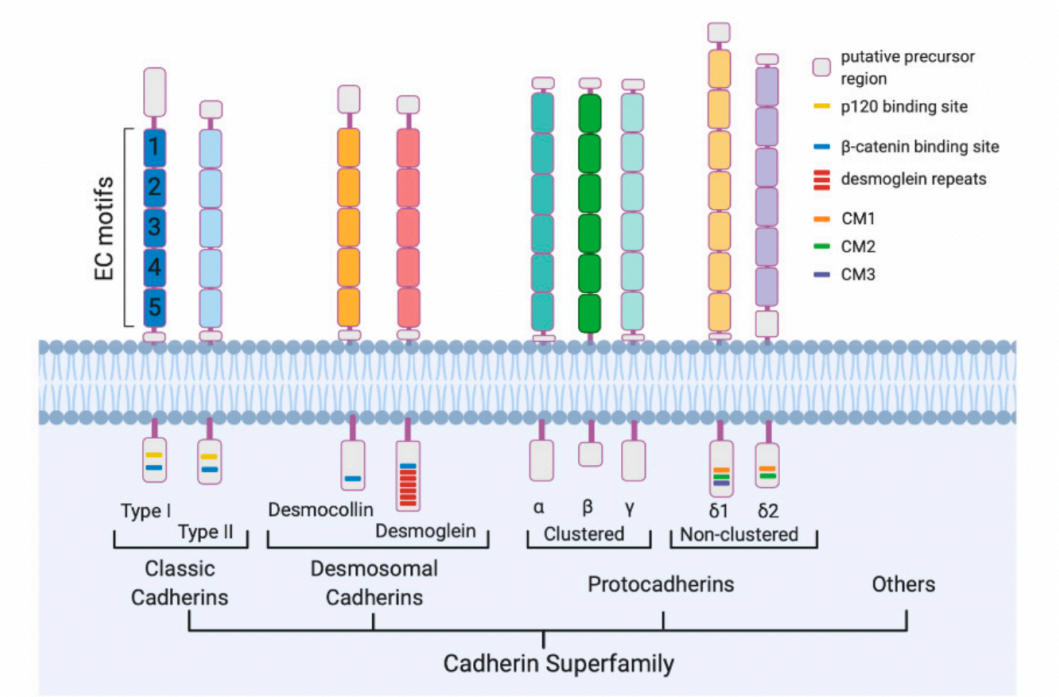

Figure 5 ***Cadherin superfamily classification and structure.*** *(EC, extracellular cadherin repeats; CM, conserved motif) (Mancini et al., 2020)*

Classical cadherins, as NCAD, are characterized by five EC domains and by a conserved intracellular domain. The intracellular domain interacts with β - catenin and p120 catenin, promoting acting remodeling and so cell adhesion (*Takeichi, 2007).* Classical cadherins are divided into type 1 and type 2, which differ for the number of conserved tryptophan (W2) residues and for the

number of hydrophobic pockets present in EC1 domain (*Hirano and Takeichi, 2012*).

Desmosomal cadherins belongs to the desmosomes, which are specialized adhesive protein complexes mainly localized at the intracellular junctions and they are involved in the maintenance of tissues mechanical integrity (*Dubash and Green., 2011*). They resemble type 1 classical cadherins, except for the different intracellular domains (*Morishita and Yagi, 2007*).

Finally, protocadherins (Pcdhs) are characterized by loop structures which are specific for this sub – family. The strong heterogeneity in this subfamily suggests a precise role in mediating specific neuronal interaction (*Morishita and Yagi, 2007*).

2.2 PROTOCADHERINS

In the cadherin superfamily, the most abundant members are the protocadherins (Pcdhs) (*Nollet et al., 2000*), which are predominantly expressed in the central nervous system (CNS) (*Vanhalst et al., 2005; Redies et al., 2005; Kim et al., 2010; Kim et al., 2011; Hertel et al., 2012*).
Pcdhs show some structural differences compared to the other members of the cadherin superfamily. They are characterized by more than five EC domains, by the absence of the W2 conserved residue and of the hydrophobic pocket, and by a different intracellular domain (*Sano et al., 1993*).
Usually, Pcdhs form weak homophilic binding and interact with specific cytoplasmic partners to promote specific neuronal connection (*Takeichi, 2007*).

More than 70 genes encode for Pcdhs. Pcdhs can be divided into clustered (cPcdhs) and non – clustered Pcdhs (ncPcdhs), according to the genomic organization (*Mancini et al., 2020*).
α - Pcdhs, β - Pcdhs and γ - Pcdhs belong to the cPcdhs, since the gene clusters are sequentially organized in a small genome locus on a single chromosome (homo sapiens: chromosome 5q31; mus musculus:

chromosome 18) (*Mancini et al., 2020*). More than 50 transcripts can be generated by these three gene clusters, since they contain multiple "variable" exons and "constant" exons (*Takeichi, 2007*). By cis – mRNA splicing, exons are combined to form isoforms with different extracellular domains (*Takeichi, 2007)* (Fig. 6).

A peculiarity of the β - Pcdhs gene clusters is that do not present constant exons and so this gene cluster encodes for proteins with a truncated intracellular domain (Fig. 6) (*Pancho et al., 2020*).

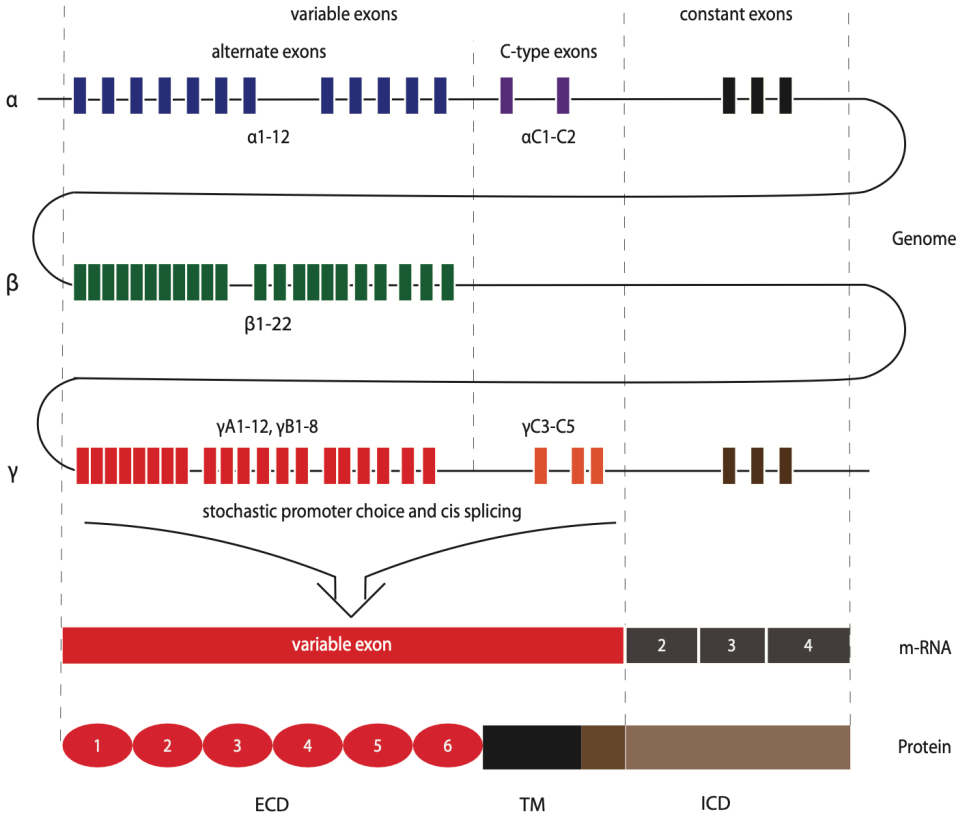

Figure 6 ***Schematic representation of clustered protocadherins gene organization and molecular structure.*** *Pre-mRNA present 2 regions: a variable portion, composed by one single long exon, which encodes for the N – terminus, the TM and a portion of the C – terminus, and a small constant portion, which encodes for the last amino acids of the C – terminus (Pancho et al.,2020)*

Besides cPcdhs, other Pcdhs were found spread along the genome and therefore they were defined as ncPcdhs. ncPcdhs are divided into δ1 (*Pcdh1, Pcdh7, Pcdh9 and Pcdh11*) and δ2 Pcdhs (*Pcdh8, Pcdh10, Pcdh17, Pcdh18 and Pcdh19*), according to their homology and number of EC domains (*Pancho*

et al., 2020) and in solitary Pcdhs or ε - Pcdhs (*Pcdh12, Pcdh20 and Pcdh24*) (*Hulpiau and van Roy, 2011*; *Mancini et al., 2020*).
δ1 – Pcdhs have seven EC domains and three conserve motifs (CM, CM1 – 3), where CM3 present a putative binding site for protein phosphatase – 1α (PP1α) (*Vanhalst et al., 2005*). On the contrary, δ2 – Pcdhs have just two CM domains (CM1 – 2) in their intracellular domain (Fig. 5) (*Wolverton and Lalande, 2001*). Still CM1 and CM2 don't have a known function, but they are fundamental for ncPcdhs classification (*Vanhalst et al., 2005*).

Mutations in δ – Pcdhs have been associated with neurodevelopmental disorders and with cancer, since they act as tumour suppressor genes (*Berx and van Roy, 2009; Hirano and Takeichi, 2012; Redies et al., 2012; van Roy, 2014*).

2.3 PROTOCADHERIN – 19 (PCDH19)

Protocadherin – 19 (PCDH19) is a member of the δ2 – ncPcdhs and it is encoded by the *PCDH19* gene, localized on the long arm of the X chromosome (Xq22.1) (*Dibbens et al., 2008; Depienne et al., 2009)*.
PCDH19 is composed by six exons, where exon 1 encodes for most of the protein: the extracellular domain, the TM domain and a portion of the intracellular domain. The remaining intracellular portion is encoded by exon 2 – 6 (*Redies et al., 2005; Dibbens et al., 2008*).

PCDH19 extracellular domain presents six EC repeats and the intracellular domain has two CM (CM1 – 2) and the WIRS sequence, recognized by the WAZE regulatory complex (WRC, highlighting in red in Fig. 7) (*Chen et al., 2013*). Exon 2 undergoes alternative splicing, promoting the formation of a shorten version of PCDH19 (canonical isoform # 1: 1148 aminoacids, aa; isoform # 2: 1101 aa) (Fig. 7) (*Depienne and Leguern, 2012*).

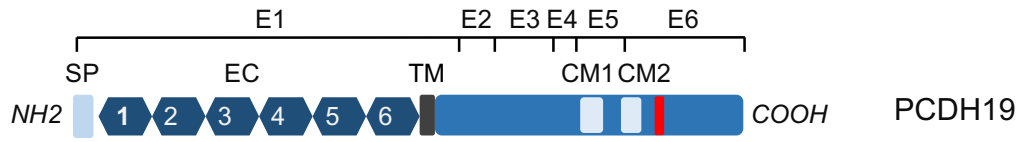

Figure 7 ***PCDH19 structure.*** *E, exon; SP, signal peptide; EC, extracellular cadherin repeats; TM, transmembrane domain; CM, conserved motif. WIRS sequence is highlighting in red.*

PCDH19 has a specific temporal and spatial expression (*Gerosa et al., 2018*). Even though PCDH19 is detectable in trachea, lung, kidney, its major expression is in the CNS (*Wolverton and Lalande, 2001; Gaitan and Bouchard, 2006*). In mouse brain, PCDH19 starts to be expressed at the embryonic day (E) 9.0 (*Gaitan and Bouchard, 2006)*. During embryonic period, PCDH19 expression increases, reaching a peak in the post – natal period, around P7 (*Bassani et al.,2018*). PCDH19 expression persists in adulthood, suggesting that PCDH19 has a role both in neuronal circuit formation and in the regulation of neuronal activity (*Gerosa et al., 2018*).

PCDH19 is expressed in the cerebral cortex and in different limbic areas, among which amygdala, hippocampus, and ventral hypothalamus (*Kim et al., 2007; Pederick et al., 2016; Schaarschch and Hertel, 2018*). More precisely, in cerebral cortex, PCDH19 is expressed in layer 2/3 and in layer 5; while in hippocampus, it is localized in *cornu ammonis* (CA) regions and in dental gyrus (DG) (*Kim et al., 2007; Pederick et al., 2016*). In mouse brain, PCDH19 is mainly expressed in CA1 and CA3 in the first postnatal period, while in adulthood it is mainly expressed in the DG (*Gaitan and Bouchard, 2006; Kim et al., 2007; Kim et al., 2010; Hertel and Redies, 2011; Krishna-K et al., 2011*).

At the cellular level, PCDH19 is expressed in neuronal progenitors (*Fujitani et al., 2017*), radial glia (*Zhang et al., 2014*) and pyramidal neurons (*Bassani et al., 2018*). Recently, PCDH19 expression has also been shown in cortical inhibitory neurons (*Galindo – Riera et al., 2021*).
Finally, at the subcellular level, PCDH19 is expressed in the perinuclear region and along dendrites (*Bassani et al., 2018*), where it partially colocalizes with excitatory and inhibitory synapses (*Hayashi et al., 2017; Bassani et al., 2018*).

In recent years, different PCDH19 functions and interactors have been described (*Gerosa et al., 2018*).

PCDH19 mediates cell – cell adhesion, a highly fundamental process which allows neuronal differentiation and migration, axon outgrowth, dendritic arborization and synapse formation and maintenance (*Weiner and Jontes, 2013*). Indeed, in Zebrafish, Pcdh19 is important for the maintenance of optical *tectum* architecture and its absence promotes aberrant cell – cell interaction and aberrant cell proliferation (*Cooper et al., 2015*).

PCDH19 is mainly involved in homophilic interaction *in trans* (*Cooper et al., 2016*); however, recently, some evidence demonstrated its capability to establish *in cis* interaction with NCAD (*Biswas et al., 2010; Emond et al., 2011*). Even though, in the beginning, PCDH19 was considered as a cofactor for NCAD complex formation, recent studies suggest the importance of PCDH19 in NCAD correct complex formation and activation (*Emond et al., 2011, Hoshina et al.,2021*). The interaction between NCAD – PCDH19 complex in the pre and post – synapsis, as well as the interaction between NCAD alone (as it occurs in male hemizygous patients) in the pre and post – synapsis, is fundamental for the correct pre – synaptic compartment development and organization, due to β - catenin clustering pathway activation (*Hoshina et al., 2021*) (Fig. 8a, 8b).

By contrast, in mutated females or somatic mutated males, where there are PCDH19 positive and PCDH19 negative synapses, trans – synaptic interaction between PCDH19 – NCAD complex and NCAD cannot occur due to mismatching. Overall, mismatch promotes reduction in β - catenin clustering and so defects in pre – synaptic compartment development, causing DEE9 cognitive impairment (Fig. 8c). This study provided the first molecular evidence of the cellular interference hypothesis (*Hoshina et al., 2021*).

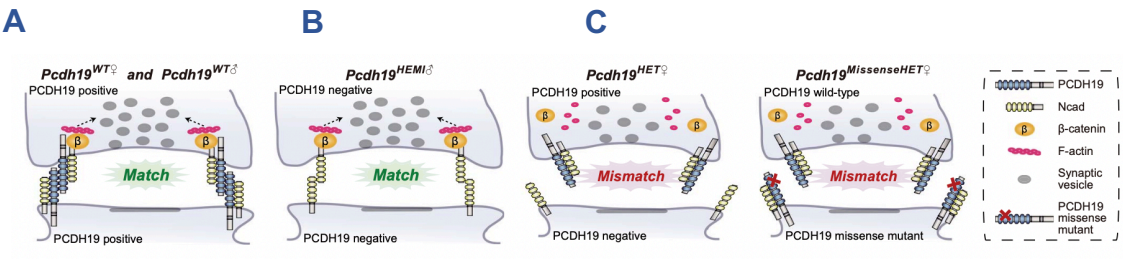

Figure 8. ***PCDH19 – NCAD mismatch alters normal pre – synaptic organization*** *(modified from Hoshina et al., 2021)*

Besides a role in cell – cell adhesion, PCDH19 promotes embryonic cortical neurogenesis between E14.5 and E16.5. PCDH19 3' – untranslated region (UTR) is targeted by miR – 484, which prevents PCDH19 mRNA stabilization and translation, thus reducing radial glia proliferation and allowing basal progenitors differentiation (*Fujitani et al., 2017*).

Recently, PCDH19 expression was found to be regulated also by the *brain and muscle Arnt – like protein 1* (*Bmal1*), one of the main clock gene involved in circadian cycle. Alterations in Bmal1 expression participates in diseases onset, among which epilepsy. Indeed, reduced Bmal1 expression was found in hippocampus during latent and chronic phases of temporal lobe epileptic (TLE) patients. Interestingly, lower level of PCDH19, due to Bmal1 targeting, was also found in the hippocampus of epileptic mice, but also in patients affected by Hippocampal Sclerosis (HS). This data suggested that reduced expression of Bmal1 can be involved in epilepsy onset, through PCDH19 expression regulation (*Wu et al., 2021*).

Through its intracellular domain, PCDH19 interacts with different proteins mediating different effect.

PCDH19 interacts with the γ - aminobutyric acid type A ($GABA_ARs$) α subunits, regulating their expression on the cellular surface and so modulating inhibitory transmission (*Bassani et al., 2018; Serrato et al.,2020).* More precisely, PCDH19 intracellular domain binds the conserved intracellular loop between TM3 – TM4 of the α subunits, a region known to regulate $GABA_ARs$ gating properties.

PCDH19 shRNA – mediated downregulation reduced $GABA_AR$s surface expression (Fig. 9a) and altered $GABA_AR$s biophysical properties (promotion of channel flickering behavior, Fig. 9b), thus affecting also neuronal functionality (*Bassani et al., 2018; Serratto et al., 2020*). Indeed, PCDH19 downregulation affected both phasic (reduced frequency of the miniature post – synaptic currents, Fig. 9c) and the tonic (reduced holding current shift, Fig. 9d) currents. The overall effect was an increased frequency in spiking activity, suggesting an increase in neuronal excitability (Fig. 9e) (*Bassani et al., 2018; Serratto et al., 2020*).

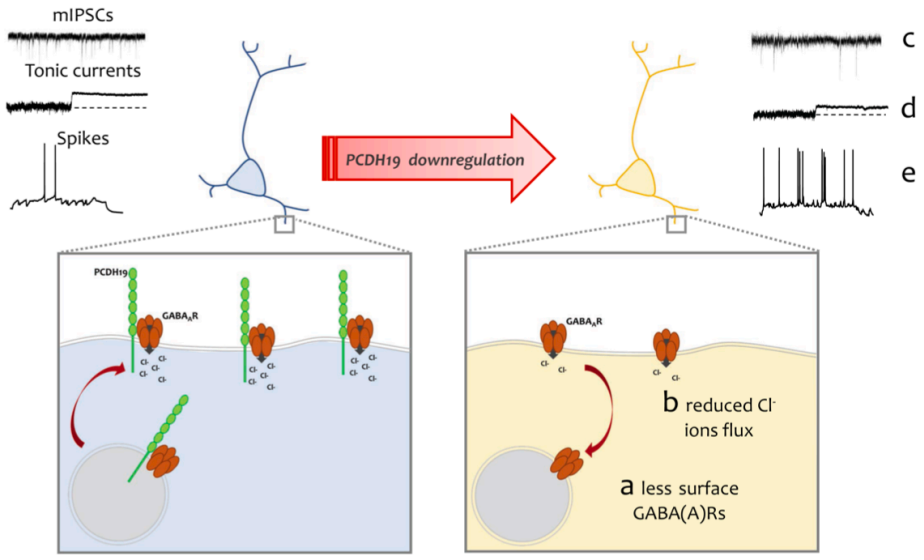

Figure 9. ***PCDH19 – $GABA_AR$s α subunits interplay and PCDH19 downregulation effects on $GABA_AR$s expression, gating properties, and functionality.*** *Cl^-, chloride; mIPSCs: miniature inhibitory post – synaptic currents. (Mazzoleni and Bassani, 2021)*

Moreover, PCDH19 also regulates actin dynamics, through its binding with WRC. Indeed, PCDH19 promotes Rac – 1 mediated WRC activation and Arp2/3 complex activation (*Nakao et al., 2008; Tai et al., 2010; Hayashi et al., 2017*). Consistent with these findings, it was demonstrated strong interactions between PCDH19 and Rho GTPases and microtubules cytoskeleton proteins (*Emond et al., 2021*). More precisely, *in vitro*, PCDH19 colocalizes with Dock7, a RacGEF protein which interacts with microtubule cytoskeleton, promoting interkinetic nuclear migration in neuronal progenitor cells (*Watabe-Uchida et al., 2006; Yang et al., 2019*). Besides Dock7, PCDH19 is supposed to interact

also with Nedd1, a centrosome protein which is important for spindle functioning (*Pinyol et al., 2012; Yonezawa et al., 2015*). Overall, these results suggest a strong involvement of PCDH19 in actin dynamics, suggesting a contact – dependent cell motility function, but also a role in neuronal progenitors proliferation and so in neurogenesis, through cytoskeleton regulation (*Emond et al., 2021*).

In addition, one evidence also suggested the possibility of PCDH19 to enter in the nucleus and to regulate gene expression. Indeed, PCDH19 is supposed to be involved in the non-POU domain – containing octamer binding protein (NONO) – estrogen receptor (ER) axis, promoting ERα - dependent regulation of a subset of target genes (*Tan et al., 2015*).
Recently, a new study confirmed the involvement of PCDH19 in a synapse – to – nucleus signaling pathway. Precisely, PCDH19 undergoes a N – methyl – D – aspartate (NMDA) receptor (NMDARs) – dependent proteolytic cleavage. This PCDH19 cleavage generates a soluble C – terminal fragment (CTF) that enters in the nucleus. Here, this CTF interacts with the epigenetic repressor Lysine – Specific Demethylase 1 (LSD1) and thus regulates immediate – early genes expression. Specifically, CTF – LSD1 complex prevents neuronal hyperexcitation, by downregulating specific gene expression (*Gerosa et al., Manuscript under revision*).

3. GABAERGIC TRANSMISSION

A correct brain functioning relies on a balanced excitatory and inhibitory transmission (*Gatto, 2010; Smith and Kittler, 2010*). In the CNS, glutamatergic transmission is responsible for excitation, promoting cellular depolarization upon ligand – receptor interaction. By contrast, inhibition is mainly promoted by γ – Aminobutyric acid (GABA). Through GABA binding to GABA receptors (GABARs), cells are hyperpolarized, decreasing neuronal probability of firing (*Petroff, 2002*).

Alterations in the balance between excitation and inhibition can induce aberrant brain functionalities and the onset of some neurodevelopmental and neuropsychiatric disorders, like ASD, schizophrenia, ID and epilepsy (*Gatto, 2010*).

3.1 GABA RECEPTORS (GABARS)

Synaptic inhibition is mostly promoted by GABA and GABARs interaction (*Jacob et al., 2008*). Indeed, one third of neurons in the brain uses GABA as major neurotransmitter (*Terunuma, 2018*).

There are two types of GABARs:

- GABARs type A ($GABA_A$Rs): they are heteropentameric ligand – gated ion channels and they promote fast inhibitory transmission (*Jacob et al., 2008)*. Indeed, in mature brain, upon GABA binding, a chloride (Cl^{2-}) pore gets open, inducing cell hyperpolarization.

  Interestingly, in the first developmental phases of the brain, the Cl^{2-} concentration inside the cell is high, due to upregulation of the NKCC1 Cl^{2-} transporter. This promotes cell depolarization (*Deidda et al., 2014*).

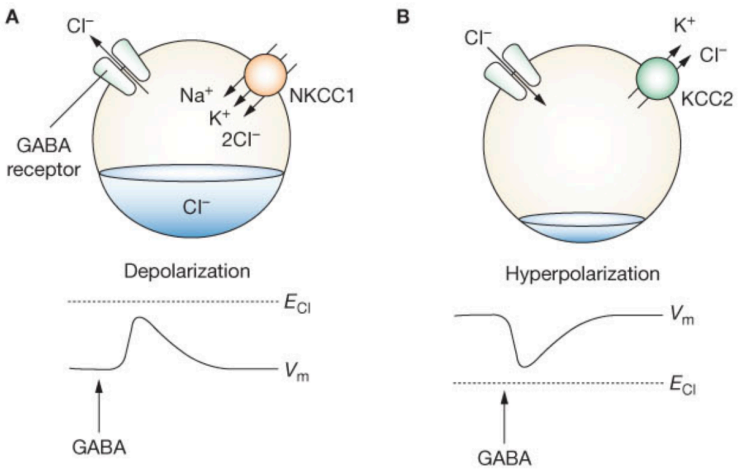

Figure 10. ***GABA switch.*** *During embryonic and post – natal period, in immature neurons, GABA has a depolarizing function, due to higher expression of the cation – chloride cotransporter NKCC1 (a). During neuronal maturation, there is an upregulation of the chloride – extruding K^+ – Cl^- cotransporter KCC2 and thus GABAergic transmission is involved in hyperpolarization (b) (Kahle et al., 2008)*

- GABARs type B ($GABA_BRs$): they are obligated heterodimeric G protein – coupled receptors composed by R1 and R2 subunits and promote slow inhibitory transmission. The inhibitory transmission is mediated by activation of inwardly rectifying potassium (K^+) channels, by inhibition of Ca^{2+} channels and inhibition of the adenylate cyclase (*Terunuma, 2018*).

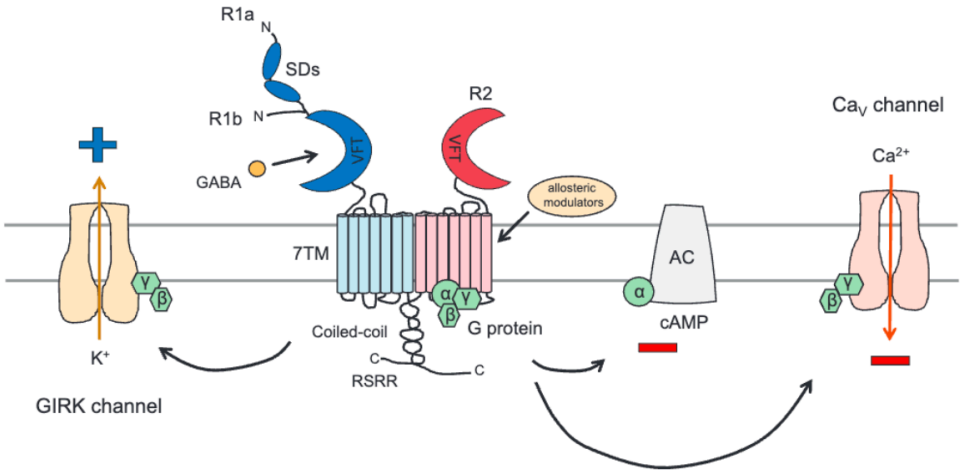

Figure 11. ***$GABA_BRs$.*** *$GABA_BRs$ are heterodimeric metabotropic receptor, composed by two different subunits, R1 and R2. Upon GABA binding, an intracellular signaling cascade starts thus promoting the activation of the GIRK K^+ channel and the inhibition of the Adenylate Cyclase and of the Ca_V channel. The overall effect is neuronal hyperpolarization. (Terunuma, 2018).*

3.2 $GABA_ARs$

$GABA_ARs$ are composed by five homologous subunits with a common structure (*Jacob et al., 2008)*. Indeed, each subunit is ~ 450 aa long and is composed by:

- A large amino – terminal hydrophobic extracellular domain, containing a Cys – loop;
- Four TM domains (TM1 – TM4), where TM2 constitutes the chloride channel;

- An intracellular loop between TM3 and TM4, target for post – translational modification which promotes receptor function modulation (*Sigel et al., 2012*);
- An extracellular carboxyl – terminal domain.

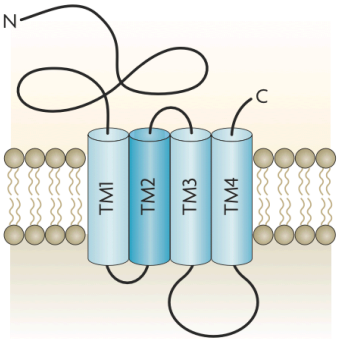

Figure 12. ***GABA$_A$Rs subunits' structure.*** *(Jacob et al., 2008)*

Up to now, 19 subunits were identified (*Simon et al., 2004*), and they are divided into seven classes. α class comprises 6 members; β ,γ, ε classes contain 3 members; while δ,θ and π are solitary members (*Sigel and Steinmann, 2012*), Moreover, receptor diversity is further increased by alternative splicing. In the brain, the majority of the receptors are composed by two α1 subunits, two β2 subunits and one γ or δ subunit (*Rudolph et al., 2004*).

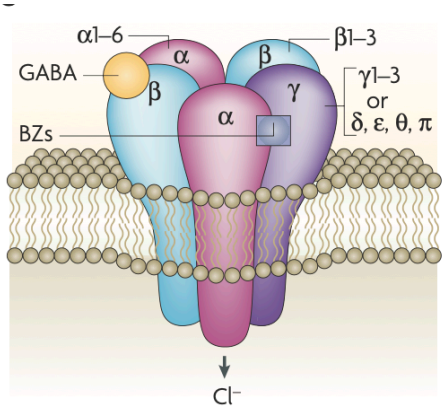

Figure 13. ***GABA$_A$Rs structure.*** *GABA$_A$Rs are heteropentameric receptors and they mediate neuronal hyperpolarization. Two molecules of GABA are required to promote Cl^- influx and GABA binding site is localized between α and β subunits. Benzodiazepines (BZs) are depressant drugs which enhance GABA transmission by binding a site between α and γ subunits. BZs effect increases the total conduction of the Cl^- channel and it occurs only if also GABA is bound to the receptor. (Jacob et al., 2008)*

$GABA_AR$s subunits composition confers specific physiological and pharmacological properties, together with specific brain region localization (*Jacob et al., 2008*).

Indeed, concerning pharmacological properties, α (1- 3), α5 associated with βγ are benzodiazepine (BZ) – sensitive; while α4 or α6 associated with βδ are insensitive to them (*Jacob et al., 2008*).

Concerning cellular localization, $GABA_AR$s subunits are widely distributed in the CNS, however, some subunits are expressed restrictively in specific cells. For instance, α6 subunit is expressed in cerebellar granule cells, while ρ subunit is predominantly expressed by retina cells (*Sigel and Steinmann, 2012)*.

Finally, $GABA_AR$s can be both synaptic and extra – synaptic, according to subunits composition. $GABA_AR$s composed by α (1- 3) subunits associated with βγ subunits are synaptic, and they are involved in phasic inhibition, promoting a fast (millisecond) increase in the anion conductance. By contrast, receptors composed by α4 or α6 subunits associated with βδ subunits or α5 subunit associated with βγ subunits are extra – synaptic and they induce tonic inhibition. Indeed, these receptors are activated by low ambient GABA concentration, and they stay open for longer period of time (*Jacob et al., 2008; Sigel and Steinmann, 2012*).

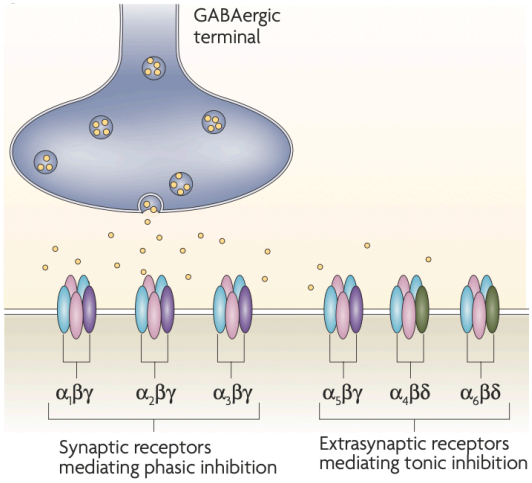

Figure 14. ***Synaptic and extra – synaptic $GABA_AR$s composition and function.*** *(Jacob et al., 2008)*

3.3 $GABA_ARs$ AND NEUROLOGICAL DISORDERS

Synaptic $GABA_ARs$ pool is finely regulated through internalization, recycling, and lateral diffusion. All these processes define the strength of the GABAergic synapses (*Mele et al., 2019*). $GABA_ARs$ are assembled in the Endoplasmic Reticulum (ER) and then receptors are transported to the Golgi Apparatus. Unassembled subunits undergo proteasomal degradation. The transport of assembled receptors on the plasma membrane is protein – dependent and it is finely regulated. Once on the plasma membrane, $GABA_ARs$ are dynamics, moving from synaptic to extra – synaptic location (*Mele et al., 2019*).

Alterations in $GABA_ARs$ expression or in turn – over are strongly associated with the onset of different neurological disorders (*Schwartz-Bloom and Sah, 2001; Rudolph and Knoflach, 2011; Kaila et al., 2014*).

For example, a correlation between seizures onset and GABAergic neurotransmission alterations has been widely documented. Indeed, mutations affecting α1, α6, β2, β3, γ2, or δ subunit were associated with epilepsy in human (*Hirose, 2014*). These mutations can enhance ER – associated degradation or perturb receptor trafficking on the plasma membrane (*Huang et al., 2014; Huang et al., 2017*). Moreover, also some pediatric monogenic epilepsies, like Dravet and Rett syndrome, were associated to GABAergic defects (*Ali Rodriguez et al., 2018; Gataullina et al., 2019*). For example, in Dravet syndrome, besides mutations in the *SCN1A* gene, also mutations in *GABRA1, GABRB2, GABRB3*, and *GABRG2* were found, altering the normal receptor surface expression (*Hernandez et al., 2021*).

Moreover, different ASD animal models showed GABAergic defects (*Mele et al., 2019*). Indeed, it is well established that one of the pathophysiological mechanisms behind ASD is an unbalance between inhibition and excitation (*Jenks and Volkers, 1992; Ramamoorthi and Lin, 2011; Yizhar et al., 2011*).

For example, in a sodium valproate-induced ASD rat model, a reduced expression of the $GABA_AR$-β3 subunits and of its phosphorylation form has

been reported. This reduction was associated with an increased receptor internalization (*Li et al., 2017b*).

Besides epilepsy and ASD, GABAergic defects are associated to neuropsychiatric disorder, like depression and anxiety disorders, as well as neurodegenerative disorders, like Parkinson and Alzheimer diseases (*Kim and Yoon, 2017*).

AIM OF THE PROJECT

Developmental and Epileptic Encephalopathy 9 (DEE9) is a severe neurodevelopmental disorder characterized by epileptic seizures occurring in clusters, intellectual disability (ID), autism spectrum disorder (ASD) and neuropsychiatric symptoms (*Dibbens et al., 2008; Depienne et al., 2009; Kolc et al.,2020*).

DEE9 is still an uncurable disorder with a strong variability among patients (*Kolc et al., 2020; Mazzoleni and Bassani, 2021*).

DEE9 is due to mutations affecting *PCDH19*, a gene localized on the X chromosome, which encodes for a calcium – dependent cell – cell adhesion molecule, called protocadherin – 19 (PCDH19) (*Dibbens et al., 2008*). PCDH19 is expressed mainly in the cerebral cortex and in the limbic system (*Kim et al., 2007; Pederick et al., 2016; Schaarschch and Hertel, 2018*).

Even though DEE9 is a X – linked disorder, it mainly affects females, sparing males. For this peculiar mechanism of inheritance, the cellular interference hypothesis was postulated: random X inactivation in females would lead to *PCDH19* mosaic expression in the brain of patients, which would in turn affect neuronal communication and circuit formation, promoting DEE9 features onset (*Dibbens et al., 2008; Hoshina et al., 2021*).

However, the role of PCDH19 in the brain is still not clear, as the pathophysiological mechanism behind this disorder (*Hoshina et al.,2021*). Therefore, generation of animal models could help in identifying some pathophysiological mechanisms responsible for DEE9 as well as possible future therapeutic targets to treat this disorder.

The aim of my project was the characterization of a new conditional knock – out (cKO) mouse model for PCDH19. Through a molecular, functional, and behavioural characterization, we wanted to validate this cKO mouse as a new DEE9 model able to recapitulate the main features of DEE9 as well as provide a tool to study signalling pathways involved in DEE9 aetiology. Moreover, we focused our attention on both female and male mice to identify a possible gender – effect in DEE9 pathophysiology.

MATERIALS AND METHODS

MICE

Animals care and all experimental procedures involving animals were performed in accordance with the CNR licensing and were approved by the Italian Ministry of Health (authorization no. 534/2017 – PR, 316/2018 – PR, 239/2018 – PR, 530/2019 – PR, 708/2019 – PR).

Pcdh19 floxed mouse was generated in collaboration with the InGenious Targeting Laboratories, Inc. (USA). A Lox P site was introduced 174 base pair (bp) upstream *Pcdh19* exon 3, while a Neomycin cassette, flanked by the Frt sites and two Lox P sites, was introduced 225 bp downstream of exon 3 (Fig.1a). After selection of neomycin – expressing clones, the neomycin cassette was excised by Flp – mediated homologous recombination. In the resulting Pcdh19 floxed allele exon 3 is flanked by two Lox P sites.

To generate the *Pcdh19* cknock out (cKO) mice, *Pcdh19* floxed female mice were crossed with Syn1 – Cre male mice, expressing the Cre recombinase under the control of the rat Synapsin I promoter (The Jackson Laboratory, stock No: 003966). Both male and female mice were used for this study. The

50% of the progeny that did not inherit the Syn1 – Cre transgene, was used as control.

MICE GENOTYPING

DNA was extracted *postmortem* from the mouse tail or cortex (Fig.3c) or from ear tissue obtained from ear punching procedure in Post – Natal Day (P) 21 mice, by using REDExtract-N-Amp™ Tissue PCR Kit Protocol (Merck). Genotyping of *Pcdh19* floxed mice and of the progeny of *Pcdh19* floxed and Syn1 – Cre mice was performed by PCR with the following primers:
Primer 1, 5' -TCTCCCCCATAGGCTCAACTTTCC - 3' and
Primer 2, 5' - AGTGCCTTTAGGATTCCGAACCACAGG - 3'.
These primers allowed the discrimination of the following Pcdh19 alleles: WT, 1053 bp; floxed allele, 1224 bp; KO allele, 379 bp (Fig.3b).
Detection of Cre recombinase in the progeny of *Pcdh19 floxed* and Syn1 – Cre mice was performed by PCR using the following primers:
Primer 1, 5' - CCAGCACCAAAGGCGGGC - 3' and
Primer 2, 5' -TGCATCGACCGGTAATGCAG - 3'.
These primers allowed the amplification of a 500 bp sequence within the Syn1 – Cre transgene.

INTRACEREBROVENTRICULAR (ICV) INJECTION IN P0 PCDH19 FLOXED MICE

P0 *Pcdh19* floxed mice were manually intracerebroventricular (ICV) injected according to the protocols in *Glacscock et al., 2011* and *Kim et al., 2014*. Briefly, pups were anesthetized via cryo – anaesthesia for 3 minutes and their heard was disinfected with 70% EtOH. The injection needle was a sterilized glass micropipette whose tip was adjusted for 3 mm penetration into the skull and the needle was attached to a 1ml Insulin syringe through a small pipe. The needle was inserted 3 mm deep into the skull of the animal, which was previously checked for anaesthesia, and the coordinates for the ventricles were as followed: 0.25 mm lateral to the sagittal suture and 0.50 – 0.75 mm

rostral to the neonatal coronary suture (*Glacscock et al., 2011*). 1 μl of solution (AAV9.hSyn.HI.eGFP-Cre.WPRE.SV40, 5,5 x 10^9 genome copy (GC)/ml; 0,05% Trypan Blue; 1X Phosphate Buffered – Saline (10X PBS: 1.37M NaCl, 27 mM KCl, 80 mM Na_2HPO_4 x $2H_2O$, 23 mM NaH_2PO_4, pH 7.4)) was slowly injected for each ventricle and the needle stayed in position for 15 seconds to prevent backflow. Pups were placed in a warmed container under a warming light until full – recover and finally returned to their home cage with their mother. Adult female and male mice (P60 – P90) were used for electrophysiological analysis and immunohistochemistry (IHC) experiments.

PRIMARY NEURONS FROM POST NATAL DAY (P)0 PCDH19 FLOXED MICE

Dissociated cortical and hippocampal neurons were obtained from P0 *Pcdh19* floxed mice of either sex. Briefly, pups were sacrificed by decapitation and cortices and hippocampi were dissected from mouse brain and cut in small pieces.

Hippocampal and cortical tissues were disaggregated with Trypsin (0.25 %, Gibco) in Hanks' Balanced Salt Solution (HBSS: 1X HBSS (Gibco); 0.5M $MgSO_4$; 1M HEPES, pH 7.4; 1% Penicillin – Streptomycin (Gibco)), for 30 minutes at 37°C. Neurobasal A (Gibco) and 10% Fetal Bovine Serum (FBS, Gibco) was added and, after centrifugation (3 minutes at 1500 Revolutions Per Minute (RPM)), the pellet was resuspended in HBSS at 37°C, 10% FBS and DNAse – I (12,5 ul/pup, Merck). Neurons were mechanically disaggregated and then centrifugated 6 minutes at 1000 RPM. Pellet was resuspended in complete medium (Neurobasal A (Gibco); 1% L – glutamine (Gibco); 1X B27 Supplement (Gibco); 1% Glucose; 1% Penicillin – Streptomycin (Gibco)) and then plated on poly – D – lysine (50 ug/ml, Sigma Aldrich) coated coverslips in 12 – multiwell plates at a density of 10^5/well for immunocytochemistry (ICC) experiments and of 1.2 X 10^5 for RT – PCR and biochemical experiments.

Neurons were grown in complete medium and maintained at 37°C, 5% CO_2. At days in vitro (DIV) 5 the 50% of the medium was replaced by fresh medium.

At DIV 0 neurons were infected with Adeno Associated Virus 9 (AAV9) encoding Cre fused to GFP (pENN.AAV.hSyn.HI.eGFP-Cre.WPRE.SV40 was a gift from James M. Wilson (Addgene plasmid # 105540; http://n2t.net/addgene:105540; RRID:Addgene_105540)) or an empty vector encoding GFP (provided by Prof. V. Broccoli, San Raffaele Institute; IN - CNR). Neurons were used at DIV 7 or DIV 10, as indicated.

REAL TIME PCR

mRNA was extracted from primary neurons and from hippocampal and cortical tissues using RNeasy mini kit (Qiagen) and Nucleozol Reagent Kit (Macherey Nagel), respectively. mRNA was retrotranscribed into cDNA using SuperScript VILO cDNA Synthesis Kit (Thermo Fisher). 2,5 ug of mRNA were retrotranscribed for all the samples, and the cDNA was diluted 1:4 for Real Time – PCR (RT – PCR).

Pcdh19 and the control *α – actin* were amplified by using SYBR Green PCR Master Mix (Applied Biosytems) in a Applied Biosystems 7000 Real – Time thermocycler.

The following primers were used:

Fw PCDH19 EX 1 – 2, 5' - ATCCGGACCTACAATTGCAG - 3';

Rev PCDH19 EX 1 – 2, 5' - ATAAAACAGCCGAGGAGACAAG - 3';

Fw PCDH19 EX 4 – 5, 5' - GCCGTGCCCATTTAATCA - 3';

Rev PCDH19 EX 4 – 5, 5' - TTCACAGCAGTATCGCAGTACAG - 3';

Fw PCDH19 EX 5 – 6, 5' - TGGGATCTCAGATGCCTG - 3';

Rev PCDH19 EX 5 – 6, 5' - CCAGCATCTATCAGAGTGGC - 3';

Fw α – actin, 5' - AGATGACCCAGATCATGTTTGAGA - 3' and

Rev α – actin, 5' - CCTCGTAGATGGGCACAGTGT - 3'.

A triplicate was prepared for each sample and data were analysed though ABI PRISM 7000 software (Applied Biosystems) to calculate the C_t, $2^{-\Delta Ct}$, $2^{-\Delta\Delta Ct}$ values, after having been normalized on *α – actin* controls.

BS3 (BIS(SULFOSUCCINIMIDYL)SUBERATE) ASSAY

20 – day – old and 3 – month – old female and male mice were sacrified by cervical dislocation and the brain was immediately cut in oxygenized artificial Cerebrospinal Fluid (aCSF: 125 mM NaCl, 2.5 mM KCl, 1.25 mM NaH_2PO_4, 1 mM $MgCl_2$, 2 mM $CaCl_2$, 25 mM glucose, and 26 mM $NaHCO_3$) with a vibrating blade microtome (VT1000S, Leica Biosystems, Italy) into 400 µm – thick coronal brain slices. Coronal brain slices were treated with 2mM BS3 (Thermo Fisher) in 5mM Sodium Citrate pH 5.0 (for treated slices) or with 5mM Sodium Citrate (for untreated slices) for 30 minutes at 4°C in slightly agitation. 100mM glycine prepared in bi-distilled water was added and left for 10 minutes at 4°C in slightly agitation. Finally, coronal brain slices were collected and centrifuged at 13.200 RPM for 2 minutes at 4°C and then lysated in Lysis Buffer (50mM Tris, 150mM NaCl, 1mM EDTA, 1% SDS, pH 7.4 and protease inhibitors). Lysates were put on a wheel at room temperature (RT) for 1h and then centrifugated at 13.200 RPM for 8 minutes at RT. Homogenates were mixed with Sample Buffer 3X and underwent SDS – PAGE and Wester Blotting (as in Wester Blotting section).

WESTERN BLOTTING

Cerebral cortex and hippocampus were collected from male and female adult mice (P90 – P120) and tissues underwent homogenization in modified Radio Immunoprecipitation Assay (RIPA) buffer (50 mM Tris – HCl, 150 mM NaCl, 1 mM EDTA, 1% NP – 40, 1% Triton X100, pH 7.4 and protease inhibitors). Cultured neurons were lysated in modified RIPA buffer at DIV 10. Homogenates from tissues and primary neurons were mixed with Sample Buffer 3X and underwent SDS – PAGE. Proteins were transferred to a 0.2 µm nitrocellulose support (Amersham GE Healthcare) through a wet – tank system (Bio – Rad). Membranes were blocked in 5% skim milk in 1X Tris Buffer Saline (10X TBS: 20mM Tris; 150mM NaCl, pH 7.4) with 0,1% Tween 20 detergent (TBST 0,1%, Sigma Aldrich) for 1 hour at RT or overnight at 4°C. Membranes were incubated with primary antibodies prepared in 5% skim milk in TBST 0,1% overnight at 4°C or for 2 hours at RT (PCDH19 1:20000, Bethyl

Laboratories; $GABA_AR$ α1 1:1000, Millipore; α - Tubulin, 1:40000, Sigma Aldrich; GAPDH 1:2000, Santa Cruz Biotechnology). After washing three times with TBST 0,1%, membranes were incubated with secondary antibodies for 1 hour at RT (1:7500, Li – Cor; 1:2000, ECL HRP – conjugated anti Mouse, Amersham; 1:20000, ECL HRP – conjugated anti Rabbit, Jackson ImmunoResearch).

Proteins were detected by using the Odyssey CLx detector system (Li – Cor) and quantified by Image Studio (Li – Cor) software program or detected by Amersham Imager 600 and quantified with Image Lab Studio (Bio – Rad) software program.

IMMUNOCYTOCHEMISTRY (ICC)

DIV 7 hippocampal and cortical neurons were fixed with 4% paraformaldehyde and 4% sucrose for 10 minutes at RT. Neurons were incubated with primary antibody prepared in gelatine detergent buffer (2X GDB: 0.2 % gelatin; 0.6 % Triton X-100, 33 mM Na_2HPO_4, 0.9 M NaCl, pH 7.4) for 2 hours at RT (MAP2 1:2000, Synaptic System; PCDH19 1:400, Bethyl Laboratories) and then with secondary antibody for 1 hour at RT (DyLight 649 1:400, Jackson Laboratories; Alexa Fluor 555 1:400, Thermo Fisher). Neuronal nuclei were detected by staining with DAPI prepared in 1X PBS for 5 minutes at RT (1:10000, Invitrogen). ICC images were acquired with an LSM 800 confocal microscope (Carl Zeiss, Italy) with a 63X oil – immersion objective at 1024 x 1024 – pixel resolution.

Images were obtained from the z – projection (maximum intensity) of 6 – 8 stacks taken at 0.75 µm intervals.

IMMUNOISTOCHEMISTRY (IHC)

2 – month – old mice were anesthetized with intraperitoneal injection of Zolazepam and Tiletamine (80 mg/Kg) and brains were washed through cardiac perfusion with 0.1M Phosphate Buffer (0.2 M PB: 33 mM Na_2HPO_4 x $2H_2O$; 192 mM NaH_2PO4, pH 7.4) and then fixed with 4% paraformaldehyde

in 0.1M PB. 100 µm – thick coronal brain slices were cut with a vibrating blade microtome (VT1000S, Leica Biosystems) and incubated with the blocking solution (0,5%Triton 100X and 10% goat serum in 0.1 M PB) for 2 hours at RT. Sections were incubated overnight at 4°C with primary antibody (PCDH19 1:50, Thermo Fisher) prepared in blocking solution and successively in secondary antibody (Alexa Fluor 488 1:400, Thermo Fisher) for 2 hours at RT. Brain slices were incubated with DAPI (1:4000, Invitrogen) for 15 minutes at RT and mounted with Fluoromount™ Aqueous Mounting Medium (Merck).
IHC images were acquired with an LSM 800 confocal microscope (Carl Zeiss) with 20X and 40X oil – immersion objective at 1024 x 1024-pixel resolution.

BEHAVIORAL TESTS

SPONTANEOUS MOTOR ACTIVITY TEST

3 – month – old female and male mice were tested for spontaneous motor activity in an activity cage (43w x 43d x 32h cm; Ugo Basile, Varese Italy), placed in a sound – attenuating room at a constant temperature (22°C ± 2°C). The cage is fitted with two horizontal and vertical infrared beams located 2 cm and 4 cm respectively from the cage floor. Mice were habituated for 45 minutes at the testing room and then each mouse performed 3 rounds of 10 minutes each (30 minutes in total). Cumulative horizontal and vertical movements counts were recorded by the machine.

SELF – GROOMING TEST

For the evaluation of self – grooming, 3 – month – old mice were habituated to a sound – attenuating room at a constant temperature (22°C ± 2°C) for 45 minutes and after to a transparent cylinder (46 x 23.5 x 20 cm) for 10 minutes. Successively, mice were assayed and recorded for 10 minutes. The number and the duration of self – grooming events were evaluated manually by the operator. A self – grooming event was considered whenever the mouse did a related self – grooming behaviors (lick, scratch, nibble) towards the self (https://conductscience.com/maze/mouse-ethogram-self-grooming-behavior/).

NOVEL OBJECT RECOGNITION (NOR) TEST

To test recognition memory, adult mice underwent Novel Object Recognition (NOR) test. In principle, 3 – month – old mice were habituated to a sound – attenuating room at a constant temperature (22°C ± 2°C) for 45 minutes and after to a white plastic box (38 x 30 x 18 cm) covered by sawdust for 10 minutes. During the familiarization phase, two identical objects were placed at the two corners with 10 cm from the box edges. Each mouse was let to explore the objects (called familiar objects) for 20 minutes and then returned to the home cage. In the object recognition phase, one of the two familiar objects was substituted after 5, 120 minutes and 24 hours from the familiarization phase with a novel object to evaluate mice capability to discriminate the new object in 20 minutes. Object exploration was considered when mice stayed within 0.5 cm from the object with the nose toward the object.

Data are expressed as discrimination index (I), calculated as difference between the exploration time of the novel object (N) and the exploration time of the familiar one (F) on the total time of exploration: $I = ((N-F)/(N+F))$.

FEAR CONDITIONING TEST

Fear conditioning test tested associative memory and conditioned fear related to hippocampus and amygdala. After 30 minutes of habituation in the room, 3 – month – old mice were placed in a sound – attenuating and ventilated cage (26x26x27 cm) connected to a PC, where through the Packwin Panlab software (Panlab Harvard Apparatus) was possible to automatize the experiment. The test was articulated in three phases:

1) Training phase: After 2 minutes of exploration of the new cage, animals were exposed for 5 following times in 5 minutes and 30 seconds to an acoustic stimulus (85db, duration 28 seconds), followed by a mild electric shock (0.25mA, duration 2 seconds; *Wahlsten, 2010*). Between mice, the cage was cleaned with 5% Acetic Acid to remove any odor cues.
2) Context phase: After 24 hours, mice were placed again in the training phase cage and the freezing time was measured in a 5 minute – time cut off.

3) Cued phase: after 24 hours, mice were placed in a new different cage with a different odor (cleaned with 4% EtOH) from the training phase one. After 2 minutes of exploration, mice were exposed to the training phase acoustic stimulus and mice were recorded for 4 minutes to measure the freezing time.

MORRIS WATER MAZE (MWM) TEST

To test hippocampal – related spatial memory, 3 – month – old mice were habituated to a sound – attenuating room at a constant temperature (22°C ± 2°C) for 45 minutes. A circular swimming pool (diameter 1,54 m and depth 0,38 m) was places under a camera connected to a computer to record the test with the Ethovision XT Software (Noldus Information Technology, the Netherlands). The swimming pool was filled with water at a constant temperature (22°C ± 2°C) and made opaque with the addition of non – toxic white tempera paint to hide the platform (diameter 13,5 cm). Visual cues were placed in the room and remained fixed during all the experiment. The swimming pool was ideally divided into four quadrants (North Ouest, Nord East, South Ouest and South East) and the platform was placed stably in one of these quadrants.

Mice were trained for 4 days with 4 trials per day and with 1 hour of inter trial per mouse. Across trials, mice were released into the pool from four different locations.

The test was articulated in three phases:

1) Habituation phase: mice were habituated to swim for 60 seconds and trained to stay on the platform for 60 seconds;
2) Learning phase: in a 60 second – cut off time, mice had to locate the hidden platform, after which they were guided to the platform by the experimenter. Mice had to remain on the platform for 60 seconds before being remove from the swimming pool.
3) Probe test: the platform was removed from the swimming pool and the latency to reach the correct quadrant and the platform zone was calculated.

At the end of each trial, mice were placed in a towel to dry and then placed in their home cage.

After 2 days from the acquisition learning test, a 4 – day reversal learning test was used to evaluate memory plasticity, by placing the platform on the opposite quadrant of the acquisition test.
Finally, a single day of visible platform training was performed, where the platform was moved in a new quadrant and made it visible by a flag.
Through Ethovision XT software, the distance moved, velocity and latency to reach the platform were calculated.

TRANSMISSION ELECTRON MICROSCOPY (TEM)

20 – day – old mice were anesthetized with intraperitoneal injection of Zolazepam and Tiletamine (80 mg/Kg) and transcardially perfused with 0.1% glutaraldehyde and 4% paraformaldehyde in 0.1M PB buffer (pH 7.4). Dissected brains were post-fixed for an additional 24 h at 4°C. Coronal sections (100 µm thickness) were obtained with a vibratome (Leica VT1000S), and hippocampi were manually dissected, and trimmed samples were processed for transmission electron microscopy (TEM) as previously described (*Murru et al., 2017*). Briefly, samples were washed with sodium cacodylate buffer (pH 7.4) and post-fixed with 2% osmium tetroxide in sodium cacodylate buffer (pH 7.4), rinsed and "*en bloc"* stained with 1% uranyl acetate in bi-distilled water. Samples were then dehydrated in EtOH and embedded in Epon-Spurr epoxy resin. 70 nm thin - sections were collected on copper grids and counter-stained with uranyl acetate in bi-distilled water and 1% lead citrate. Grids were observed with a Talos L120C TEM (FEI) equipped with a Ceta 4kX4k digital camera. Images were acquired at 28000x magnification for the quantitative analysis of excitatory synapses and at 8500x for the estimation of synapse density.

MORPHOMETRIC AND STEREOLOGICAL ANALYSES OF EXCITATORY SYNAPSES

Excitatory synapse profiles were included in the analyses when they met the following criteria: presence of at least three synaptic vesicles in the pre-synaptic terminal, clear defined synaptic cleft and post synaptic density (PSD) within the post-synaptic terminal. Quantitative and stereological analyses were

performed using the Fiji 1.53c software, as described elsewhere (*Colombo et al., 2021*).

The verification of the normal data distribution was performed using the Shapiro-Wilk test and for the comparison we used the parametric student's *t*-test for normally distributed data or the Mann-Whitney non parametric test for not normally distributed data.

ELECTROPHYSIOLOGY

270 µm thick - coronal slices from *Pcdh19* cKO and control mice were prepared as previously described (Murru et al., 2017). Briefly, mice were sacrificed by decapitation, the brain was rapidly removed and placed in an ice-cold solution at pH 7.4, equilibrated with 95% O_2 and 5% CO_2 [for patch-clamp recordings: 220 mM sucrose, 2 mM KCl, 1.3 mM NaH_2PO_4, 12 mM $MgSO_4$, 0.2 mM $CaCl_2$, 10 mM glucose, 2.6 mM $NaHCO_3$, 3 mM kynurenic acid; for field excitatory post synaptic potentials (fEPSPs) recordings: artificial cerebrospinal fluid (aCSF) containing 125 mM NaCl, 2.5 mM KCl, 1.25 mM NaH_2PO_4, 1 mM $MgCl_2$, 2 mM $CaCl_2$, 25 mM glucose, and 26 mM $NaHCO_3$]. Immediately after the cutting procedure, slices were incubated at 37°C for 40 min and then at RT for 1 h in standard aCSF solution before recordings.

Slices containing the hippocampus were transferred to a recording chamber and perfused with aCSF at a rate of ~2 mL/min and at RT. Whole-cell patch-clamp electrophysiological recordings were performed with a Multiclamp 700B amplifier (Axon CNS Molecular Devices, USA) and using an infrared-differential interference contrast microscope (Nikon Eclipse FN1). Patch electrodes (borosilicate capillaries with a filament and an outer diameter of 1.5 µm; Sutter Instruments) were prepared with a four-step horizontal puller (Sutter Instruments) and had a resistance of 3–5 MΩ.

Current-clamp experiments were performed using an intracellular solution containing (in mM): 126 K-gluconate, 4 NaCl, 1 EGTA, 1 MgSO4, 0.5 CaCl2, 3 ATP (magnesium salt), 0.1 GTP (sodium salt), 10 glucose, and 10 HEPES–

KOH (pH 7.4), while fEPSPs recordings were obtained using aCSF as internal solution.

The analysis of neuronal AP firing activity was conducted at resting membrane potential (RMP) in whole-cell configuration according to the literature (*Weiss and Veh, 2011*). To evaluate DG neurons active membrane properties, a series of current steps (ranging from -60 to +150 pA) were injected (10 pA per step, 1 s duration) to evoke AP firing. The AP frequency was correlated to the current injected in an input/output (I/O) curve. AP feature analysis were performed for the first AP evoked by current injection.

fEPSPs responses were evoked stimulating the Schaffer-collateral fiber bundles using a glass pipette filled with aCSF and placed at 200/300 μm from the recording electrode in the stratum radiatum. The stimulus intensity that evoked a half maximal response was chosen. For paired pulse ratio (PPR) experiments, pairs of stimuli were delivered at 50-ms intervals every 20 s (0.05 Hz) and the ratio was calculated by dividing the amplitude of the second response by the first one. Access resistance was between 10 and 20 MΩ; if it changed by >20% during the recording, the recording was discarded.

After 10 min of stable baseline (fEPSPs evoked every 20 s), LTP was induced stimulating Schaffer-collaterals pathway with one train of 100 stimuli at 100 Hz according to *Murru et al., 2017.* To quantify the LTP induction, the fEPSPs slopes were analyzed before and after LTP induction. Currents and potentials were filtered at 2 kHz through the amplifier and digitized at 20 kHz using Clampex 10.1 software. The analysis was performed offline with Clampfit 10.1 software.

STATISTICAL ANALYSIS

Data were analysed with GraphPad Prism software (9.0.2 version) and results were expressed as mean ± standard error of the mean (SEM). Unpaired two tailed Student's t – test was used to assess the significancy of the data. When three categories were evaluated, One – Way ANOVA was assayed; instead, for group analysis, Two – Way ANOVA. For growth curve analysis and MWM,

multiple t - test was used. Significancy was given when p value was < 0.05 (* p value < 0.05; ** p value < 0.01; *** p value < 0.001). Significant outliers were excluded according to the Grubbs' test. Experiments on cultured neurons were done on three independent cultures.

REAGENTS AND RESOURCES TABLE

REAGENT or RESOURCE	SOURCE	IDENTIFIER
Antibodies		
α - PCDH19 Rabbit Polyclonal	Bethyl Laboratories	Cat. No A304 – 468A
α - MAP2 Guinea Pig Monoclonal	Synaptic System	Cat. No 1880 – 004
α - GAPDH Rabbit Monoclonal	Santa Cruz Biotechnology	Cat. No sc - 47724
α - alpha Tubulin Mouse Monoclonal	Sigma Aldrich	Cat. No T5168
α - $GABA_A$Rs α1 Rabbit polyclonal	Millipore	Cat. No 06 - 868
α - Rabbit IgG – Alexa 488	Invitrogen	Cat. No A11034
α - Rabbit IgG – Alexa 555	Invitrogen	Cat. No A21429
α - Mouse IgG – Alexa 488	Invitrogen	Cat. No A11029
α - Guinea Pig IgG – DyLight 649	Jackson ImmunoResearch	N/A
α - Rabbit IgG – HRP	Jackson ImmunoResearch	Cat. No 111 – 035 - 00
α - Mouse IgG – HRP	Amersham	Cat. No NA 931
α - Rabbit IgG – Dye800CW	Li - Cor	Cat. No 926 - 32211
α - Mouse IgG – Dye680RD	Li - Cor	Cat. No 926 - 68072
AAV		
AAV - GFP	Dr. Vania Broccoli	N/A
AAV9.hSyn.HI.eGFP-Cre.WPRE.SV40	AddGene	Cat. No 105540 – AAV9
Software and algorithms		
Clampex 10.1	Axon Instruments, Molecular Devices	N/A
Clampfit 10.1	Axon Instruments, Molecular Devices	N/A
Image Lab 6.0	Bio - Rad	N/A
Li - Cor Image Studio	Li - Cor	N/A
Fiji	ImageJ	N/A
Ethovision XT	Noldus InformationTechnology	N/A

RESULTS

1. GENERATION OF *PCDH19* FLOXED MOUSE MODEL

To recreate a model of DEE9 *in vivo*, we generated a new conditional knock – out (cKO) mouse model for *Pcdh19* by exploiting the Cre recombinase (Cre) – LoxP technology.

Pcdh19 is a six – exons gene encoding the transmembrane protein protocadherin-19 (PCDH19). *Pcdh19* exon 1 contains different regulatory elements (*http://www.ensembl.org/Mus_musculus/Gene/Summary?g=ENSMUSG00000051323;r=X:132483609-132589736*), while exon 2 undergoes alternative splicing (*Depienne and LeGuern, 2012*). Therefore, we decided to target exon 3 to remove alternative isoforms deriving from exon 2 and not to alter the normal expression of the protein before Cre expression in the newly generated mice.

To generate the *Pcdh19* floxed mouse, we entrusted the InGenious Targeting Laboratories, Inc. (USA). The *Pcdh19* – targeting vector contained a Lox P site and the neomycin cassette which were flanked by two Lox P sites and a Frt sequence, which is recognized by the flippase (FLP) protein. This vector was electroporated into FLP C57BL6 embryonic stem (ES) cells. Upon G418 antibiotic selections, five clones were screened for homologous recombination

by Southern Blot analysis and among these, four clones satisfied the euploid cut – off, according to the Cold Spring Harbor Laboratory's chromosome counting protocol (*Nagy et al., 2009*) and therefore they were injected into Balb/c blastocysts to obtain chimeras. Chimeras were crossbred with C57BL/6 wild – type (WT) to obtain a germ – line neomycin cassette depleted F1 heterozygous mice. By this, *Pcdh19* exon 3 was flanked by two Lox P sites and mice were crossbred with C57/BL6 to establish the *Pcdh19* floxed mouse line (Fig.1a).

General health status parameters were checked in the newly formed mouse line. Homozygous ($Pcdh19^{Flox/Flox}$) and heterozygous ($Pcdh19^{Flox/x}$) female mice and hemizygous ($Pcdh19^{Flox/y}$) male mice for the *Pcdh19* floxed allele had a normal growth compared to wild – type (WT) mice and they were fertile. Moreover, $Pcdh19^{Flox/Flox}$, $Pcdh19^{Flox/x}$ and $Pcdh19^{Flox/y}$ and $Syn1^{Cre}$ male mice expressed PCDH19 at comparable level to WT mice in hippocampal tissues (Fig.1b, 1c).

These data suggested that insertion of the Floxed allele did not alter either PCDH19 normal expression or viability and fertility of the mice and therefore we could consider these mice as control mice for the future experiments.

2. VALIDATION OF CRE – MEDIATED EXON 3 EXCISION *IN VITRO*

The *Pcdh19* exon 3 targeting by Cre was assumed to cause reading frame shift and the generation of premature stop codons and as consequence the activation of the mRNA Nonsense – mediated Decay (NMD) (Fig.1a). To effectively validate the effect of *Pcdh19* exon 3 excision mediated by Cre, cortical and hippocampal neurons obtained from Post Natal (P) 0 *Pcdh19* floxed mice were infected with an Adeno – Associated Virus (AAV) 9 expressing Cre fused to GFP (AAV9 Cre – GFP) or with a control vector (AAV9 GFP). At days in vitro (DIV) 7, *Pcdh19* mRNA was analysed by Real Time – PCR (RT – PCR). Almost no transcript levels were detected both by using probes amplifying downstream exons (probes spanning the junction between exon 4 – 5 and 5 – 6) and upstream exons (probes

spanning the junction between exon 1 – 2), indicating *Pcdh19* mRNA absence and no formation of aberrant transcripts encoding for truncated *Pcdh19* isoforms (deriving from exon 1 and 2) (Fig. 2a). Western Blot (WB) analysis and Immunocytochemistry (ICC) at DIV 10 reconfirmed RT – PCR results at the protein level (Fig. 2b, 2c).

To conclude, our results demonstrated that the Cre recognition of the Lox P sites flanking exon 3 caused the depletion of PCDH19 expression.

3. GENERATION OF *PCDH19* cKO MOUSE LINE

Once evaluated the effect of exon 3 excision *in vitro*, we wanted to deplete *Pcdh19* expression also *in vivo*. We exploited two different strategies to deliver Cre (Fig.3a):
1) by crossbreeding *Pcdh19* floxed mice with mice expressing Cre under a specific promoter;
2) by intracerebroventricular (ICV) injecting P0 *Pcdh19* floxed mice with an AAV9 expressing Cre fused to GFP (AVV9 Cre – GFP). The second approach was used whenever we needed to discriminate between neuronal genotypes (PCDH19 positive neurons and PCDH19 negative neurons).

Initially, we focused our attention on the crossbreeding model.
To obtain a *Pcdh19* cKO mouse line, we crossbred *Pcdh19* floxed mice with mice expressing Cre under the rat Synapsin – 1 promoter ($Syn1^{Cre}$, The Jackson Laboratory, stock No: 003966). In this way, we depleted specifically *Pcdh19* expression in neuronal cells. PCR genotyping was used to identify the WT, floxed and KO allele (Fig. 3b, 3c). As expected, 50% of the progeny inherited the $Syn1^{Cre}$ transgene and displayed *Pcdh19* exon 3 excision specifically in brain tissue (Fig. 3c). Since *Pcdh19* cKO female mice displayed one WT allele and one floxed allele, we expected a mosaic expression of *Pcdh19* in their brain. Indeed, by RT - PCR, *Pcdh19* cKO female mice showed a mRNA reduction of ~ 56% in cerebral cortex and of ~ 40% in hippocampus compared to control female mice (Fig. 4a). *Pcdh19* reduction was also

confirmed at the protein level by WB analysis. *Pcdh19* cKO female mice confirmed a PCDH19 reduction of ~ 40% both in cerebral cortex and in hippocampus compared to their female counterparts (Fig. 4b). A further validation of *Pcdh19* mosaicism in mouse brain was provided by Immunohistochemistry (IHC). It was possible to appreciate the coexistence of *Pcdh19* positive neurons and *Pcdh19* negative neurons in the cerebral cortex and in the hippocampal CA1 and dental gyrus (DG) areas of *Pcdh19* cKO female mice compared to their sex – related controls (Fig. 4c).
Even though, *Pcdh19* cKO male mice have just one X chromosome which is floxed and so they should be full KO mice, RT – PCR demonstrated that *Pcdh19* cKO male mice also had a mosaic expression of *Pcdh19* in their brain. Indeed, *Pcdh19* cKO male mice showed a mRNA reduction of ~ 68% in the cerebral cortex and of ~ 63% in the hippocampus compared to their controls (Fig. 5a). By WB analysis, PCDH19 protein was confirmed to be reduced of ~ 60% both in cerebral cortex and in hippocampus in *Pcdh19* cKO male mice (Fig. 5b) and the *Pcdh19* mosaicism was also confirmed by IHC (Fig. 5c).

To conclude, Cre delivery was able to promote *Pcdh19* exon 3 excision specifically in the brain confirming the generation of a cKO mouse model for *Pcdh19*. Moreover, we demonstrate that not only *Pcdh19* cKO female mice, which are heterozygous for the floxed allele, but also *Pcdh19* cKO male mice are mosaic for *Pcdh19* (*Pcdh19* cKO female mice: -40%; *Pcdh19* cKO male mice: -60%). This last aspect could be due to that Cre has a mosaic expression itself, as reported by *Corbetta et al., (2009*). Corbetta et al. showed that in Syn-Cre mice there was an inhomogeneous expression of Cre in different brain areas and that not all the cells expressed the Cre transgene.
Pcdh19 mosaicism is a key aspect in DEE9 pathophysiology, therefore we wanted to investigate if the mosaicism could have a different impact on female and male mice and if the gender could have a role in DEE9. That is why for future experiments, we concentrated both on female and male mice.

4. *Pcdh19* cKO FEMALE MICE DISPLAY A DELAYED GROWTH CLOSE TO THE WEANING TIME

Since it was a new mouse model, *Pcdh19* cKO mice were monitored from birth to the 3rd month to evaluate general physical parameters (body appearance, motility, and posture). No gross defects were identified in the *Pcdh19* cKO mice compared to their control littermates (data not shown). Moreover, no differences in brain dimension or gross structural abnormalities were observed between cKO and control mice (Fig. 6a). Furthermore, mice were weighted from the 3rd week to the 3rd month to evaluate their growth. Interestingly, *Pcdh19* cKO female mice were characterized by a transient growth delay close the weaning time (P21 – 26, *Brust et al., 2015*). Indeed, *Pcdh19* cKO female mice weighted significantly less than control females during the 4th and the 6th week (P28 – 42, Fig.6b, 6c), which was compensated over the time by an increased in weight gain between the 5th and the 8th week (P35 – 56, Fig. 6d). At the end, *Pcdh19* cKO and control female mice reached a comparable weight (P90, Fig. 6e).

Concerning *Pcdh19* cKO male mice, no differences in growth and in weight gain were observed compared to control mice during the monitoring time (Fig. 6f, 6g, 6h, 6i), even though *Pcdh19* cKO male mice were characterized by a strong intra – group variability, which could mask this subtle growth delay (Fig.6g).

Since DEE9 is characterized by epilepsy, spontaneous seizures were verified. *Pcdh19* cKO mice didn't display any spontaneous seizures, in accordance with constitutive *Pcdh19* mouse models (*Pederick et al., 2016; Hoshina et al., 2021*). However, constitutive *Pcdh19* mouse models underlined an increased susceptibility to seizures when these were induced (*Rakotomamonjy et al., 2020*).

Moreover, also Dravet syndrome mouse models were characterized by a similar growth delay, which was close to seizures onset (*Talbot et al., 2020; Ricobaraza et al., 2019; Martin et al., 2010; Mijanovic et al., 2021*).

To conclude, even though our *Pcdh19* cKO mouse model didn't display any spontaneous seizures, there were cues of a possible increased susceptibility to the induction of seizures.

5. *PCDH19* cKO FEMALE MICE DISPLAY AN ALTERED SYNAPTIC PLASTICITY AND STRUCTURE

It is well established that spine structural plasticity correlates with synaptic function and synaptic plasticity. Indeed, spines undergo experience – dependent morphological changes, that if aberrant, they can affect synaptic functionality (*Forrest et al., 2018).*
Therefore, synaptic dysfunction is at the base of many neuropsychiatric and neurological disorders (*Forrest et al., 2018*).
To investigate if *Pcdh19* cKO female mice displayed some functional and morphological synaptic defects, we performed some electrophysiological and ultrastructural analysis.

First, *Pcdh19* cKO female mice displayed ultrastructural synaptic defects compared to control female mice. Precisely, the excitatory synapses of the hippocampal stratum radiatum CA1 area from *Pcdh19* ckO female mice showed a reduced synaptic vesicles density and a reduced number of synapses. Moreover, *Pcdh19* cKO mice also presented an increased post-synaptic density (PSD) length, but with a reduced thickness (Fig.7a).

To investigate synaptic plasticity, Long Term Potentiation (LTP) and Paired Pulse Ratio (PPR) were measured on acute hippocampal brain slices from adult *Pcdh19* cKO and control female mice. *Pcdh19* cKO female mice showed a strong reduction in LTP between Shaffer collateral and CA1 synapses both in the early phase (first 10 minutes) and in the late phase (last 10 minutes) (Fig.7b, 7c). Moreover, also short – term plasticity was impaired in *Pcdh19* cKO female mice compared to control mice, represented by a significantly reduced PPR (Fig.7d).

6. *PCDH19* NEGATIVE AND POSITIVE NEURONS DISPLAY AN HETEROGENOUS EXCITABILITY WITHIN *PCDH19* FLOXED MOUSE BRAIN

The main feature of DEE9 is the presence of an early – onset epilepsy which occurs in clusters (*Dibbens et al., 2008*).
Even though *Pcdh19* cKO mice didn't show any spontaneous seizures, we investigated if *Pcdh19* cKO mice displayed any clues of increased neuronal excitability.
Indeed, it was recently demonstrated by our laboratory that PCDH19 downregulation was associated with an increased in the intrinsic excitability of primary hippocampal neurons (*Serrato et al.,2020*).

To evaluate neuronal excitability *in vivo*, P0 *Pcdh19* floxed mice were ICV injected with an AAV9 expressing the Cre fused to GFP (Cre – GFP). This approach allowed to reproduce a PCDH19 mosaic extended to all brain regions and to discriminate the genotype of the two neuronal populations: PCDH19 negative neurons (GFP expressing cells) and PCDH19 positive neurons (no GFP expressing cells) (Fig.8a). First, we checked if the virus expression was distributed in all the brain areas and if we were able to obtain a mosaicism of neurons expressing and not expressing PCDH19. Afterwards, we needed to verify that whenever Cre – GFP was expressed, no PCDH19 signal was detected in neurons (Fig.8b). To verify neuronal excitability, we focused our attention on the DG area, which is the gateway to the hippocampus, protecting it from overexcitation (*Buckmaster, 2009*).

Once again, a sex difference was observed. Indeed, PCDH19 negative DG Granule Cells (DGGCs) in female mice were characterized by a reduced Resting Membrane Potential (RMP) and a reduced rheobase (Fig. 8c) and by an unaltered Action Potential (AP) amplitude and threshold (Fig. 8d) compared to neighbouring DDGCs retaining PCDH19 expression. Moreover, increased excitability was confirmed by a higher firing frequency in response to injected currents in PCDH19 negative DGGCs compared to control neurons (Fig. 8e).

Concerning male mice, PCDH19 negative DGGCs were characterized by a reduced rheobase (Fig. 8f, right panel) and by a higher firing frequency in response to injected currents until 70pA, where for higher pA, they behaved like PCDH19 positive DGGCs (Fig. 8h). RMP, AP amplitude and threshold were unaltered between PCDH19 positive and negative DGGCs (Fig. 8f, left panel, 8g).

To conclude, PCDH19 negative DGGCs were characterized by an increased excitability compared to PCDH19 retaining DGGCs, possible underlying increased susceptibility to seizures. Moreover, this alteration in excitability was different in the two sexes, suggesting even a possible sex susceptibility.

7. *PCDH19* cKO MICE SHOW AN ALTERED SURFACE EXPRESSION OF $GABA_AR$s α1 SUBUNIT

Bassani et al., (2018) demonstrated that PCDH19 interacts with the $GABA_AR$ α subunits, modulating the receptor expression on the surface. Since $GABA_AR_s$ are the main component involved in the regulation of the inhibitory tone in the brain (*Terunuma, 2018*) and any alterations in the $GABA_AR$s receptors can promote onset of epilepsy and other neurodevelopmental disorders (*Mele et al., 2019*), we investigated if *Pcdh19* cKO mice showed any defects in the expression of the $GABA_AR$ α1 subunit, which is ubiquitously expressed in the brain (*Rudolph et al., 2004*).

Through BS3 assay, we assessed that *Pcdh19* cKO male mice displayed a reduced $GABA_AR$ α1 subunit expression on the surface with an unaltered total pool compared to control male mice. This defect was present both during the weaning time (P20) and in adulthood (P90) (Fig. 9a, 9b, 9c, 9d).
Surprisingly, *Pcdh19* cKO female mice showed an opposite phenotype. Indeed, *Pcdh19* cKO female mice were characterized by a significant increase in $GABA_AR$ α1 subunit and by an unaltered total pool compared to control

female mice. The α1 increase was observed at both P20 and P90 (Fig. 9e, 9f, 9g, 9h).

To conclude, *Pcdh19* cKO mice were characterized by an aberrant surface expression of $GABA_AR$ α1 subunit compared to their sex – related control mice, suggesting a possible GABAergic defect connected to seizures susceptibility. Moreover, once again, *Pcdh19* cKO female and male mice displayed differences, confirming a possible sex determinant in DEE9 aetiology.

8. *PCDH19* cKO MICE DISPLAY FEATURES OF AUTISM AND INTELLECTUAL DISABILITY

DEE9 is characterized by epilepsy, ASD and ID. To verify if our mouse model displayed features of ASD and ID, mice underwent different behavioural tests. We analysed male and female mice separately. Whenever mice of the two sexes showed the same phenotype, we pooled the data together.
First, we checked if *Pcdh19* cKO mice had a normal motor capacity and a normal visual acuity, which are necessary to perform the behavioural tests.
Pcdh19 cKO mice didn't display any defects in spontaneous motor activity compared to control mice, as revealed by the counting of the number of horizontal and vertical movements (Fig. 10a). Moreover, *Pcdh19* cKO mice had a normal visual acuity comparable to their controls, evaluated in Morris Water Maze (MWM) with a visible platform (data not shown).

To test ASD repetitive and stereotyped movements features, self – grooming was performed. *Pcdh19* cKO mice showed both an increase in the number and in the duration of the self – grooming events, suggesting the presence of some ASD features (Fig. 10b).

Concerning ID, Novel Object Recognition (NOR) test was performed to evaluate the recognition memory. By varying the retention intervals, it was also possible to test short – term memory (5 minutes), intermediate – term memory

(2 hours) and long – term memory (24 hours) (*Taglialatela et al. 2009; Antunes and Biala, 2012*). No significant differences were observed between *Pcdh19* cKO mice and control mice in any retention interval (Fig. 10c).

However, some memory defects emerged by the MWM test, which assayed hippocampal – related spatial memory. No differences were noticed between mean distanced moved and mean speed during the training days between *Pcdh19* cKO and control mice (Fig. 10d, 10f). During the acquisition phase, *Pcdh19* cKO mice started to learn the hidden platform location on the 3rd day compared to controls mice, which learnt immediately on the 2nd day. No differences in the probe test were found between the two groups (Fig. 10e). Concerning the reversal phase, which assayed the memory plasticity, *Pcdh19* cKO mice displayed a slight difficulty in remembering the new position of the hidden platform, showed by an increased latency to reach the platform on the 4th day of the training, defect that was also reconfirmed in the probe test (Fig. 10g).

MWM test suggested that *Pcdh19* cKO mice needed a persistent recall during the training days of the acquisition phase to perfectly remember the position of the hidden platform on the 4th day and especially during the probe test. Moreover, it emerged that *Pcdh19* cKO mice had also some memory plasticity defects, represented by difficulties in learning the new position of the platform.

A first difference between sexes was observed in the Fear Conditioning Test, which investigate the associative memory and the conditioned fear mainly associated to hippocampus and amygdala (*Heise et al., 2017*). During the first day, mice were exposed to a new cage and a paired auditory cue (conditioned stimuli) and to a mild electric foot shock (aversive unconditioned stimulus). No statistically significant differences in freezing time were seen during the training (day 1) among sex and genotype (Fig.10h, left panel). On the contrary, when *Pcdh19* cKO female mice were exposed 24h later to the same cage of the training (day2, context), they showed a reduced time spent in freezing compared to control female mice, suggesting a hippocampal memory defect (Fig. 10h, middle panel). No differences in freezing time were noticed when female mice were exposed to the same auditory tone of the training (day 3, cued), suggesting no defects in the amygdala – related memory (Fig. 10h, right

panel). Interestingly, no differences in freezing time were noticed between *Pcdh19* cKO and control male mice in day 2 (context – related memory) and day 3 (cued – related memory) (Fig. 10i).

To conclude, *Pcdh19* cKO mice displayed an increased number and duration of stereotyped movements, suggesting the presence of some ASD features. Moreover, *Pcdh19* cKO mice showed some memory defects associated to hippocampus. These defects were more pronounced in *Pcdh19* cKO female mice, suggesting that females might be more susceptible to the loss of *Pcdh19*.

Up to now, our *Pcdh19* cKO mouse model recapitulated the main DEE9 features: the *Pcdh19* mosaicism in the brain and evidence of ASD and ID. Moreover, *Pcdh19* cKO female mice presented also some synaptic functional and morphological defects.
All these data suggest that our *Pcdh19* cKO mouse model could be a good model to investigate molecular and functional alterations implicated in DEE9 pathophysiology.

FIGURES

a

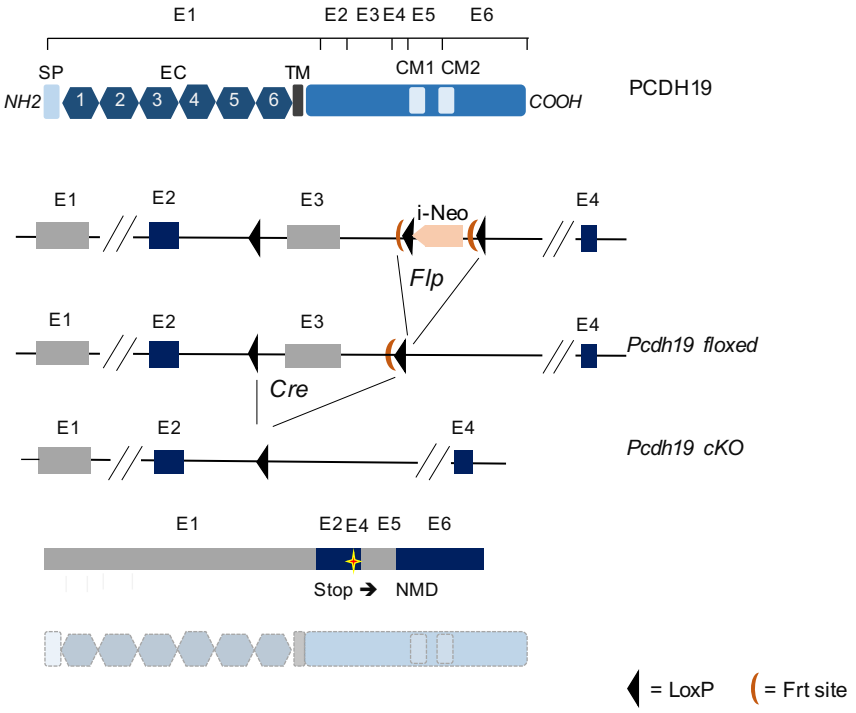
E1
E2 E3 E4 E5
E6
SP
EC
TM
CM1 CM2
NH2
1 2 3 4 5 6
COOH
PCDH19
E1
E2
E3
i-Neo
E4
Flp
Pcdh19 floxed
Cre
Pcdh19 cKO
E2 E4
Stop
NMD
= LoxP
= Frt site

b

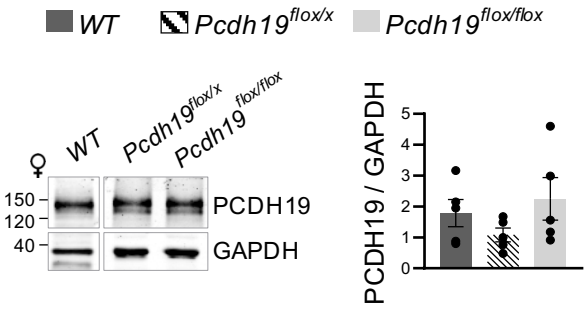
WT
Pcdh19flox/x
Pcdh19flox/flox
♀
150
120
40
PCDH19
GAPDH
PCDH19 / GAPDH
0
1
2
3
4
5

c

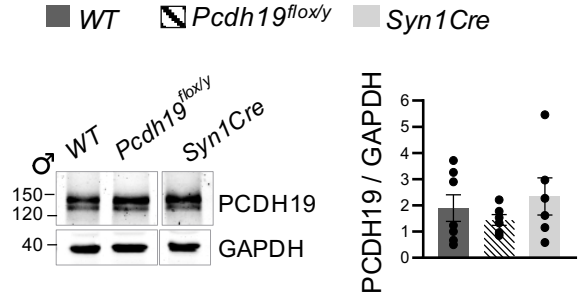
WT
Pcdh19flox/y
Syn1Cre
♂
150
120
40
PCDH19
GAPDH
PCDH19 / GAPDH
0
1
2
3
4
5
6

Figure 1. Generation of the *Pcdh19* floxed mouse. a) A Lox P site was introduced upstream exon 3, while a Neomycin cassette, flanked by Frt sites and two Lox P sites were introduced downstream exon 3. Upon Flp – mediated Frt recognition, exon 3 is flanked by two Lox P sites. The Cre - mediated excision of exon 3 causes the splicing of exon 2 into exon 4 (*Pcdh19* cKO allele) with subsequent frameshift and the generation of premature stop codons, which are expected to activate the NMD of *Pcdh19* transcript. (E = exon; SP = signal peptide; EC = extracellular cadherin domain; TM = transmembrane domain; CM = conserved motif). **b**) Representative Western blot and relative quantification showing PCDH19 expression in the hippocampus of three different groups of female mice: WT, heterozygous *Pcdh19* floxed ($Pcdh19^{fl/x}$) and homozygous *Pcdh19* floxed ($Pcdh19^{fl/fl}$). PCDH19 was normalized on GAPDH. Data are shown as means ± SEM and statistical significance was calculated by one-way ANOVA (WT = 5; n° $Pcdh19^{fl/x}$ = 5; $Pcdh19^{fl/fl}$ = 5; $p > 0.05$ n.s.). **c**) Representative Western blot and relative quantification showing PCDH19 expression in the hippocampus of three different groups of male mice: WT, hemizygous *Pcdh19* floxed ($Pcdh19^{fl/y}$) and Syn1Cre mice. PCDH19 was normalized on GAPDH. Data are shown as means ± SEM and statistical significance was calculated by one-way ANOVA (WT = 7; n° $Pcdh19^{fl/y}$ = 6; Syn1Cre = 6; $p > 0.05$ n.s.).

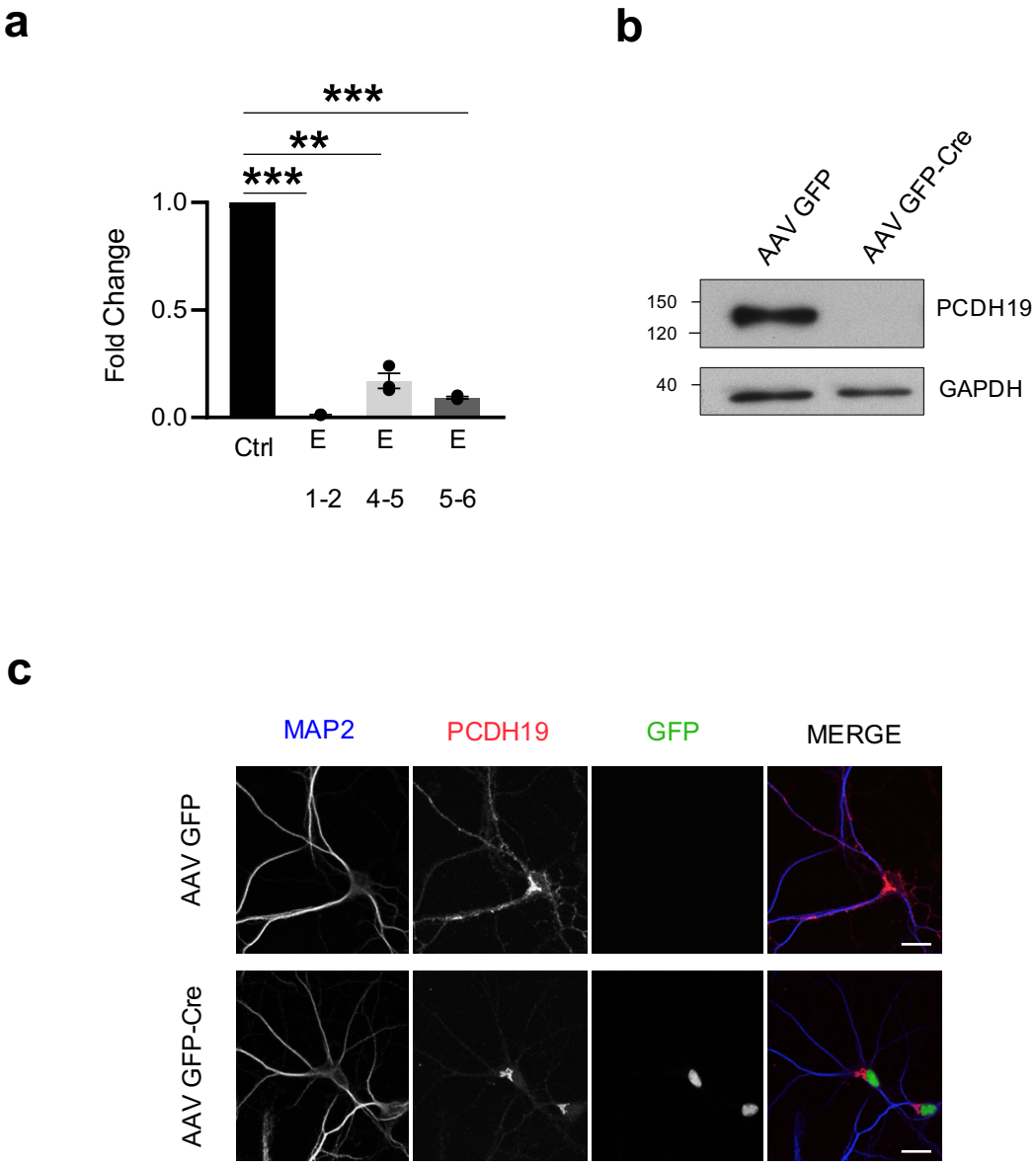
a
***
**
***
1.0
0.5
0.0
Fold Change
Ctrl
E
1-2
E
4-5
E
5-6
b
AAV GFP
AAV GFP-Cre
150
120
PCDH19
40
GAPDH
c
MAP2
PCDH19
GFP
MERGE
AAV GFP
AAV GFP-Cre

Figure 2. Exon 3 excision by Cre recombinase prevents *Pcdh19* expression in vitro. a) PCDH19 transcripts upstream (exon (E) 1 – 2) and downstream (E 4 – 5 and E 5 – 6) exon 3 were assayed with RT – PCR in neurons from P0 *Pcdh19* floxed mice infected at DIV 0 with either AAV Cre – GFP or GFP and lysated at DIV 7. PCDH19 mRNA expression was quantified with the $2^{-\Delta\Delta Ct}$ method and normalized on actin mRNA levels. Data are shown as means ± SEM. Statistical significance was calculated referring each category to the control (normalize to 1 as reference value) by two – tailed unpaired Student's t – test (n = 3; ** $p < 0.01$; *** $p < 0.001$). **b**) WB on mixed cortical and hippocampal neuronal lysates from three different P0 *Pcdh19* floxed mice (shown a representative image) infected as in a, and lysated at DIV 10. An antibody against PCDH19 C-terminus was used. GAPDH was used as loading control. **c**) ICC on mixed hippocampal and cortical neurons prepared from neonatal *Pcdh19* floxed mice (P0) of either sex. Neurons were infected at DIV 0 as in a) and stained at DIV 7 with MAP2 (Microtubule associated protein 2) and PCDH19 (antibody against PCDH19 C – terminal portion) (Scale bar: 20 μm).

a

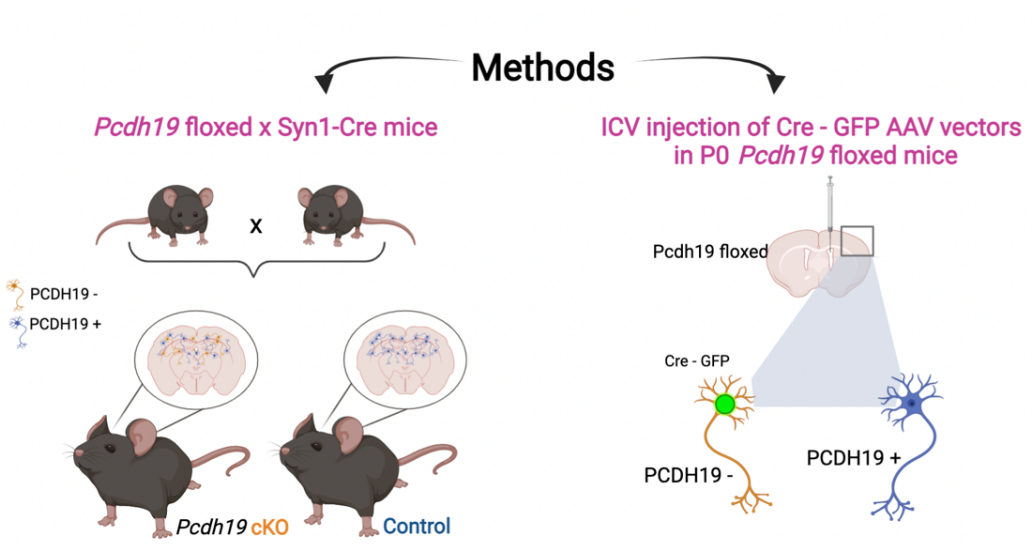
Methods
Pcdh19 floxed x Syn1-Cre mice
ICV injection of Cre - GFP AAV vectors in P0 Pcdh19 floxed mice
x
PCDH19 -
PCDH19 +
Pcdh19 cKO
Control
Pcdh19 floxed
Cre - GFP
PCDH19 -
PCDH19 +

b

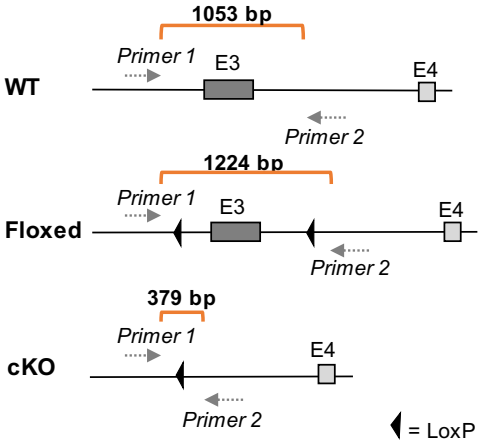
1053 bp
Primer 1
E3
E4
WT
Primer 2
1224 bp
Primer 1
E3
E4
Floxed
Primer 2
379 bp
Primer 1
E4
cKO
Primer 2
= LoxP

c

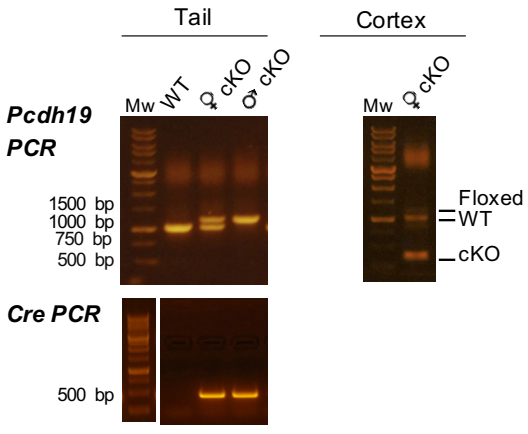
Tail
Cortex
Mw
WT
♀ cKO
♂ cKO
Mw
♀ cKO
Pcdh19 PCR
1500 bp
1000 bp
750 bp
500 bp
Floxed
WT
cKO
Cre PCR
500 bp

Figure 3. Generation of the *Pcdh19* cKO mouse model. a) Schematic representation of the two approaches used to deliver Cre. Left) Cre was delivered by crossbreeding *Pcdh19* floxed mice with rat – Synapsin 1 – Cre (Syn1 – Cre) expressing mice. 50% of the progeny expressed Cre allele (*Pcdh19* cKO); while the other 50% not (Control). Right) Cre was also delivered by ICV injecting in P0 *Pcdh19* floxed mice an AAV – Cre – GFP. This allowed to obtain two populations of neurons with known genotype (PCDH19 positive neurons, no GFP expressing cells; PCDH19 negative neurons, GFP expressing cells). **b**) Schematic representation of PCR primers annealing on *Pcdh19* WT, floxed and cKO alleles and amplification products length (base pairs, bp: WT 1053 bp, floxed 1224 bp, cKO 379 bp). **c**) Representative results of PCR-based genotyping for *Pcdh19* WT, cKO female (*Pcdh19*$^{fl/x}$ Syn1^{Cre}) and cKO male (*Pcdh19*$^{fl/y}$ Syn1Cre) mouse by using genomic DNA extracted from the tail (left panel) or from the cortex (right panel). The *Pcdh19* floxed allele (1224 bp) is converted in the cKO allele (379 bp) selectivity in the brain tissue.

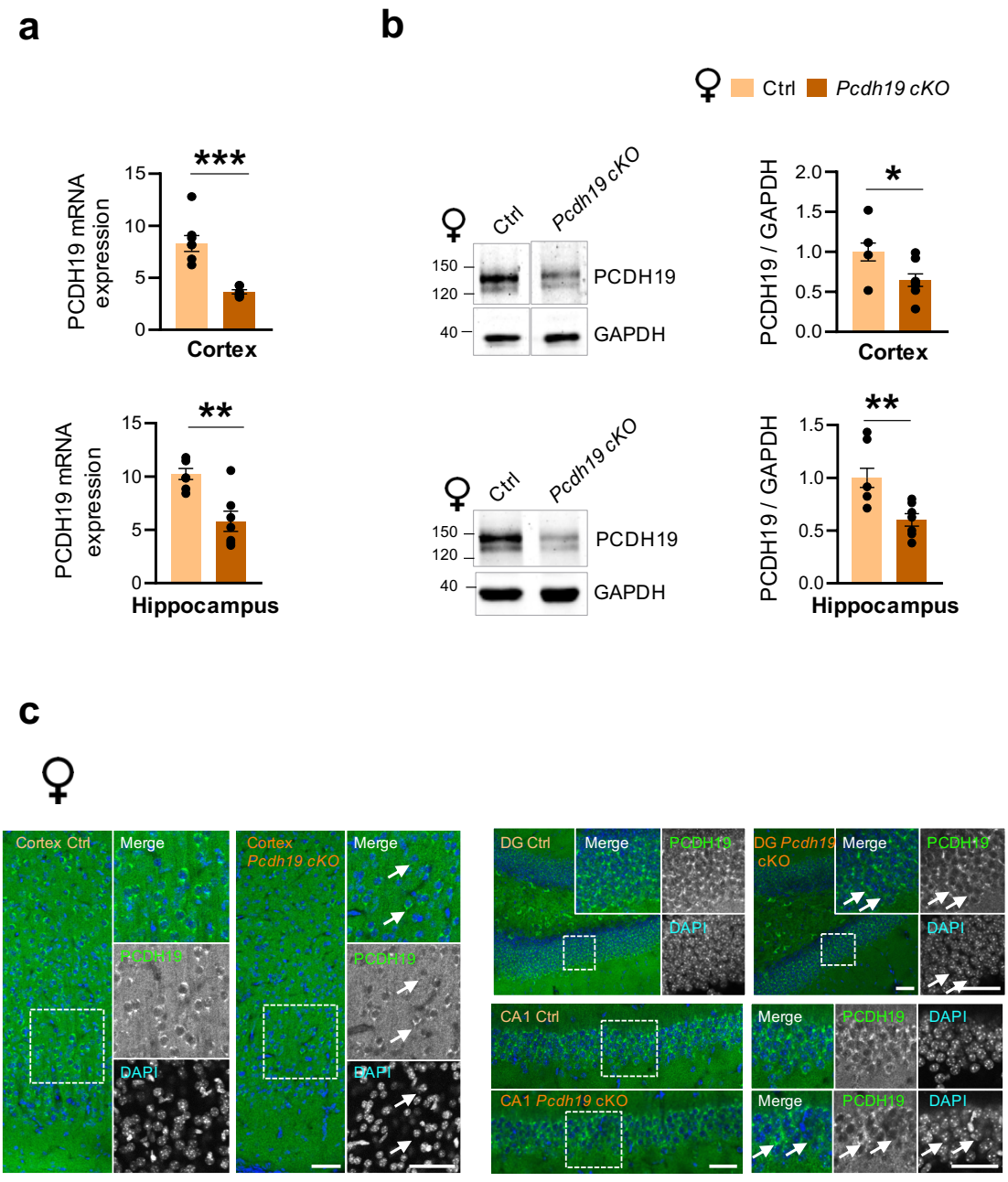
a
b
♀ Ctrl Pcdh19 cKO
PCDH19 mRNA expression
***
15
10
5
0
Cortex
**
Hippocampus
Ctrl
Pcdh19 cKO
150
120
40
PCDH19
GAPDH
PCDH19 / GAPDH
2.0
1.5
1.0
0.5
0.0
*
**
c
♀
Cortex Ctrl
Merge
PCDH19
DAPI
Cortex Pcdh19 cKO
DG Ctrl
DG Pcdh19 cKO
CA1 Ctrl
CA1 Pcdh19 cKO

Figure 4. Mosaic *Pcdh19* expression in *Pcdh19* cKO female mice. a) Quantification of *Pcdh19* expression (RT-PCR, $2^{-\Delta Ct}$ method) in cerebral cortex (upper panel) and in hippocampus (lower panel) from adult (P90) *Pcdh19* cKO female mice ($Pcdh19^{fl/x}$ / $Syn1^{Cre}$) compared to sex-matched control littermates ($Pcdh19^{fl/x}$, referred as Ctrl). *Pcdh19* mRNA expression was normalized on actin mRNA levels and data are shown as means ± SEM. Statistical significance was calculated by two-tailed unpaired Student's t-test (hippocampus: Ctrl = 7, *Pcdh19* cKO = 7; cerebral cortex: Ctrl = 8, *Pcdh19* cKO = 6; ** $p < 0.01$; *** $p < 0.001$). **b**) Representative PCDH19 Western blot and relative quantification in cerebral cortex (upper panel) and hippocampus (lower panel) from adult (P90-120) female mice. PCDH19 expression was normalized on GAPDH expression. Data are shown as means ± SEM and statistical significance was calculated by two-tailed unpaired Student's t-test (Hippocampus: Ctrl = 8, *Pcdh19* cKO = 7; Cerebral Cortex: Ctrl = 7, *Pcdh19* cKO = 8; * $p < 0.05$; ** $p < 0.01$). **c**) Immunohistochemistry (IHC) on P30 mouse coronal brain slices focusing on cerebral cortex (left) and hippocampus (right: DG, upper panel; CA1, lower panel) (scale bar: 20 µm).

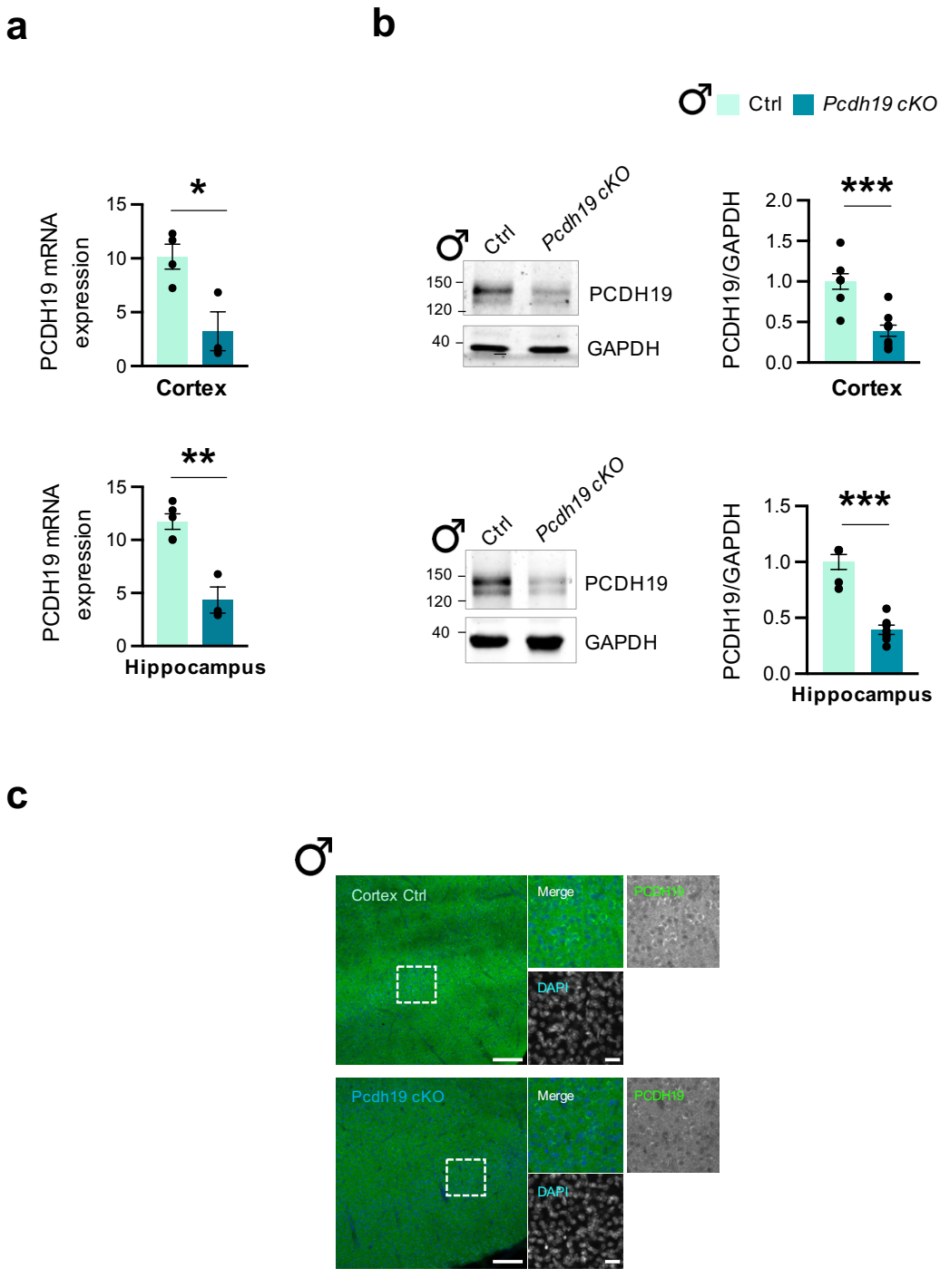
a
b
♂
Ctrl
Pcdh19 cKO
PCDH19 mRNA expression
15
10
5
0
*
Cortex
**
Hippocampus
Ctrl
Pcdh19 cKO
150
120
40
PCDH19
GAPDH
PCDH19/GAPDH
2.0
1.5
1.0
0.5
0.0
***
Cortex
Hippocampus
c
♂
Cortex Ctrl
Merge
PCDH19
DAPI
Pcdh19 cKO

Figure 5. *Pcdh19* cKO male mice are also characterized by a PCDH19 mosaic expression in their brain. a) Quantification of *Pcdh19* expression (RT-PCR, $2^{-\Delta Ct}$ method) in cerebral cortex (upper panel) and in hippocampus (lower panel) from adult (P90) *Pcdh19* cKO male mice ($Pcdh19^{fl/y}$ / $Syn1^{Cre}$) compared to sex-matched control littermates ($Pcdh19^{fl/y}$, referred as Ctrl). Pcdh19 mRNA expression was normalized on actin mRNA levels and data are shown as means ± SEM. Statistical significance was calculated by two-tailed unpaired Student's t-test (hippocampus: Ctrl = 5, *Pcdh19* cKO = 3; cerebral cortex: Ctrl = 5, *Pcdh19* cKO = 3; ** $p < 0.01$; *** $p < 0.001$) **b)** Representative PCDH19 Western blot and relative quantification in hippocampus and cerebral cortex from adult (P90-120) *Pcdh19* cKO male mice and controls (Ctrl). PCDH19 expression was normalized on GAPDH expression. Data are shown as means ± SEM and statistical significance was calculated by two-tailed unpaired Student's t-test (Hippocampus: Ctrl = 6, *Pcdh19* cKO = 7; Cerebral Cortex: Ctrl = 8, *Pcdh19* cKO = 9; *** $p < 0.001$). **c**) Immunohistochemistry (IHC) on P30 mouse brain slices (cerebral cortex is highlighted in c). Coronal brain slices were stained for PCDH19 and DAPI (scale bar: 20 µm).

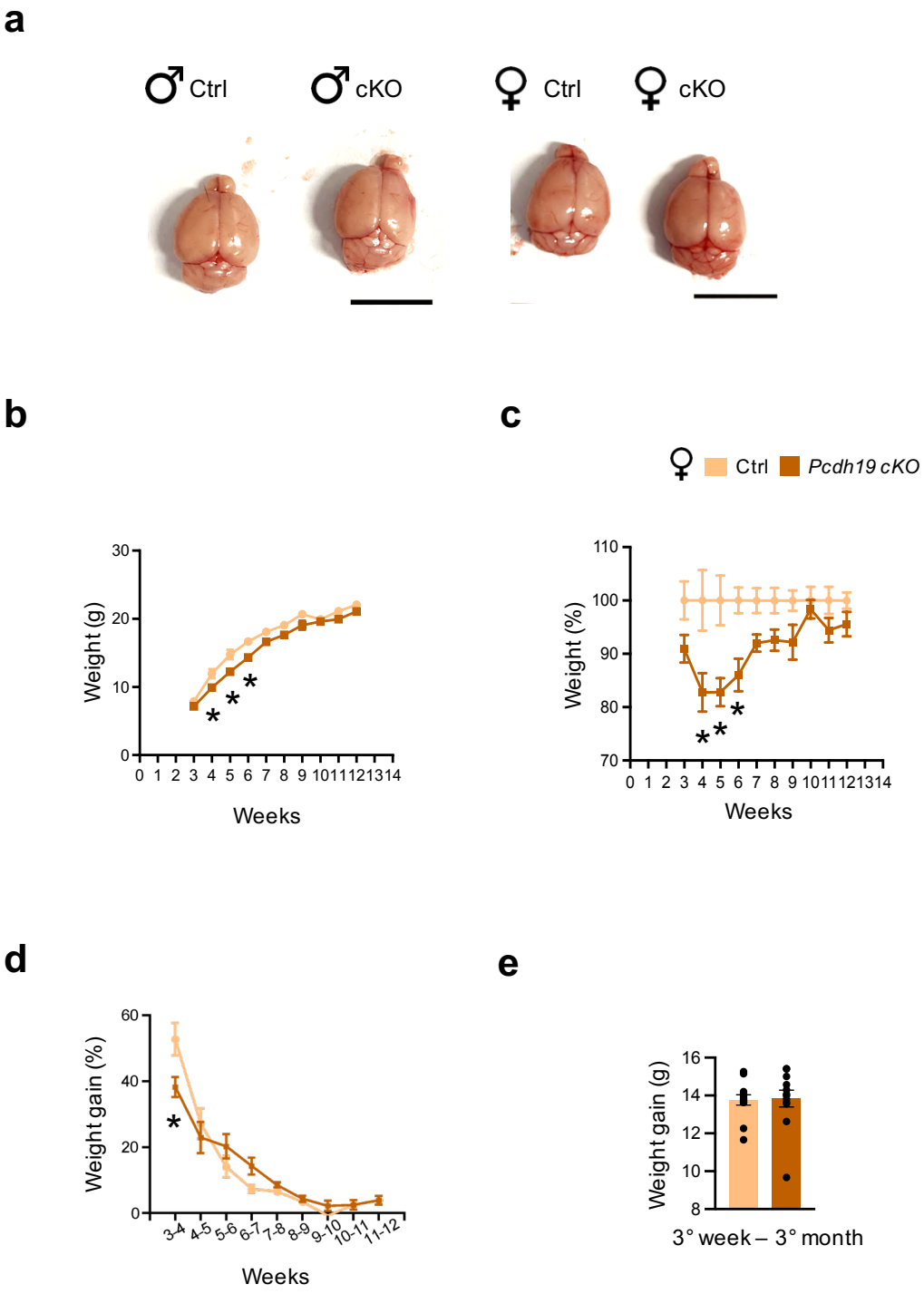
a
♂ Ctrl
♂ cKO
♀ Ctrl
♀ cKO
b
Weight (g)
Weeks
c
♀ Ctrl
Pcdh19 cKO
Weight (%)
Weeks
d
Weight gain (%)
3-4
4-5
5-6
6-7
7-8
8-9
9-10
10-11
11-12
Weeks
e
Weight gain (g)
3° week – 3° month

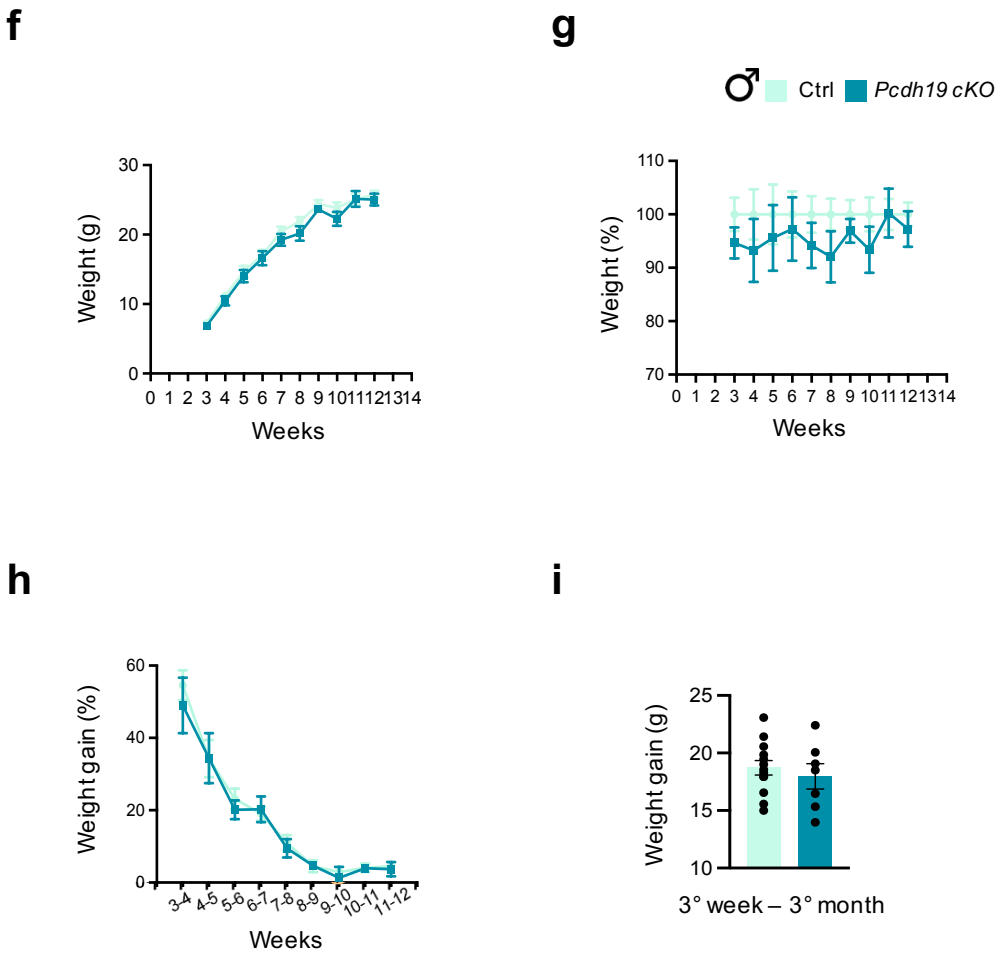
f
g
♂
Ctrl
Pcdh19 cKO
Weight (g)
Weeks
Weight (%)
Weeks
h
i
Weight gain (%)
Weeks
Weight gain (g)
3° week – 3° month

Figure 6. *Pcdh19* cKO female mice are characterized by a transient growth retardation close to the weaning time. a) Brain appearance from P90 Ctrl and *Pcdh19* cKO male and female mice. Scale bar: 1cm. **b – c**) Growth curve of *Pcdh19* cKO female mice (*Pcdh19*$^{fl/x}$ / Syn1Cre) and sex-matched controls (*Pcdh19*$^{fl/x}$ or *Pcdh19*$^{fl/fl}$) showing mice weight expressed in grams (g) or in percentage (normalized on Ctrl) (**c**). *Pcdh19* cKO mice display a reduced weight compared to controls between the 4th and 6th postnatal week (*Pcdh19* cKO: N=20; Ctrl mice: N= 22; multiple Student's t-test; * $p < 0.05$). Data are shown as means ± SEM. **d – e**) Weight gain calculated between two consecutive weeks (6d, gain expressed as percentage) or between the 3rd postnatal week and 3 months of age (6e, gain expressed in grams). *Pcdh19* cKO mice gain significantly less weight between postnatal weeks 3rd and 4th, but tended to gain more weight in subsequent weeks (5th-8th weeks) (multiple Student's t-test; * $p < 0.05$). Total weight gain (3rd week – 3rd month) is the same between *Pcdh19* cKO and control mice. Data are shown as means ± SEM (*Pcdh19* cKO =20; Ctrl mice = 22, multiple Student's t-test). **f – g**) Growth curve of *Pcdh19* cKO male mice (*Pcdh19*$^{fl/y}$ / Syn1Cre) and sex-matched controls (*Pcdh19*$^{fl/y}$ or *Pcdh19*$^{fl/fl}$) showing mice weight expressed in grams (g) or in percentage (normalized on Ctrl). Data are shown as means ± SEM (*Pcdh19* cKO: N=14; Ctrl mice: N= 22; multiple Student's t-test, $p > 0.05$, n.s). **h – i**) Weight gain calculated between two consecutive weeks (6h, gain expressed as percentage) or between the 3rd postnatal week and 3 months of age, (6i, gain expressed in grams). Data are shown as means ± SEM (*Pcdh19* cKO =14; Ctrl mice = 22; multiple Student's t-test, $p > 0.05$, n.s.).

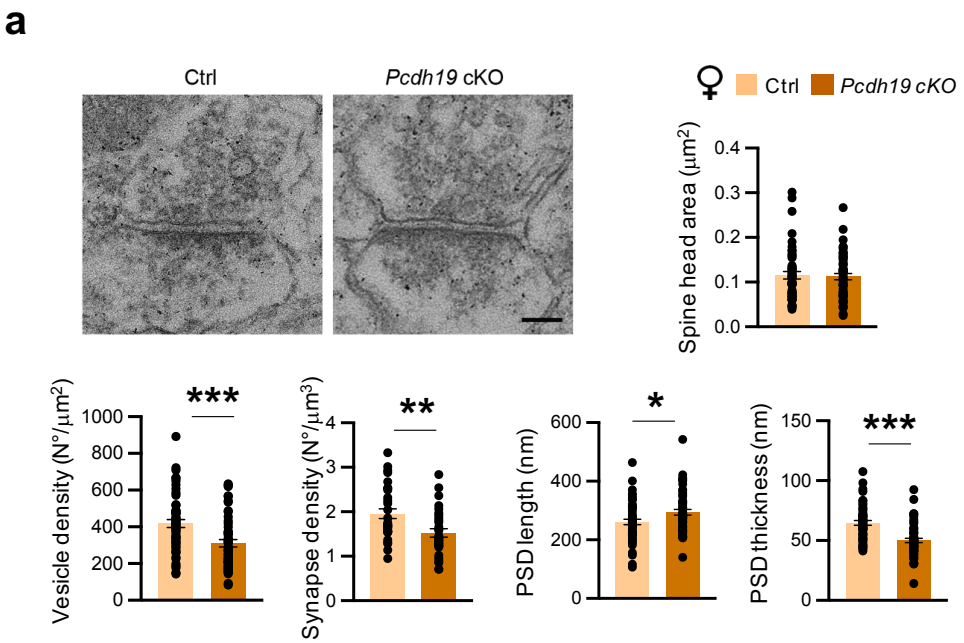
a
Ctrl
Pcdh19 cKO
♀ Ctrl Pcdh19 cKO
Spine head area (µm²)
0.4
0.3
0.2
0.1
0.0
Vesicle density (N°/µm²)
1000
800
600
400
200
0
***
Synapse density (N°/µm³)
4
3
2
1
0
**
PSD length (nm)
600
400
200
0
*
PSD thickness (nm)
150
100
50
0
***

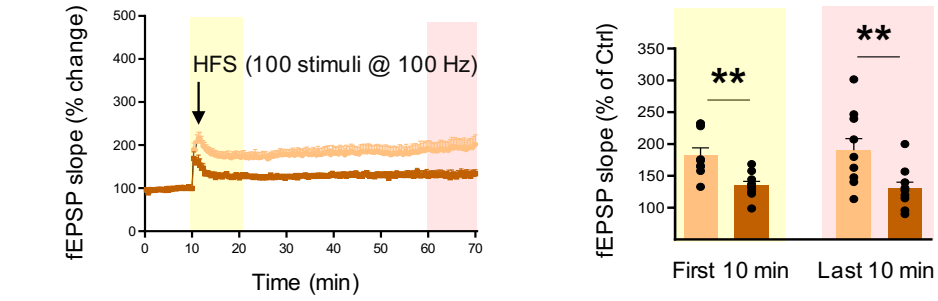
b
fEPSP slope (% change)
500
400
300
200
100
0
HFS (100 stimuli @ 100 Hz)
0
10
20
30
40
50
60
70
Time (min)
c
fEPSP slope (% of Ctrl)
350
300
250
200
150
100
**
**
First 10 min
Last 10 min

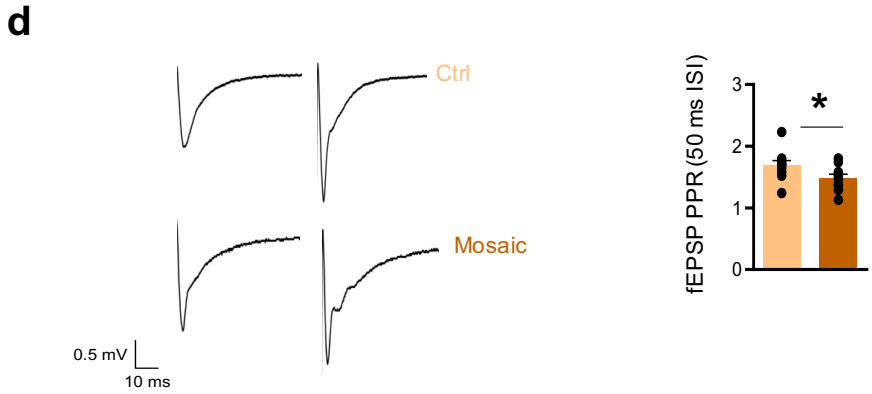
d
Ctrl
Mosaic
0.5 mV
10 ms
fEPSP PPR (50 ms ISI)
3
2
1
0
*

Figure 7. *Pcdh19* cKO females display structural and functional synaptic defects in the hippocampus. a) Electron micrographs of excitatory synapses on apical dendrites from hippocampal CA1 regions of P20 Ctrl (left) and *Pcdh19* cKO (right) female mice. The data were obtained from more than 50 synapses (Ctrl = 2; *Pcdh19* cKO = 2). Scale bar, 100 nm. Analyses confirm no alteration in spine head dimension, but a reduced vesicle and synaptic density. Moreover, *Pcdh19* cKO mice show alterations both in PSD length and thickness. For the stereological evaluation of synaptic density, a total surface of 615.00 μm^2 per genotype was analysed. All the data are reported as mean ± SEM (Mann-Whitney non parametric test or Student's *t*-test, * $p < 0.05$; ** $p < 0.01$; *** $p < 0.001$). **b – c**) LTP was recorded in hippocampal slices from P90 *Pcdh19* cKO female mice and control littermates. fEPSPs were recorded from CA1 in response to Schaffer collaterals stimulation. *Pcdh19* cKO female mice display a significantly reduced LTP compared to controls both in the first 10 minutes (**c, left**) and in the last 10 minutes (**c, right**). Data are shown as means ± SEM (Ctrl = 4; *Pcdh19* cKO = 5; two-tailed unpaired Student's t-test, ** $p < 0.01$). **d**) Presynaptic short-term plasticity was assessed by paired-pulse ratio (PPR) with an interstimulus interval of 50 ms. PPR is reduced in P90 *Pcdh19* cKO female mice compared to controls, thus suggesting a presynaptic defect upon mosaic depletion of PCDH19. Data are shown as means ± SEM (Ctrl = 4; *Pcdh19* cKO = 5; two-tailed unpaired Student's t-test, * $p < 0.05$; the stimulus artifact has been removed from the traces).

a

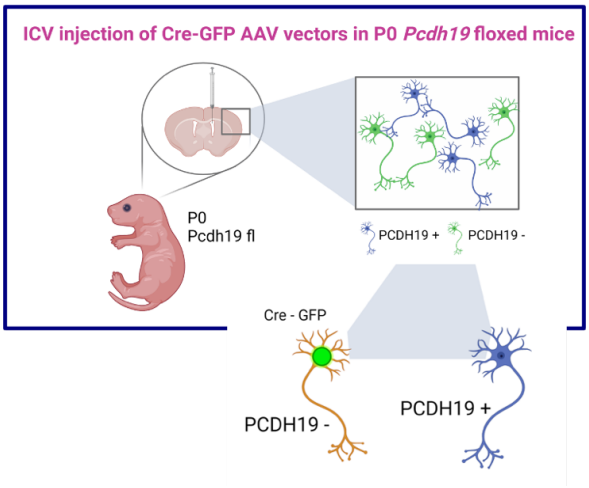
ICV injection of Cre-GFP AAV vectors in P0 *Pcdh19* floxed mice
P0
Pcdh19 fl
PCDH19 +
PCDH19 -
Cre - GFP
PCDH19 -
PCDH19 +

b

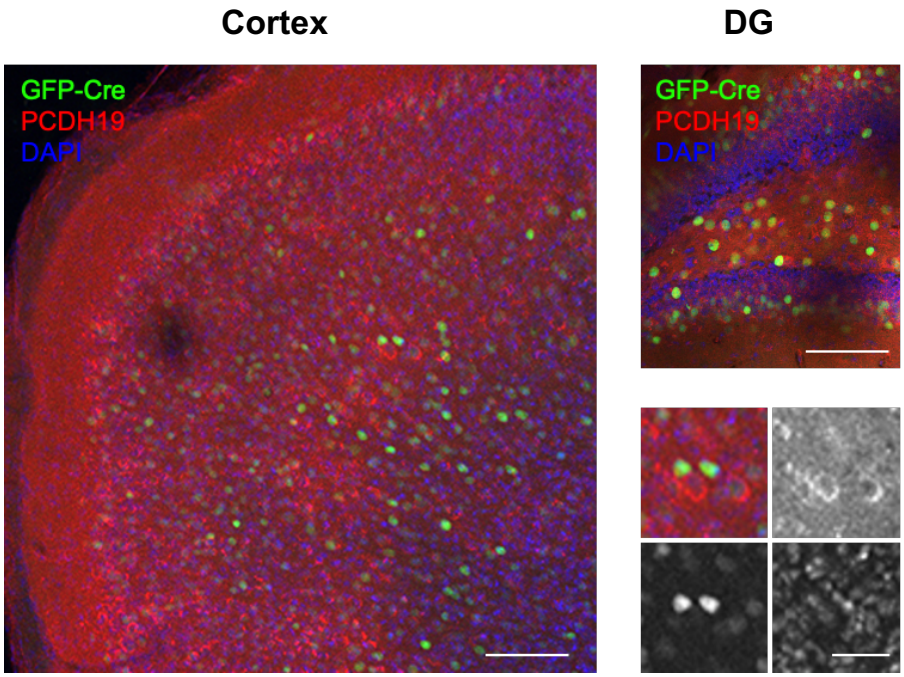
Cortex
DG
GFP-Cre
PCDH19
DAPI
GFP-Cre
PCDH19
DAPI

c

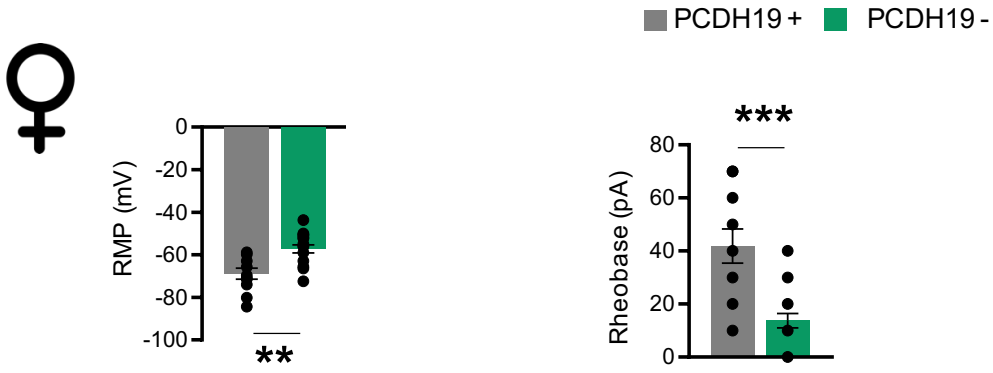
PCDH19 +
PCDH19 -
RMP (mV)
0
-20
-40
-60
-80
-100
**
Rheobase (pA)
***
80
60
40
20
0

d

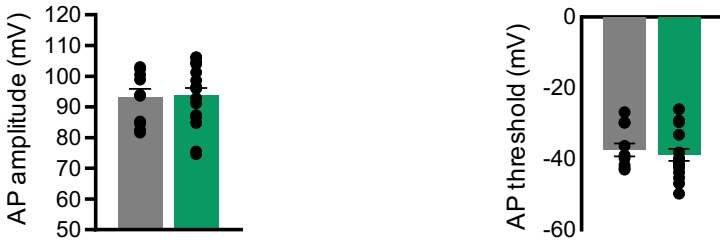
AP amplitude (mV)
120
110
100
90
80
70
60
50
AP threshold (mV)
0
-20
-40
-60

e

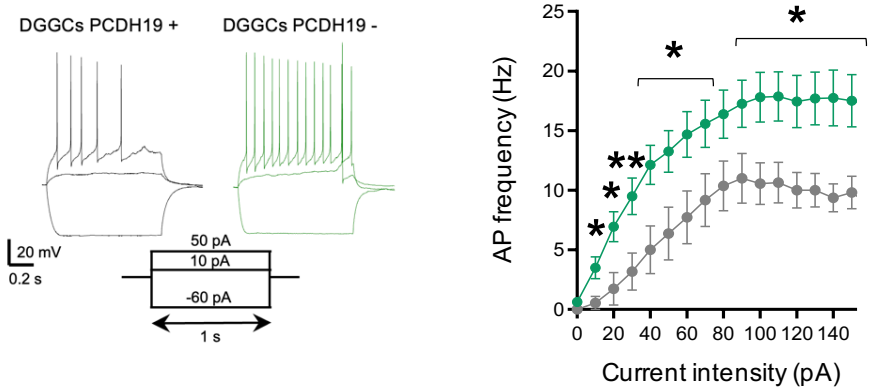
DGGCs PCDH19 +
DGGCs PCDH19 -
20 mV
0.2 s
50 pA
10 pA
-60 pA
1 s
AP frequency (Hz)
25
20
15
10
5
0
0 20 40 60 80 100 120 140
Current intensity (pA)
*
**
*
*
*

f

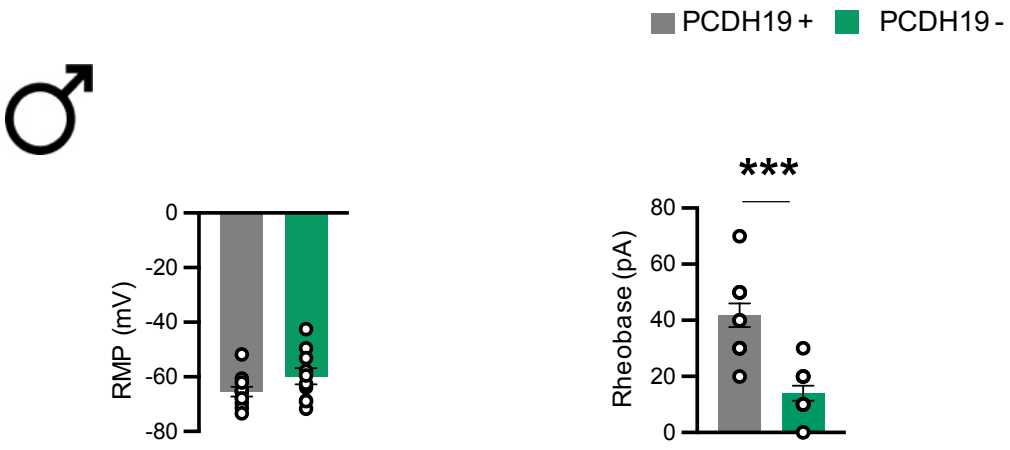
PCDH19 +
PCDH19 -
♂
RMP (mV)
0
-20
-40
-60
-80
***
Rheobase (pA)
80
60
40
20
0

g

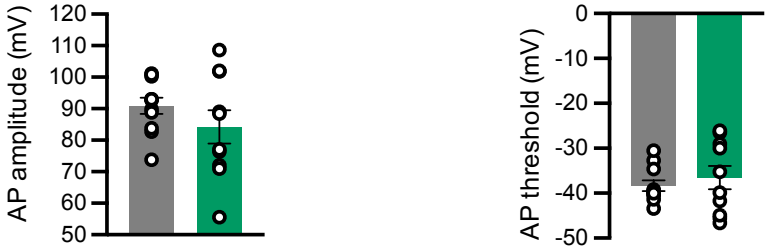
AP amplitude (mV)
120
110
100
90
80
70
60
50
AP threshold (mV)
0
-10
-20
-30
-40
-50

h

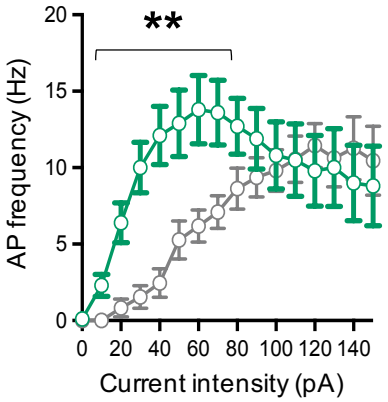
**
AP frequency (Hz)
20
15
10
5
0
0 20 40 60 80 100 120 140
Current intensity (pA)

Figure 8. PCDH19 negative DGGCs show an aberrant excitability compared to PCDH19 retaining neurons. a) Schematic representation of the ICV injection model in a P0 *Pcdh19* floxed mouse. **b**) Evaluation of AAV – Cre -GFP diffusion in cerebral cortex (left) and in DG (right). ICC confirmed the absence of PCDH19 expression in Cre-GFP expressing neurons. **c – e**) Firing properties were evaluated in adult *Pcdh19* floxed female mice (P55 – P90). Data are shown as means ± SEM (*Pcdh19* floxed = 3). **c**) PCDH19 negative DGGCs show a depolarized resting membrane potential (RMP) and needed less depolarizing current (Rheobase) to fire the first AP, respect to PCDH19 positive DGGCs. **d**) PCDH19 negative DGGCs show no differences in AP amplitude and in AP threshold compared to PCDH19 positive DGGCs. **e**) Representative traces of AP evoked by 10 and 50 pA of injected current in current-clamp mode (left). Analysis of AP frequency highlights hyperexcitability of PCDH19 negative DGGCs with respect to PCDH19 positive DGGCs (right). Data are shown as means ± SEM. **f - h**) Firing properties evaluated in adult *Pcdh19* floxed male mice (P55 – P90). Data are shown as means ± SEM (*Pcdh19* floxed = 5). **f**) PCDH19 negative DGGCs show no differences in RMP, but a reduced rheobase compared to PCDH19 positive DGGCs. **g**) No differences in AP amplitude and threshold are noticed in PCDH19 negative DGGCs compared to PCDH19 positive ones. **h**) PCDH19 negative DGGCs show an hyperexcitable phenotype until 70pA, after that, they behave like PCDH19 positive DGGCs.

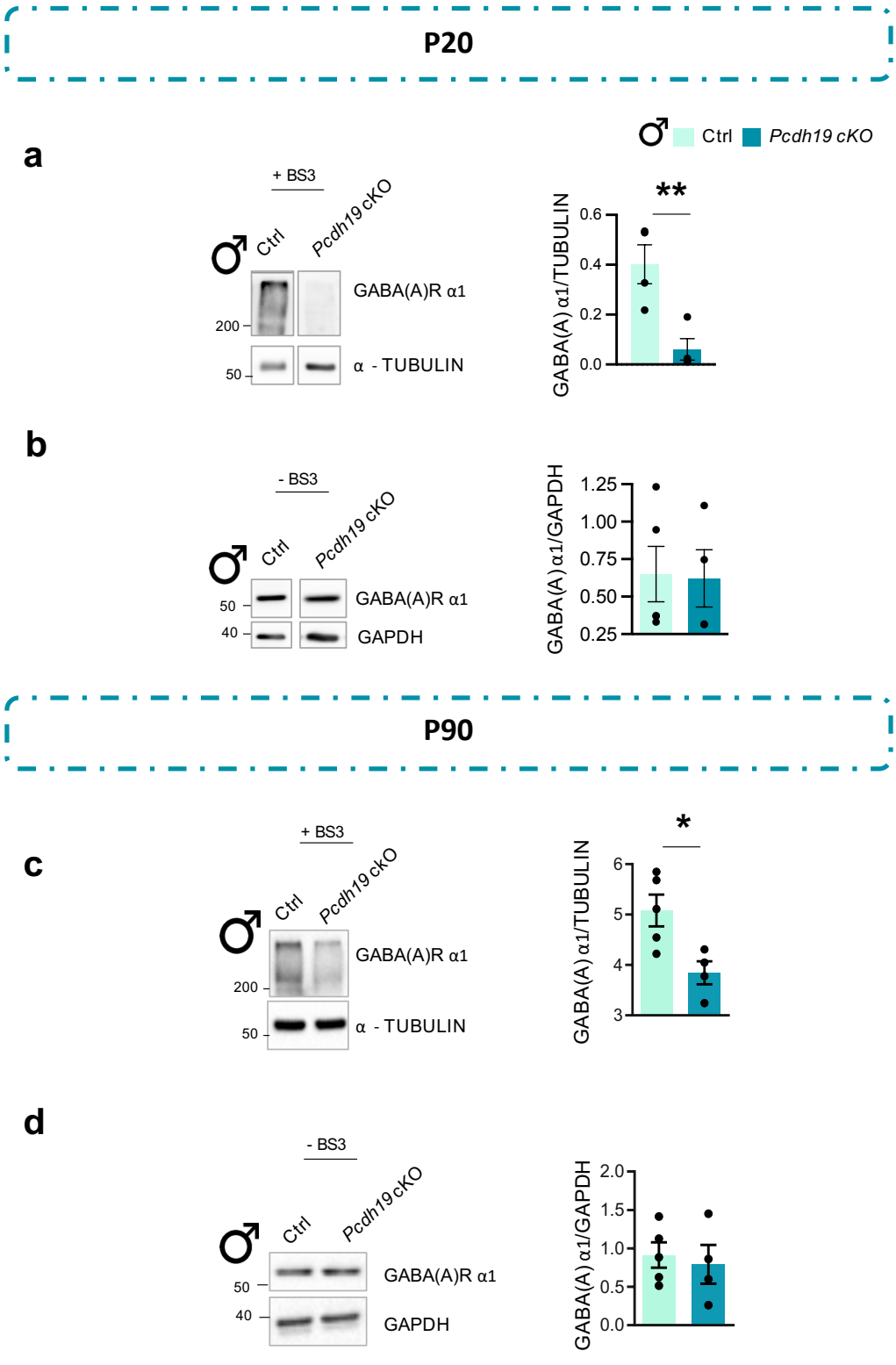
P20
a
♂ Ctrl Pcdh19 cKO
+ BS3
♂ Ctrl Pcdh19cKO
GABA(A)R α1
200
50
α - TUBULIN
**
GABA(A) α1/TUBULIN
0.6
0.4
0.2
0.0
b
- BS3
♂ Ctrl Pcdh19cKO
50
40
GABA(A)R α1
GAPDH
GABA(A) α1/GAPDH
1.25
1.00
0.75
0.50
0.25
P90
c
+ BS3
♂ Ctrl Pcdh19cKO
GABA(A)R α1
200
50
α - TUBULIN
*
GABA(A) α1/TUBULIN
6
5
4
3
d
- BS3
♂ Ctrl Pcdh19cKO
50
40
GABA(A)R α1
GAPDH
GABA(A) α1/GAPDH
2.0
1.5
1.0
0.5
0.0

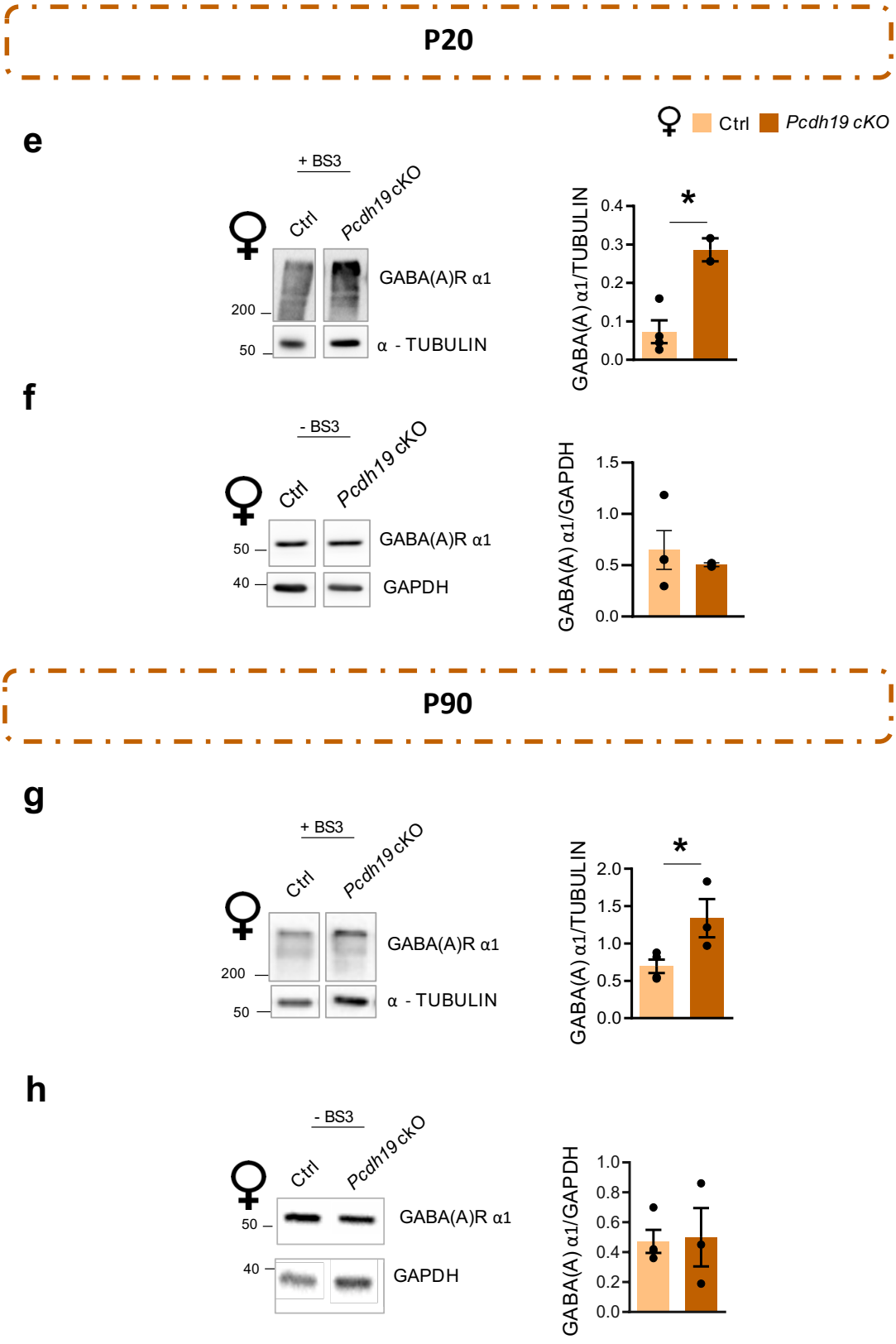
P20
Ctrl
Pcdh19 cKO
e
+ BS3
Ctrl
Pcdh19cKO
GABA(A)R α1
200
50
α - TUBULIN
GABA(A) α1/TUBULIN
0.4
0.3
0.2
0.1
0.0
*
f
- BS3
Ctrl
Pcdh19 cKO
50
40
GABA(A)R α1
GAPDH
GABA(A) α1/GAPDH
1.5
1.0
0.5
0.0
P90
g
+ BS3
Ctrl
Pcdh19cKO
200
50
GABA(A)R α1
α - TUBULIN
GABA(A) α1/TUBULIN
2.0
1.5
1.0
0.5
0.0
*
h
- BS3
Ctrl
Pcdh19cKO
50
40
GABA(A)R α1
GAPDH
GABA(A) α1/GAPDH
1.0
0.8
0.6
0.4
0.2
0.0

Figure 9. *Pcdh19* cKO mice display an aberrant surface expression of $GABA_ARs$ α1 subunit. a – b) By BS3 assay, P20 *Pcdh19* cKO male mice display a reduced surface expression of the $GABA_ARs$ α1 subunit compared to control mice (a), with an unaltered total pool (b). Data are shown as means ± SEM (Ctrl = 4; *Pcdh19* cKO = 4; 2 slices/genotype; two-tailed unpaired Student's t-test, * $p < 0.05$). **c – d**) A reduced surface expression (c) and unchanged total pool (d) of $GABA_ARs$ α1 in *Pcdh19* cKO male mice is also confirmed at P90. Data are shown as means ± SEM (Ctrl = 5; *Pcdh19* cKO = 4; 4 slices/genotype; two-tailed unpaired Student's t-test, * $p < 0.05$). **e – f**) P20 *Pcdh19* cKO female mice are characterized by an increased surface expression of $GABA_ARs$ α1 (e) and by an unaltered total pool (f) compared to their control littermates. Data are shown as means ± SEM (Ctrl = 4; *Pcdh19* cKO = 3; 2 slices/genotype; two-tailed unpaired Student's t-test, * $p < 0.05$). **g – h**) $GABA_ARs$ α1 aberrant expression (g) is also confirmed in P90 *Pcdh19* cKO female. mice, without changing in the amount of total pool (h). Data are shown as means ± SEM (Ctrl = 4; *Pcdh19* cKO = 3; 4 slices/genotype; two-tailed unpaired Student's t-test, * $p < 0.05$).

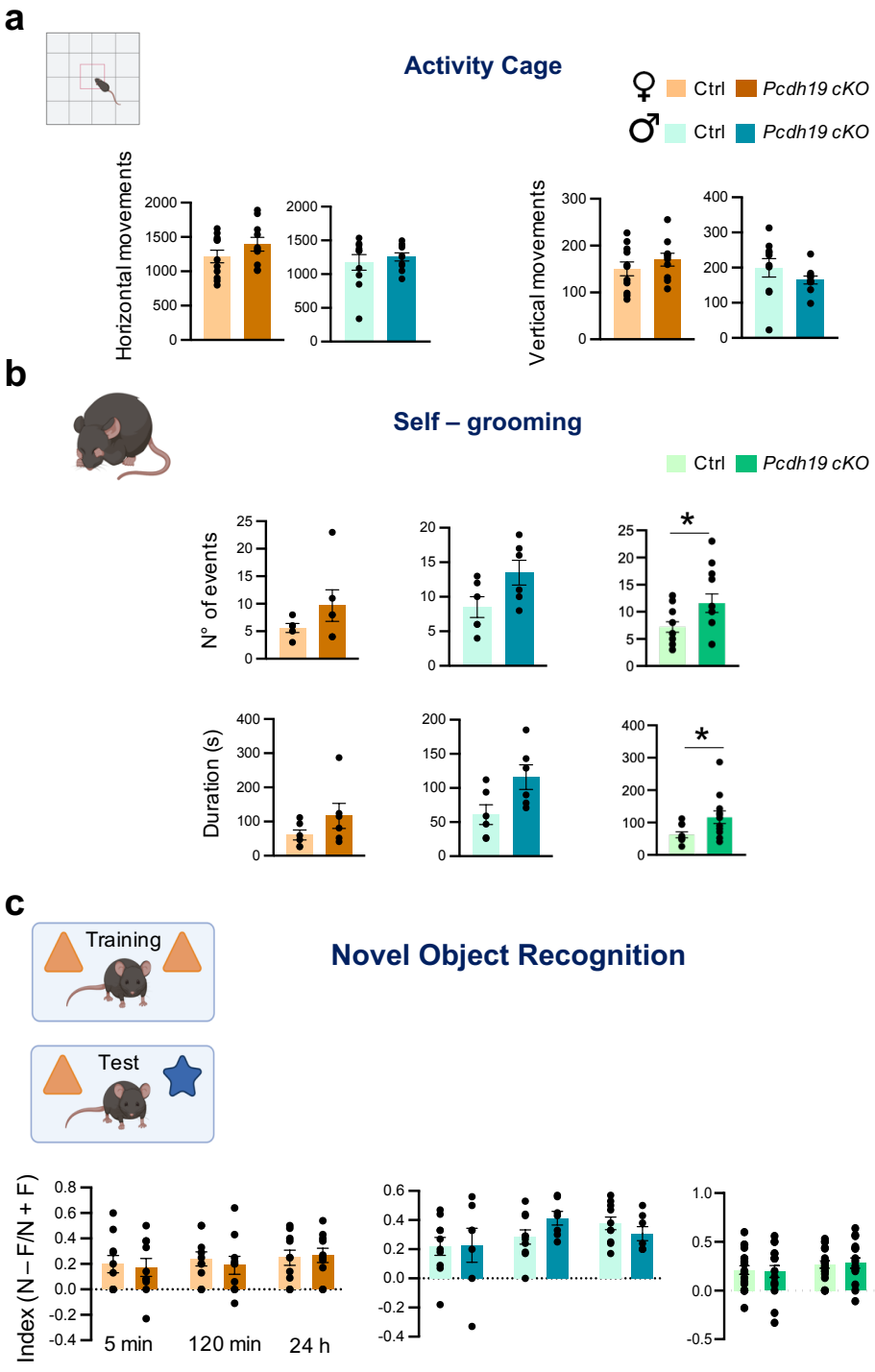
a
Activity Cage
♀ Ctrl Pcdh19 cKO
♂ Ctrl Pcdh19 cKO
Horizontal movements
Vertical movements
b
Self – grooming
Ctrl Pcdh19 cKO
N° of events
Duration (s)
*
*
c
Training
Test
Novel Object Recognition
Index (N – F/N + F)
5 min
120 min
24 h

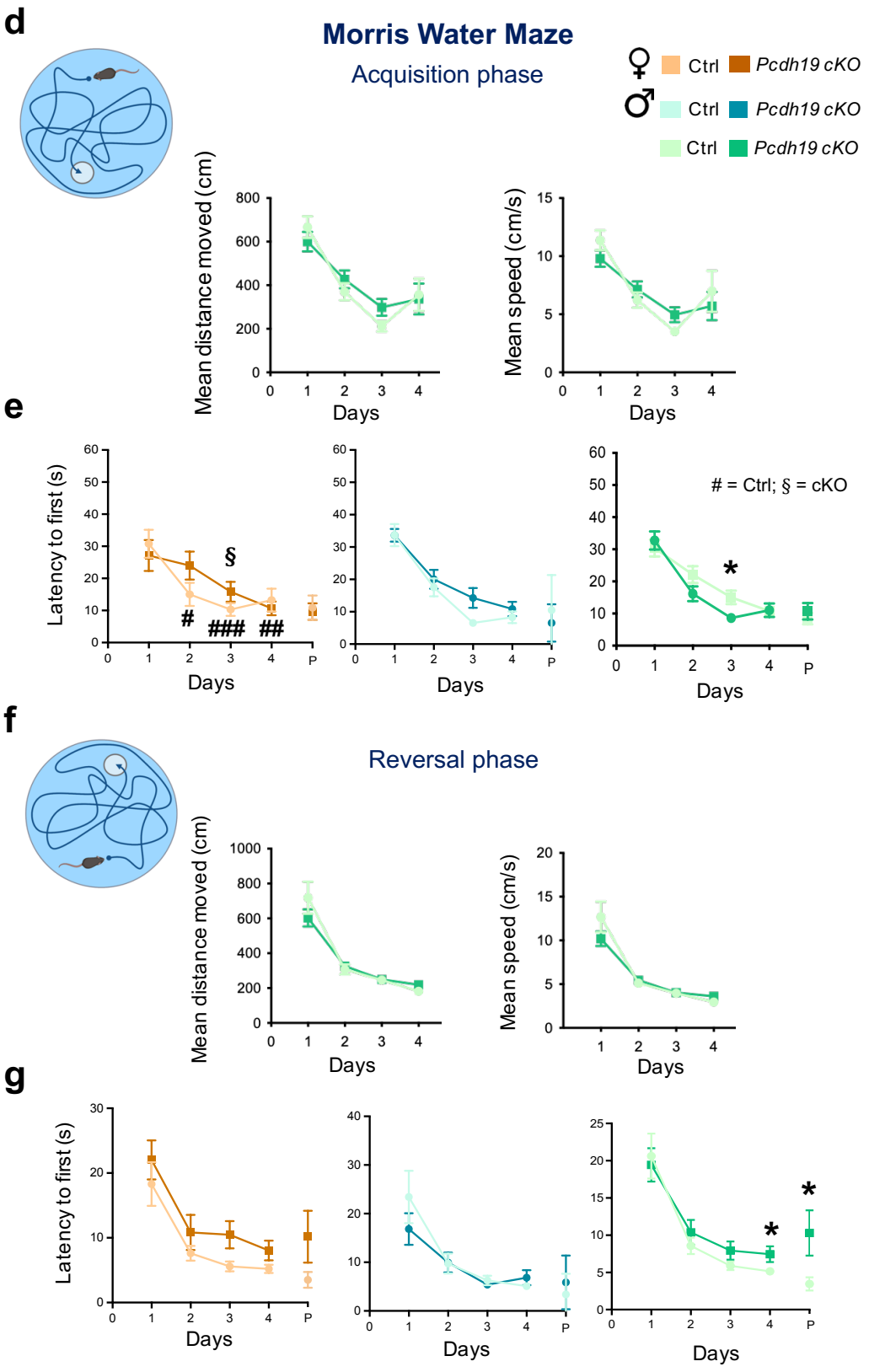
d
Morris Water Maze
Acquisition phase
♀ Ctrl Pcdh19 cKO
♂ Ctrl Pcdh19 cKO
Ctrl Pcdh19 cKO
Mean distance moved (cm)
Mean speed (cm/s)
Days
e
Latency to first (s)
§
#
###
##
= Ctrl; § = cKO
*
Days
f
Reversal phase
Mean distance moved (cm)
Mean speed (cm/s)
Days
g
Latency to first (s)
*
*
Days

h

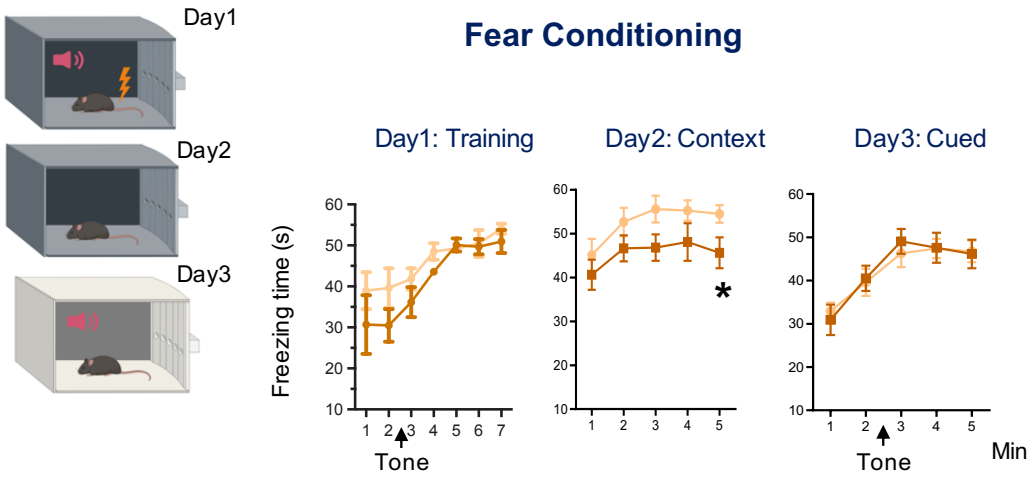
Day1
Day2
Day3
Fear Conditioning
Day1: Training
Day2: Context
Day3: Cued
Freezing time (s)
Tone
Tone
Min
*

i

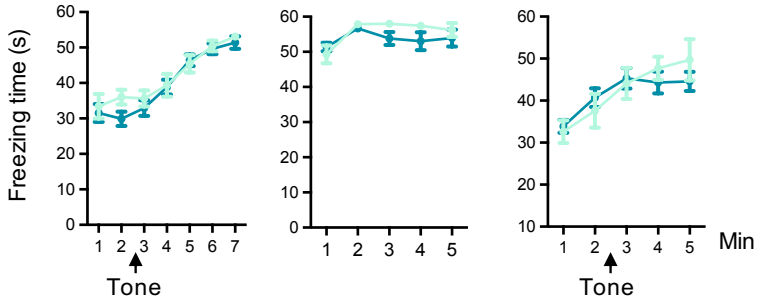
Freezing time (s)
Tone
Tone
Min

Figure 10. *Pcdh19* cKO mice display ASD and ID behavioral deficits. a) The spontaneous motor activity of mice is evaluated through activity cage test. The number of horizontal and vertical movements is calculated in *Pcdh19* cKO mice and control littermates (Ctrl). Data are shown as means ± SEM. (Ctrl female = 11; *Pcdh19* cKO female = 10; Ctrl male = 10; *Pcdh19* cKO male = 10; unpaired two-tailed Student's t-test, $p > 0.05$ n.s). **b**) *Pcdh19* cKO mice display an increase in the number and in the duration of self-grooming events compared to controls (Ctrl female = 6; *Pcdh19* cKO female = 6; Ctrl male = 6; *Pcdh19* cKO male = 6; two-tailed unpaired Student's t-test,* $p < 0.05$). **c**) *Pcdh19* cKO mice show no impairment in recognition memory as assayed by novel object recognition test (NOR). The discrimination index ((N-F)/(N+F), N= novel object; F = familiar object) is comparable between *Pcdh19* cKO mice and control littermates at all retention intervals (5 min, 120min, 24h). Data are shown as means ± SEM. (Ctrl female = 10; *Pcdh19* cKO female = 10; Ctrl male = 10; *Pcdh19* cKO male = 7; two-tailed unpaired Student's t-test $p > 0.05$ n.s.) **d – e – f – g**) Spatial memory is tested in the Morris Water Maze test. **d**) Mean distance moved and mean speed parameters are evaluated in the acquisition phase between *Pcdh19* cKO and control mice during the training. No differences are noticed between the two groups (two-way ANOVA, $p > 0.05$, n.s). **e**) No significant differences are observed during the acquisition between control and *Pcdh19* cKO mice of either sexes when analyzed separately (multiple t-test, $p > 0.05$, n.s.). However, *Pcdh19* cKO female mice take significantly less time to reach the platform at day 4 of the acquisition phase compared to day 1 (one-way ANOVA, § $p < 0.05$), whereas control mice take significantly less time to reach the platform as early as day 2 of training (one-way ANOVA, # $p < 0.05$). If analyzed together, *Pcdh19* cKO male and female mice take significant more time to reach the platform at day 3 of the acquisition phase (multiple t-test, *$p < 0.05$). No differences are observed in probe test (P). Data are shown as means ± SEM. (Ctrl female = 10; *Pcdh19* cKO female = 10; Ctrl male = 10; *Pcdh19* cKO male = 10; two-tailed unpaired Student's t-test $p > 0.05$ n.s.) **f**) Mean distance moved and mean speed parameters are also evaluated for the reversal phase between *Pcdh19* cKO and control mice during the four – day training. No differences are noticed between the two groups (two-way ANOVA, $p > 0.05$, n.s). **g**) During the reversal phase, mice are tested for memory plasticity. No statistically significant differences are noticed between the two groups (*Pcdh19* cKO and Ctrl), when they are analyzed separately (multiple t-test, $p > 0.05$, n.s). However, when female and male mice are analyzed together, *Pcdh19* cKO mice take significantly more time to find the platform at day 4 compared to controls. Indeed, in the probe test, *Pcdh19* cKO mice require more time to reach the platform zone compared to Ctrl mice. Data are shown as means ± SEM. (Ctrl female = 10; *Pcdh19* cKO female = 10; Ctrl male = 10; *Pcdh19* cKO male = 10; multiple t-test, *$p < 0.05$; two-tailed unpaired Student's t-test, * $p < 0.05$). **h – i**) Associative learning is tested in the fear-conditioning test. **h**) *Pcdh19* cKO female mice freezing time is significantly reduced compared to control during the context test (middle panel), while there are no differences groups during the conditioning phase (left panel) and cued test (right panel). Data are shown as means ± SEM (Ctrl = 10; *Pcdh19* cKO = 10; two-way ANOVA, * $p < 0.05$). **i**) *Pcdh19* cKO male mice

don’t show any statistically significant difference in the conditioning phase (left panel), in the context phase (middle panel) and in the cued phase (right panel) compared to control mice. Data are shown as means ± SEM (Ctrl = 10; *Pcdh19* cKO = 10; two-way ANOVA, $p > 0.05$, n.s.)

DISCUSSION AND CONCLUSIONS

Mutations in the X – linked gene *PCDH19* cause a severe neurological disorder, called DEE9 (OMIM #300088) (*Dibbens et al., 2008; Depienne et al., 2009*).
DEE9 patients displayed epilepsy and ASD, ID and neuropsychiatric alterations with heterogeneity in the severity of the symptoms (*Smith et al., 2018; Kolc et al., 2020*).
Up to now, the pathophysiological mechanisms behind DEE9 are still unknown.

To try to fill this gap, we generated a new *Pcdh19* cKO mouse model for DEE9 by exploiting the Cre – Lox P system.
Cre was delivered either by crossbreeding *Pcdh19* floxed mice with Syn1 – Cre expressing mice or by ICV injecting AAV Cre – GFP into P0 *Pcdh19* floxed mice. In both cases, we obtained a *Pcdh19* cellular mosaicism in the brain.
The cellular mosaicism is an important feature for DEE9 aetiology, since it is thought to be the trigger of the symptomatology and it is at the base of the pathophysiological hypothesis of cellular interference (*Dibbens et al., 2008*).

Interestingly, not only heterozygous female mice, as expected, but also hemizygous male mice were mosaic for *Pcdh19* expression. This allowed us to conduct some analyses on both sexes, to evaluate if also gender, in addition to PCDH19 mosaic expression, might play a role in in DEE9.

1. Pcdh19 cKO MICE DISPLAY SIGNS OF HYPEREXCITABILITY

In accordance with other DEE9 constitutive mouse models (*Pederick et al., 2016; Hoshina et al., 2021*), our *Pcdh19* cKO mouse model didn't display spontaneous seizures. However, a feature of *Pcdh19* cKO female mice captured our attention.

Pcdh19 cKO female mice were characterized by a transient growth delay during adolescence (P28 – P42), which was recovered in the following weeks (P35 – P56). This delayed growth was not statistically significant in *Pcdh19* cKO male mice, although this might have been masked by their stronger inter-variability.

Even though we do not know the reason of this phenotype, it is interesting to note that different Dravet – syndrome constitutive mouse models showed a similar growth retardation in concomitance with seizure onset (*Ricobaraza et al., 2019; Almog et al.,2019; Mijanovic et al., 2021*).

Pcdh19 cKO mice might, therefore, display subclinical signs of hyperexcitability and might be more susceptible to seizure induction.

Future experiments will test this hypothesis and evaluate seizures threshold in *Pcdh19* cKO and control mice in response to hyperthermia, since patients' epilepsy is fever – sensitive (*Marini et al., 2012, Smith et al., 2018),* during this time window.

Indeed, adolescence is a key phase for mice, allowing the transition from childhood to adulthood (P22 – P60, *Brust et al., 2015*). During this phase, different hormonal and behavioral changes happen, associated also with alterations in brain structures. Indeed, remodeling of cortical and limbic circuits, where *Pcdh19* is highly expressed (*Brust et al., 2015, Pederick et al., 2016; Schaarschch and Hertel, 2018),* occurs.

Notably, at cellular level, we observed signs of hyperexcitability in *Pcdh19* floxed mice ICV injected at P0 with an AAV associated with Cre fused to GFP. Indeed, we discovered that PCDH19 negative neurons within the mosaic brain, showed an altered excitability compared to PCDH19 positive neurons.
More precisely, PCDH19 negative DGGCs presented increased excitability (reduced rheobase and increased AP firing frequency) compared to neighboring PCDH19 positive ones.
These data were in line with previous *in vitro* study in primary hippocampal neurons in which PCDH19 was downregulated by shRNA expression and could be ascribed to a reduced surface expression of $GABA_A$Rs subunits and a reduced GABAergic tone (*Bassani et al., 2018; Serratto et al., 2020*).

One peculiarity of the hippocampal DG is that is one of few brain areas where adult neurogenesis occurs. Indeed, new immature neurons are generated and functionally inserted into the DG circuitry (*Jonas and Lisman, 2014*).
Interestingly, immature DGGCs, that represent the ~10% of the total DG population, present a higher excitability compared to mature DGGCs (*Rojas and Kreutz, 2016*).
So, we could speculate that PCDH19 negative DGGCs resemble immature DGGCs in their firing properties and alteration in the ratio between mature and immature DGGCs could impact hippocampal correct circuit functioning.
It is interesting to notice that an immature DG (iDG) is at the base of different neuropsychiatric disorder (*Hagihara et al.,2013)*, like schizophrenia, which is one of the late – onset symptoms of DEE9 (*Vlaskamp et al.,2018*).
Indeed, it was demonstrated, in different animal models for schizophrenia, the presence of iDG features (*Hagihara et al.,2013)*. As further validation, postmortem tissues from schizophrenic and bipolar disorder patients presented molecular markers which were representative for an iDG (*Hagihara et al.,2013*).
Future experiments are meant to better investigate the impact of PCDH19 negative neurons on hippocampal circuitry.

2. *PCDH19* cKO MICE DISPLAY SYNAPTIC DEFECTS ASSOCIATED WITH ASD AND ID – LIKE PHENOTYPES

Brain circuits formation is shaped by the highly – specialized neuronal morphology and these circuits are highly dynamics and plastic, since they respond to activity – dependent mechanism and to environmental stimuli (*Forrest et al., 2018*).
Dendritic spines are highly responsive to neuronal activity. Therefore, we evaluated synaptic plasticity and morphology in *Pcdh19* cKO and control female mice.

Pcdh19 cKO female mice were characterized by an overall reduction in the number of excitatory synapses. This could be hypothesized to be a compensatory mechanism to face PCDH19 negative neurons hyperexcitability and so to promote a balanced circuit, as it has been proposed for immature DG neurons, whose hyperexcitability is kept under control by reducing their synaptic inputs (*Dieni et al., 2016*).

Moreover*, Pcdh19* cKO female mice displayed a longer and a thinner PSD compared to control mice. PSD is a protein supercomplex associated to the glutamatergic post – synaptic membrane. Among the PSD proteins, there are the NMDARs and the α-amino-3-hydroxy-5-methyl-4-isoxazolepropionate (AMPA) receptors (AMPARs), which are fundamental for learning and memory processes. Thus, PSD properties correlates with synaptic strength (*Borczyk et al., 2021*).
Coherently with PSD defects, *Pcdh19* cKO female mice were characterized by a reduced LTP.
We can hypothesize that pre and post – synaptic PCDH19 mismatch promotes an aberrant post – synaptic organization, so possible impairment in learning and memory.

Finally, *Pcdh19* cKO mice presented a reduced pre – synaptic vesicles density, even though, we found a reduced PPR, which suggested an increase in

vesicles release probability. However, this last aspect could also represent a depletion of synaptic vesicles following the first stimulus, in accordance with a reduced number of vesicles.
Reduced pre – synaptic vesicles density was also found in another mouse model for DEE9, confirming our results (*Hoshina et al., 2021*). In this mouse model, it was clarified the role of PCDH19 in assembling the pre – synaptic compartment.

As previously underlined, synaptic function and structure is fundamental for cognition and behavior.
In our case, defects in synapses correlated with ASD and ID like phenotype in *Pcdh19* cKO mice.
Indeed, *Pcdh19* cKO mice displayed slightly defects in learning and memory plasticity related to hippocampus and increase in the number of stereotype and repetitive movements associated to ASD.
Also other DEE9 constitutive mouse models displayed ID – like phenotype (*Hayashi et al., 2017; Hoshina et al., 2021*) and ASD traits (*Lim et al., 2019; Galindo – Riera et al., 2021*), supporting our results.

3. *PCDH19* cKO MICE SHOW SOME DIFFERENCES RELATED TO GENDER

In DEE9, most of the patients are females (*Shibata et al., 2021*). Indeed, PCDH19 mutated males are usually healthy carriers, even though it has been recently reported that they can suffer from a milder phenotype, typically characterized by ID or by a more rigid personality with ASD and obsessive-compulsive disorder traits (*van Harssel et al., 2013; Scheffer et al., 2018; Kolc et al., 2020).* Few DEE9 patients are males with somatic mutations in *PCDH19*. Up to now, only 12 somatic mutated males were identified and they display a phenotype closer to female patients (*Niazi et al., 2019*). No differences between the phenotype of somatic mutated male patients and female patients were noticed until now (*Niazi et al., 2019*). However, given DEE9 incomplete

penetrance (*Kolc et al., 2019*), the strong heterogeneity in the DEE9 symptoms and the low number of identified somatic mutated male cases, a putative gender-effect could be masked.

We hypothesize that, besides *PCDH19* mosaicism, also the gender could have an impact on DEE9 pathology.
In agreement with this, we identified few differences between *Pcdh19* cKO male and female mice in our model.

1) *Growth*: *Pcdh19* cKO female mice were characterized by a transient growth delay, which was not statistically evident in *Pcdh19* cKO male mice;
2) *Behavioral defects*: even though *Pcdh19* cKO male and female mice displayed similar behavioral alterations, *Pcdh19* cKO female mice showed impairment also in the Fear Conditioning Test, suggesting a more severe phenotype;
3) *Molecular differences: Pcdh19* cKO female and male mice showed both an aberrant $GABA_A$Rs α1 expression, but in opposite direction (deeply discussed in the following paragraph).

Indeed, PCDH19 intracellular domain binds a conserved region of the α subunits (TM3 – TM4 region). It was demonstrated that downregulation of PCDH19 promoted a reduced surface expression of $GABA_A$Rs α1 subunit (*Bassani et al., 2018*).

GABAergic transmission is a fundamental key player for a correct brain development and function. Indeed, many neurological disorders are characterized by an aberrant GABAergic transmission.
It is important to note that too much or too low inhibition is detrimental for brain functioning.

Dysregulation of the $GABA_AR$s can promote hyperexcitability in different ways (*Briggs and Galanopoulou, 2011)*:

1) *GABAergic cell loss* or *$GABA_ARs$ loss*;
2) *Excitatory GABA*: there is a defect in the GABA switch (Chapter Introduction, 3.1; Fig.10), which is a fundamental event during post – natal period that allows the shift from excitatory to inhibitory $GABA_AR$s activity;
3) *Miswiring* or *malformation*: defects in the inhibitory circuits or aberrant synapses between inhibitory neurons and their targets.

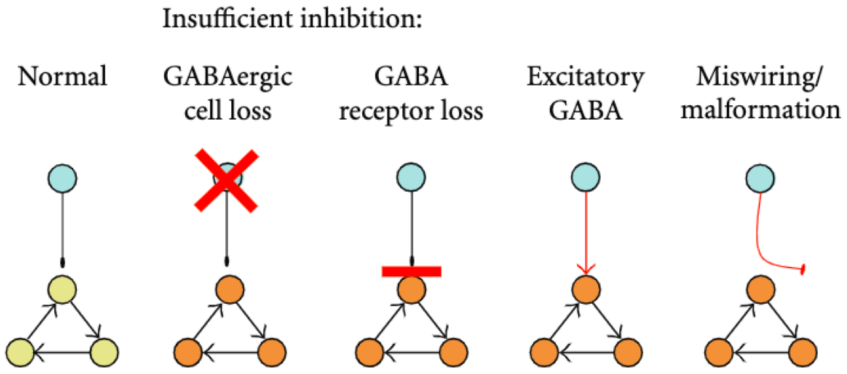

Figure 1 ***Schematic representation of the possible pathological mechanisms characterized by a reduced $GABA_ARs$ inhibition.*** *In blue, inhibitory neurons; in orange, excitatory/targets neurons, in yellow, balanced neurons (modified from Briggs and Galanopoulou, 2011)*

We can instead hypothesize two possible pathological mechanisms associated with an excessive inhibitory tone (*Briggs and Galanopoulou, 2011)*.

1) *Disinhibition*: increased GABAergic signalling and/or $GABA_AR$s are upregulated in neurons, which disinhibit inhibitory targets;
2) *Hyper – synchrony*: inhibitory neurons are known to regulate circuit synchronization and too much synchronization correlates with higher probability to the development of epilepsy (*Whittington et al., 1995*).

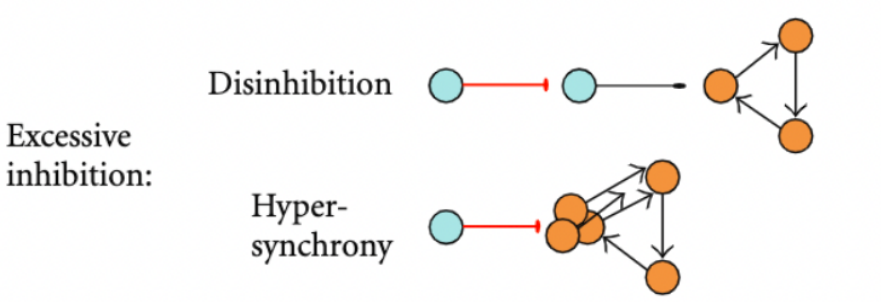

Figure 2 ***Schematic representation of two possible pathological mechanisms characterized by excessive $GABA_ARs$ inhibition.*** *In blue, inhibitory neurons; in orange, excitatory/targets neurons (modified from Briggs and Galanopoulou, 2011)*

Supporting this hypothesis, enhanced GABAergic signaling was found in two mouse models for autosomal dominant nocturnal frontal lobe epilepsy (ADNFLE) and moreover, increased inhibition is a known common mechanism in absence epilepsy (*Klaassen et al., 2006; Cope et al., 2009*).

Since in epilepsy and in different neurological disorders, there are alteration in the GABAergic transmission and since PCDH19 interacts with $GABA_ARs$ α subunits, we investigated if *Pcdh19* cKO mice were characterized by an altered expression of the $GABA_ARs$ $\alpha1$, through BS3 assay.
We focused our attention on the $GABA_ARs$ $\alpha1$ subunit, because it is involved both in tonic and phasic currents and it is one of the most expressed subunits in the brain.

Pcdh19 cKO mice were characterized by an aberrant surface expression of $GABA_ARs$ $\alpha1$, with an unaltered total pool. This data suggested defects in the $GABA_ARs$ trafficking and not in protein production.
Interestingly, we noticed that $GABA_ARs$ $\alpha1$ surface pool alteration was opposite in *Pcdh19* cKO female compared to male mice, suggesting a possible gender – effect in DEE9 aetiologia. This defect was conserved from late post – natal period (P20) to adulthood (P90).

Pcdh19 cKO male mice were characterized by a reduced surface expression of $GABA_ARs$ $\alpha1$. This data is in line with *in vitro* study, where PCDH19 downregulation promotes a reduction of $GABA_ARs$ $\alpha1$ expression on the surface (*Bassani et al., 2018*).
It is well known that decreased surface expression of $GABA_ARs$ correlates with an increased susceptibility to seizures, since $GABA_ARs$ favor the inhibitory tone. Indeed, different animal models for temporal lobe epilepsy (TLE) or for status epilepticus (SE) showed reduced expression of different $GABA_ARs$ subunit, especially $\alpha1$ one (*Friedman et al., 1994; Brooks – Kayal et al., 1998*).

On contrary, *Pcdh19* cKO female mice were characterized by an increased surface expression of $GABA_ARs$ $\alpha1$. This increase could appear as counterintuitive, especially in a mouse model for epilepsy. However, explanations could be hypothesized, due to a difference in phenotype severity, gender effect or both.

One possibility could be that in *Pcdh19* cKO female mice, there is an increase of $GABA_ARs$ $\alpha1$ as protective mechanism, since they displayed a more severe phenotype compared to *Pcdh19* cKO male mice.

Indeed, new evidence highlighted changes in $GABA_ARs$ subunits expression after epilepsy. Precisely, it was demonstrated in different rat models, that after seizures induction, $GABA_ARs$ $\alpha1$ subunit increased especially in hippocampus DG area, protecting rats from future epileptogenic activity (*Schwarzer et al., 1997; Raol et al., 2006*).
An interesting work also highlighted an age – dependent change in $GABA_ARs$ $\alpha1$ according to the onset of epilepsy. Indeed, they demonstrated that if SE occurred around P10, $GABA_ARs$ $\alpha1$ subunit was upregulated in DG and rats were protected against future episodes. On the contrary, if SE occurred during adulthood, $GABA_ARs$ $\alpha1$ subunit was reduced and rat underwent spontaneous seizures (*Zhang et al., 2004*).
So, we could hypothesize that during post – natal period and adolescence, *Pcdh19* cKO female mice could display an aberrant neuronal activity, which

can increase seizures susceptibility. A possible overall effect is the upregulation of $GABA_ARs$ $\alpha1$ subunit on the surface, as future compensatory and protective mechanism.
Indeed, also in a Dravet – syndrome mouse model, increased level of $GABA_ARs$ $\alpha1$ subunit, together with other $GABA_ARs$ and $GABA_BRs$ subunits, was found in brain lysates after epilepsy manifestation (*Mijanovic et al., 2021).*

On the other hand, the increase in $GABA_ARs$ $\alpha1$ expression could be due to a sex – effect.
In recent years, new awareness is arising in considering sex as a biological variable. Indeed, it is emerging how much the brain is shaped by gender and how different are males and females considering brain features and morphology (*Shansky and Murphy, 2021*).
Accordingly, it is now established that females and males could have different pathophysiological mechanisms, which can promote the onset of the same identical pathological phenotype (*Shansky and Murphy, 2021*).
So, we could state that the increased in the $GABA_ARs$ $\alpha1$ subunit in *Pcdh19* cKO female could be still a pathological mechanism like the one of *Pcdh19* cKO male mice, even if it is different.

However, we do not know why female and male mice aberrantly expressed $GABA_AR$ $\alpha1$ differently. One possible explanation can rely on sexual hormones. Indeed, estrogen and progesterone and its active metabolites, called neurosteroids (allopregnanolone and pregnanolone), influences $GABA_ARs$ function and expression. Usually, estrogen is associated to $GABA_ARs$ inhibition; progesterone metabolites work as allosteric modulators, enhancing $GABA_ARs$ transmission (*Barth et al., 2015*).
Recently, different works also highlighted the capability of progesterone neurosteroids to reorganize $GABA_ARs$ subunits, in response to stress (*Maguire and Mody, 2007*; *Reddy et al., 2017*).
Interestingly, PCDH19 was also found involved in the NONO - ERα pathway, where NONO is known to regulate progesterone receptor and androgen receptor gene regulation (*Pham et al., 2017*).

So, PCDH19 can regulate sexual hormones gene transcription, affecting potentially GABAergic transmission.

Still few aspects concerning the GABAergic alteration need to be clarified in our *Pcdh19* cKO mouse model.

1) We just took consideration of one $GABA_AR$ subunit (α1) among the 19 subunits expressed in the brain. Even though it provided an important information, we cannot exclude changing or compensation by other $GABA_AR$ subunits. So further $GABA_AR$ subunits investigation is needed.

2) We do not know exactly where $GABA_AR$ α1 subunit is aberrantly expressed, since we had a global result from brain slices. Indeed, some studies suggested a specific change in spatial expression, mostly CA3 and DG hippocampal areas (*Friedman et al., 1994*).

3) It is important to reiterate that *Pcdh19* cKO female and male mice have a different grade of mosaicism (PCDH19-positive neurons / PCDH19-negative neurons: females 60% / 40%; males 40% / 60%). Even though, according to the cellular interference theory, these percentages should result in a common phenotype, since they are specular, we cannot exclude that the different PCDH19 expression could have an impact on the phenotype of our mice.
   If the phenotype severity is due to the number of PCDH19 negative cells, *Pcdh19* cKO female mice should displayed a less severe phenotype. However, in our case, *Pcdh19* cKO female mice had a more severe phenotype compared to male mice. So, we can assume that also sex play a role in DEE9 pathophysiology.

To conclude, we generated a new *Pcdh19* cKO mouse model to investigate DEE9, a still largely unknown disorder. Our mouse model was able to recapitulate important features of the disease: brain *Pcdh19* mosaicism and the presence of ID and ASD features.

Even though, our *Pcdh19* cKO mouse model didn't display any spontaneous seizures, we had signs of hyperexcitability.

It is important to highlight that our data provided evidence of the significant role of mosaicism in DEE9. Interestingly, we also noticed some differences between *Pcdh19* cKO male and female mice, suggesting that also a sex – effect could be involved in the pathology.

ACKNOWLEDGMENTS

I would like to thank

My tutor, Prof. Diego Maria Michele FORNASARI, and my supervisor, Dr. Silvia BASSANI, who guided me all along these three years of scientific and personal education;

Dr. Maria PASSAFARO and my laboratory, with whom I shared this experience;

All the collaborators, who actively participated to this work:

- Dr. Luca MURRU (IN – CNR),
- Prof. Maura FRANCOLINI (UNIMI) and her laboratory (Anna Ghilardi and Greta Maiellano),
- Dr. Maria Elvina SALA (IN – CNR) and Luisa Ponzoni

The financial support of Fondazione Telethon-Italy (Dr. Silvia Bassani) and of University of Milan (UNIMI) is gratefully acknowledged.

REFERENCES

Almog Y, Fadila S, Brusel M, Mavashov A, Anderson K, Rubinstein M. Developmental alterations in firing properties of hippocampal CA1 inhibitory and excitatory neurons in a mouse model of Dravet syndrome. Neurobiology of Disease. 2021 Jan 1;148:105209.

Antunes M, Biala G. The novel object recognition memory: Neurobiology, test procedure, and its modifications. Cognitive Processing [Internet]. 2012 May 9 [cited 2021 Dec 15];13(2):93–110. Available from: https://link.springer.com/article/10.1007/s10339-011-0430-z

Barth C, Villringer A, Sacher J. Sex hormones affect neurotransmitters and shape the adult female brain during hormonal transition periods. Frontiers in Neuroscience. 2015;9(FEB):37.

Bassani S, Cwetsch AW, Gerosa L, Serratto GM, Folci A, Hall IF, et al. The female epilepsy protein PCDH19 is a new GABAAR-binding partner that regulates GABAergic transmission as well as migration and morphological maturation of hippocampal neurons. Human Molecular Genetics. 2018;27(6):1027–38.

Biswas S, Emond MR, Jontes JD. Protocadherin-19 and N-cadherin interact to control cell movements during anterior neurulation. The Journal of Cell Biology [Internet]. 2010 Nov 29 [cited 2021 Dec 14];191(5):1029. Available from: /pmc/articles/PMC2995167/

Borczyk M, Radwanska K, Giese KP. The importance of ultrastructural analysis of memory. Brain Research Bulletin. 2021 Aug 1;173:28–36.

Breuillard D, Leunen D, Chemaly N, Auclair L, Pinard JM, Kaminska A, et al. Autism spectrum disorder phenotype and intellectual disability in females with epilepsy and PCDH-19 mutations. Epilepsy and Behavior. 2016 Jul 1;60:75–80.

Brooks-Kayal AR, Shumate MD, Jin H, Rikhter TY, Coulter DA. Selective changes in single cell GABA(A) receptor subunit expression and function in temporal lobe epilepsy. Nature medicine. 1998 Oct;4(10):1166–72.

Brust V, Schindler PM, Lewejohann L. Lifetime development of behavioural phenotype in the house mouse (Mus musculus). Frontiers in Zoology [Internet]. 2015 Aug 24 [cited 2021 Dec 15];12(Suppl 1):S17. Available from: /pmc/articles/PMC4722345/

Buckmaster PS. INTERNEURONS | GABAergic Interneurons of the Dentate Gyrus and Entorhinal Cortex. Encyclopedia of Basic Epilepsy Research. 2009 Jan 1;614–8.

Cappelletti S, Specchio N, Moavero R, Terracciano A, Trivisano M, Pontrelli G, et al. Cognitive development in females with PCDH19 gene-related epilepsy. Epilepsy and Behavior. 2015 Jan 1;42:36–40.

Chen W v., Maniatis T. Clustered protocadherins. Development (Cambridge, England) [Internet]. 2013 Aug 15 [cited 2021 Dec 14];140(16):3297. Available from: /pmc/articles/PMC3737714/

Colombo MN, Maiellano G, Putignano S, Scandella L, Francolini M. (2021) Comparative 2D and 3D Ultrastructural Analyses of Dendritic Spines from CA1 Pyramidal Neurons in the Mouse Hippocampus. Int J Mol Sci. 2021 Jan 26;22(3):1188. doi: 10.3390/ijms22031188

Cooper SR, Emond MR, Duy PQ, Liebau BG, Wolman MA, Jontes JD. Protocadherins control the modular assembly of neuronal columns in the zebrafish optic tectum. The Journal of Cell Biology [Internet]. 2015 Nov 23 [cited 2021 Dec 14];211(4):807. Available from: /pmc/articles/PMC4657173/

Cooper SR, Jontes JD, Sotomayor M. Structural determinants of adhesion by protocadherin-19 and implications for its role in epilepsy. eLife. 2016;5(OCTOBER2016):1–22.

Corbetta S, Gualdoni S, Ciceri G, Monari M, Zuccaro E, Tybulewicz VLJ, et al. Essential role of Rac1 and Rac3 GTPases in neuronal development. The FASEB Journal [Internet]. 2009 May 1 [cited 2021 Dec 14];23(5):1347–57. Available from: https://onlinelibrary.wiley.com/doi/full/10.1096/fj.08-121574

de Lange IM, Rump P, Neuteboom RF, Augustijn PB, Hodges K, Kistemaker AI, et al. Male patients affected by mosaic PCDH19 mutations: five new cases. Neurogenetics. 2017 Jul 1;18(3):147–53.

Depienne C, Bouteiller D, Keren B, Cheuret E, Poirier K, Trouillard O, et al. Sporadic infantile epileptic encephalopathy caused by mutations in PCDH19 resembles Dravet syndrome but mainly affects females. PLoS Genet. 2009 Feb;5(2).

Depienne C, Leguern E. PCDH19-related infantile epileptic encephalopathy: an unusual X-linked inheritance disorder. Human Mutation [Internet]. 2012 [cited 2021 Dec 6];33(4). Available from: https://www.hal.inserm.fr/inserm-00669941

Depienne C, Trouillard O, Bouteiller D, Gourfinkel-An I, Poirier K, Rivier F, et al. Mutations and deletions in PCDH19 account for various familial or isolated epilepsies in females. Hum Mutat. 2011 Jan;32(1):E1959–75.

Dibbens LM, Tarpey PS, Hynes K, Bayly MA, Scheffer IE, Smith R, et al. X-linked protocadherin 19 mutations cause female-limited epilepsy and cognitive impairment. Nat Genet. 2008 Jun;40(6):776–81.

Dieni, C., Panichi, R., Aimone, J. *et al.* Low excitatory innervation balances high intrinsic excitability of immature dentate neurons. *Nat Commun* **7,** 11313 (2016). https://doi.org/10.1038/ncomms11313

Dubash AD, Green KJ. Desmosomes. CURBIO. 2011;21:R529–31.

Emond MR, Biswas S, Blevins CJ, Jontes JD. A complex of Protocadherin-19 and N-cadherin mediates a novel mechanism of cell adhesion. The Journal of Cell Biology [Internet]. 2011 Dec [cited 2021 Dec 15];195(7):1115. Available from: /pmc/articles/PMC3246890/

Emond MR, Biswas S, Jontes JD. Protocadherin-19 is essential for early steps in brain morphogenesis. Developmental Biology [Internet]. 2009;334(1):72–83. Available from: http://dx.doi.org/10.1016/j.ydbio.2009.07.008

Emond MR, Biswas S, Morrow ML, Jontes JD. Proximity-dependent Proteomics Reveals Extensive Interactions of Protocadherin-19 with Regulators of Rho

GTPases and the Microtubule Cytoskeleton. Neuroscience. 2021 Jan 1;452:26–36.

Forrest MP, Parnell E, Penzes P. Dendritic structural plasticity and neuropsychiatric disease. Nature Reviews Neuroscience 2018 19:4 [Internet]. 2018 Mar 16 [cited 2021 Dec 14];19(4):215–34. Available from: https://www-nature-com.pros2.lib.unimi.it/articles/nrn.2018.16

Friedman, L. K., Pellegrini-Giampietro, D. E., Sperber, E. F., Bennett, M. V., Moshé, S. L., & Zukin, R. S. (1994). Kainate-induced status epilepticus alters glutamate and GABAA receptor gene expression in adult rat hippocampus: an in situ hybridization study. *The Journal of neuroscience : the official journal of the Society for Neuroscience*, *14*(5 Pt 1), 2697–2707. https://doi.org/10.1523/JNEUROSCI.14-05-02697.1994

Fujitani M, Zhang S, Fujiki R, Fujihara Y, Yamashita T. A chromosome 16p13.11 microduplication causes hyperactivity through dysregulation of miR-484/protocadherin-19 signaling. Molecular Psychiatry [Internet]. 2017;22(3):364–74. Available from: http://dx.doi.org/10.1038/mp.2016.106

Gaitan Y, Bouchard M. Expression of the δ-protocadherin gene Pcdh19 in the developing mouse embryo. Gene Expression Patterns. 2006;6(8):893–9.

Galanopoulou AS, Briggs SW. Altered GABA Signaling in Early Life Epilepsies. Neural Plasticity [Internet]. 2011 [cited 2021 Dec 14];2011:16. Available from: /pmc/articles/PMC3150203/

Galindo-Riera N, Adriana Newbold S, Sledziowska M, Llinares-Benadero C, Griffiths J, Mire E, et al. Cellular and Behavioral Characterization of Pcdh19 Mutant Mice: subtle Molecular Changes, Increased Exploratory Behavior and an Impact of Social Environment. eNeuro [Internet]. 2021 Jul 1 [cited 2021 Dec 3];8(4). Available from: https://www.eneuro.org/content/8/4/ENEURO.0510-20.2021

Gataullina S, Bienvenu T, Nabbout R, Huberfeld G, Dulac O. Gene mutations in paediatric epilepsies cause NMDA-pathy, and phasic and tonic GABA-pathy. Developmental Medicine & Child Neurology [Internet]. 2019 Aug 1 [cited 2021 Dec 14];61(8):891–8. Available from: https://onlinelibrary.wiley.com/doi/full/10.1111/dmcn.14152

Gatto CL, Broadie K. Genetic controls balancing excitatory and inhibitory synaptogenesis in neurodevelopmental disorder models. Frontiers in Synaptic Neuroscience. 2010;(JUN).

Gerosa L, Francolini M, Bassani S, Passafaro M. The Role of Protocadherin 19 (PCDH19) in Neurodevelopment and in the Pathophysiology of Early Infantile Epileptic Encephalopathy-9 (EIEE9). Vol. 79, Developmental Neurobiology. John Wiley and Sons Inc.; 2019. p. 75–84.

Glascock JJ, Osman EY, Coady TH, Rose FF, Shababi M, Lorson CL. Delivery of Therapeutic Agents Through Intracerebroventricular (ICV) and Intravenous (IV) Injection in Mice. Journal of Visualized Experiments : JoVE [Internet]. 2011 [cited 2021 Dec 14];(56):2968. Available from: /pmc/articles/PMC3227174/

Hagihara H, Takao K, Walton NM, Matsumoto M, Miyakawa T. Immature Dentate Gyrus: An Endophenotype of Neuropsychiatric Disorders. Neural Plasticity [Internet]. 2013 [cited 2021 Dec 14];2013. Available from: /pmc/articles/PMC3694492/

Hayashi S, Inoue Y, Hattori S, Kaneko M, Shioi G, Miyakawa T, et al. Loss of X-linked Protocadherin-19 differentially affects the behavior of heterozygous female and hemizygous male mice. Scientific Reports 2017 7:1 [Internet]. 2017 Jul 19 [cited 2021 Dec 14];7(1):1–15. Available from: https://www.nature.com/articles/s41598-017-06374-x

Heise C, Taha E, Murru L, Ponzoni L, Cattaneo A, Guarnieri FC, et al. eEF2K/eEF2 Pathway Controls the Excitation/Inhibition Balance and Susceptibility to Epileptic Seizures. Cerebral Cortex (New York, NY) [Internet]. 2017 [cited 2021 Dec 15];27(3):2226. Available from: /pmc/articles/PMC5963824/

Hernandez CC, Tian X, Hu N, Shen W, Catron MA, Yang Y, et al. Dravet syndrome-associated mutations in GABRA1, GABRB2 and GABRG2 define the genetic landscape of defects of GABA A receptors. Brain communications [Internet]. 2021 Apr 5 [cited 2021 Dec 13];3(2). Available from: https://pubmed.ncbi.nlm.nih.gov/34095830/

Hertel N, Redies C. Absence of Layer-Specific Cadherin Expression Profiles in the Neocortex of the Reeler Mutant Mouse. Cerebral Cortex [Internet]. 2011 May 1 [cited 2021 Dec 14];21(5):1105–17. Available from: https://academic.oup.com/cercor/article/21/5/1105/425333

Hirano S, Takeichi M. Cadherins in Brain Morphogenesis and Wiring. Physiol Rev [Internet]. 2012;92:597–634. Available from: www.prv.org

Hirose S. Mutant GABAA receptor subunits in genetic (idiopathic) epilepsy. Progress in Brain Research. 2014 Jan 1;213(C):55–85.

Hoshina N, Johnson-Venkatesh EM, Hoshina M, Umemori H. Female-specific synaptic dysfunction and cognitive impairment in a mouse model of PCDH19 disorder. Science (New York, NY) [Internet]. 2021 Apr 16 [cited 2021 Dec 14];372(6539). Available from: https://pubmed.ncbi.nlm.nih.gov/33859005/

Huang X, Hernandez CC, Hu N, Macdonald RL. Three epilepsy-associated GABRG2 missense mutations at the γ+/β- interface disrupt GABAA receptor assembly and trafficking by similar mechanisms but to different extents. Neurobiology of disease [Internet]. 2014 [cited 2021 Dec 15];68:167–79. Available from: https://pubmed.ncbi.nlm.nih.gov/24798517/

Huang X, Zhou C, Tian M, Kang JQ, Shen W, Verdier K, et al. Overexpressing wild-type γ2 subunits rescued the seizure phenotype in Gabrg2 +/Q390X Dravet syndrome mice. Epilepsia [Internet]. 2017 Aug 1 [cited 2021 Dec 15];58(8):1451–61. Available from: https://pubmed.ncbi.nlm.nih.gov/28586508/

Hulpiau P, van Roy F. Molecular evolution of the cadherin superfamily. International Journal of Biochemistry and Cell Biology. 2009;41(2):349–69.

Jacob TC, Moss SJ, Jurd R. [GABA.sub.A] receptor trafficking and its role in the dynamic modulation of neuronal inhibition. Nature Reviews Neuroscience [Internet]. 2008 May 1 [cited 2021 Dec 10];9(5):331–44. Available from: https://go-gale-com.pros2.lib.unimi.it/ps/i.do?p=AONE&sw=w&issn=1471003X&v=2.1&it=r&id=GALE%7CA193446733&sid=googleScholar&linkaccess=fulltext

Jacob TC, Moss SJ, Jurd R. GABAA receptor trafficking and its role in the dynamic modulation of neuronal inhibition. Nature Reviews Neuroscience. 2008;9(5):331–43.

Jonas P, Lisman J. Structure, function, and plasticity of hippocampal dentate gyrus microcircuits. Frontiers in Neural Circuits. 2014;8:107.

Juberg RC, Hellman CD. A new familial form of convulsive disorder and mental retardation limited to females. J Pediatr. 1971;79(5):726–32.

Kahle KT, Staley KJ, Nahed B v., Gamba G, Hebert SC, Lifton RP, et al. Roles of the cation–chloride cotransporters in neurological disease. Nature Clinical Practice Neurology 2008 4:9 [Internet]. 2008 [cited 2021 Dec 13];4(9):490–503. Available from: https://www.nature.com/articles/ncpneuro0883

Kaila K, Price TJ, Payne JA, Puskarjov M, Voipio J. Cation-chloride cotransporters in neuronal development, plasticity and disease. 2014;

Kim JY, Ash RT, Ceballos-Diaz C, Levites Y, Golde TE, Smirnakis SM, et al. Viral transduction of the neonatal brain delivers controllable genetic mosaicism for visualising and manipulating neuronal circuits in vivo. European Journal of Neuroscience. 2013;37(8):1203–20.

Kim JY, Grunke SD, Levites Y, Golde TE, Jankowsky JL. Intracerebroventricular viral injection of the neonatal mouse brain for persistent and widespread neuronal transduction. Journal of Visualized Experiments. 2014;(91):1–7.

Kim SY, Chung HS, Sun W, Kim H. Spatiotemporal expression pattern of non-clustered protocadherin family members in the developing rat brain. Neuroscience [Internet]. 2007 Jul 29 [cited 2021 Dec 6];147(4):996–1021. Available from: https://pubmed.ncbi.nlm.nih.gov/17614211/

Kim SY, Mo JW, Han S, Choi SY, Han SB, Moon BH, et al. The expression of non-clustered protocadherins in adult rat hippocampal formation and the connecting brain regions. Neuroscience. 2010 Sep 29;170(1):189–99.

Kim SY, Yasuda S, Tanaka H, Yamagata K, Kim H. Non-clustered protocadherin. Cell Adhesion & Migration [Internet]. 2011 [cited 2021 Dec 14];5(2):97. Available from: /pmc/articles/PMC3084973/

Kim YS, Yoon BE. Altered GABAergic Signaling in Brain Disease at Various Stages of Life. Experimental Neurobiology [Internet]. 2017 Jun 1 [cited 2021 Dec 10];26(3):122. Available from: /pmc/articles/PMC5491580/

Klaassen A, Glykys J, Maguire J, Labarca C, Mody I, Boulter J. Seizures and enhanced cortical GABAergic inhibition in two mouse models of human autosomal dominant nocturnal frontal lobe epilepsy. Proceedings of the National Academy of Sciences of the United States of America [Internet]. 2006 Dec 12 [cited 2021 Dec 12];103(50):19152. Available from: /pmc/articles/PMC1681351/

Kolc KL, Møller RS, Sadleir LG, Scheffer IE, Kumar R, Gecz J. PCDH19 Pathogenic Variants in Males: Expanding the Phenotypic Spectrum. Advances in experimental medicine and biology [Internet]. 2020 [cited 2021 Nov 29];1298:177–87. Available from: https://pubmed.ncbi.nlm.nih.gov/32852734/

Kolc KL, Sadleir LG, Depienne C, Marini C, Scheffer IE, Møller RS, et al. A standardized patient-centered characterization of the phenotypic spectrum of PCDH19 girls clustering epilepsy. Translational Psychiatry. 2020 Dec 1;10(1).

Kolc KL, Sadleir LG, Scheffer IE, Ivancevic A, Roberts R, Pham DH, et al. A systematic review and meta-analysis of 271 PCDH19-variant individuals identifies psychiatric comorbidities, and association of seizure onset and disease severity. Molecular Psychiatry [Internet]. 2019;24(2):241–51. Available from: http://dx.doi.org/10.1038/s41380-018-0066-9

Krishna-K K, Hertel N, Redies C. Cadherin expression in the somatosensory cortex: evidence for a combinatorial molecular code at the single-cell level. Neuroscience. 2011 Feb 17;175:37–48.

Leckband DE, le Duc Q, Wang N, de Rooij J. Mechanotransduction at cadherin-mediated adhesions. Current Opinion in Cell Biology. 2011 Oct 1;23(5):523–30.

Li Y, Zhou Y, Peng L, Zhao Y. Reduced protein expressions of cytomembrane GABAARβ3 at different postnatal developmental stages of rats exposed prenatally to valproic acid. Brain Research. 2017 Sep 15;1671:33–42.

Lim J, Ryu J, Kang S, Noh HJ, Kim CH. Autism-like behaviors in male mice with a Pcdh19 deletion. Molecular Brain [Internet]. 2019 Nov 20 [cited 2021 Dec 14];12(1):1–4. Available from: https://molecularbrain.biomedcentral.com/articles/10.1186/s13041-019-0519-3

Lopez-Rojas J, Kreutz MR. Mature granule cells of the dentate gyrus—Passive bystanders or principal performers in hippocampal function? Neuroscience & Biobehavioral Reviews. 2016 May 1;64:167–74.

Maguire J, Mody I. Neurosteroid Synthesis-Mediated Regulation of GABAA Receptors: Relevance to the Ovarian Cycle and Stress. Journal of Neuroscience [Internet]. 2007 Feb 28 [cited 2021 Dec 14];27(9):2155–62. Available from: https://www.jneurosci.org/content/27/9/2155

Mancini M, Bassani S, Passafaro M. Right Place at the Right Time: How Changes in Protocadherins Affect Synaptic Connections Contributing to the Etiology of Neurodevelopmental Disorders. Cells [Internet]. 2020 Dec 18 [cited 2021 Dec 14];9(12). Available from: /pmc/articles/PMC7766791/

Marini C, Darra F, Specchio N, Mei D, Terracciano A, Parmeggiani L, et al. Focal seizures with affective symptoms are a major feature of PCDH19 gene-related epilepsy. Epilepsia. 2012 Dec;53(12):2111–9.

Marini C, Mei D, Parmeggiani L, Norci V, Calado E, Ferrari A, et al. Protocadherin 19 mutations in girls with infantile-onset epilepsy. Neurology. 2010 Aug 17;75(7):646–53.

Martin P, Rautenstrau B, Abicht A, Fahrbach J, Koster S. Severe Myoclonic Epilepsy in Infancy – Adult Phenotype with Bradykinesia, Hypomimia, and Perseverative Behavior: Report of Five Cases. Molecular Syndromology [Internet]. 2010 May [cited 2021 Dec 14];1(5):231–8. Available from: https://www.karger.com/Article/FullText/326746

Mazzoleni S, Bassani S. PCDH19 interplay with GABA(A) receptors: a window to DEE9 pathogenetic mechanisms. Vol. 17, Neural Regeneration Research. Wolters Kluwer Medknow Publications; 2022. p. 803–5.

Mele M, Costa RO, Duarte CB. Alterations in GABAA-receptor trafficking and synaptic dysfunction in brain disorders. Frontiers in Cellular Neuroscience. 2019 Jan 29;13:77.

Miljanovic N, van Dijk RM, Buchecker V, Potschka H. Metabolomic signature of the Dravet syndrome: A genetic mouse model study. Epilepsia [Internet]. 2021 Aug 1 [cited 2021 Dec 14];62(8):2000–14. Available from: https://onlinelibrary.wiley.com/doi/full/10.1111/epi.16976

Morishita H, Yagi T. Protocadherin family: diversity, structure, and function. Current Opinion in Cell Biology. 2007 Oct 1;19(5):584–92.

Murru A, Torra M, Callari A, Pacchiarotti I, Romero S, Gonzalez de la Presa B, et al. A study on the bioequivalence of lithium and valproate salivary and blood levels in the treatment of bipolar disorder. European Neuropsychopharmacology. 2017 Aug 1;27(8):744–50.

Murru, Luca, Elena Vezzoli, Anna Longatti, Luisa Ponzoni, Andrea Falqui, Alessandra Folci, Edoardo Moretto, et al. 2017. ‘Pharmacological Modulation of AMPAR Rescues Intellectual Disability-Like Phenotype in Tm4sf2-/y Mice’. *Cerebral Cortex (New York, N.Y.: 1991)* 27 (11): 5369–84. https://doi.org/10.1093/cercor/bhx221.

Nagy A, Gertsenstein M, Vintersten K, Behringer R. Counting Chromosomes in Embryonic Stem (ES) Cells. Cold Spring Harbor Protocols [Internet]. 2009 Jun

1 [cited 2021 Dec 15];2009(6):pdb.prot4404. Available from: http://cshprotocols.cshlp.org/content/2009/6/pdb.prot4404.full

Nakao S, Platek A, Hirano S, Takeichi M. Contact-dependent promotion of cell migration by the OL-protocadherin–Nap1 interaction. The Journal of Cell Biology [Internet]. 2008 Jul 28 [cited 2021 Dec 15];182(2):395. Available from: /pmc/articles/PMC2483522/

Niazi R, Fanning EA, Depienne C, Sarmady M, Abou Tayoun AN. A mutation update for the PCDH19 gene causing early-onset epilepsy in females with an unusual expression pattern. Human Mutation [Internet]. 2019 Mar 1 [cited 2021 Dec 2];40(3):243–57. Available from: https://onlinelibrary.wiley.com/doi/full/10.1002/humu.23701

Nollet F, Kools P, van Roy F. Phylogenetic Analysis of the Cadherin Superfamily allows Identification of Six Major Subfamilies Besides Several Solitary Members. 2000 [cited 2021 Dec 3]; Available from: http://www.idealibrary.com

Pancho A, Aerts T, Mitsogiannis MD, Seuntjens E. Protocadherins at the Crossroad of Signaling Pathways. Frontiers in Molecular Neuroscience. 2020 Jun 30;13:117.

Parrish JZ, Emoto K, Kim MD, Yuh NJ. Mechanisms that regulate establishment, maintenance, and remodeling of dendritic fields. Vol. 30, Annual Review of Neuroscience. 2007. p. 399–423.

Pederick DT, Homan CC, Jaehne EJ, Piltz SG, Haines BP, Baune BT, et al. Pcdh19 Loss-of-Function Increases Neuronal Migration In Vitro but is Dispensable for Brain Development in Mice. Scientific Reports 2016 6:1 [Internet]. 2016 May 31 [cited 2021 Dec 14];6(1):1–10. Available from: https://www.nature.com/articles/srep26765

Perez D, Hsieh DT, Rohena L. Somatic mosaicism of PCDH19 in a male with early infantile epileptic encephalopathy and review of the literature. Am J Med Genet A. 2017 Jun 1;173(6):1625–30.

Petroff OAC. GABA and glutamate in the human brain. Neuroscientist [Internet]. 2002 Dec 29 [cited 2021 Dec 14];8(6):562–73. Available from: https://journals.sagepub.com/doi/10.1177/1073858402238515?url_ver=Z39.88-2003&rfr_id=ori%3Arid%3Acrossref.org&rfr_dat=cr_pub++0pubmed

Pham DH, Tan CC, Homan CC, Kolc KL, Corbett MA, McAninch D, et al. Protocadherin 19 (PCDH19) interacts with paraspeckle protein NONO to co-

regulate gene expression with estrogen receptor alpha (ERα). Human Molecular Genetics. 2017;26(11):2042–52.

Pinyol R, Scrofani J, Vernos I. The role of NEDD1 phosphorylation by aurora a in chromosomal microtubule nucleation and spindle function. Current Biology [Internet]. 2013 Jan 21 [cited 2021 Dec 15];23(2):143–9. Available from: http://www.cell.com/article/S0960982212013905/fulltext

Rakotomamonjy J, Sabetfakhri NP, McDermott SL, Guemez-Gamboa A. Characterization of seizure susceptibility in Pcdh19 mice. Epilepsia [Internet]. 2020 Oct 1 [cited 2021 Dec 14];61(10):2313. Available from: /pmc/articles/PMC7722218/

Raol YSH, Lund I v., Bandyopadhyay S, Zhang G, Roberts DS, Wolfe JH, et al. Enhancing GABAA Receptor α1 Subunit Levels in Hippocampal Dentate Gyrus Inhibits Epilepsy Development in an Animal Model of Temporal Lobe Epilepsy. Journal of Neuroscience [Internet]. 2006 Nov 1 [cited 2021 Dec 11];26(44):11342–6. Available from: https://www.jneurosci.org/content/26/44/11342

Reddy DS, Gangisetty O, Wu X. PR-Independent Neurosteroid Regulation of α2-GABA-A Receptors in the Hippocampus Subfields. Brain research [Internet]. 2017 Mar 15 [cited 2021 Dec 14];1659:142. Available from: /pmc/articles/PMC5367384/

Redies C, Hertel N, Hübner CA. Cadherins and neuropsychiatric disorders. Brain Research. 2012 Aug 27;1470:130–44.

Redies C, Vanhalst K, van Roy F. δ-Protocadherins: Unique structures and functions. Cellular and Molecular Life Sciences. 2005;62(23):2840–52.

Ricobaraza A, Mora-Jimenez L, Puerta E, Sanchez-Carpintero R, Mingorance A, Artieda J, et al. Epilepsy and neuropsychiatric comorbidities in mice carrying a recurrent Dravet syndrome SCN1A missense mutation. Scientific Reports 2019 9:1 [Internet]. 2019 Oct 2 [cited 2021 Dec 11];9(1):1–15. Available from: https://www.nature.com/articles/s41598-019-50627-w

Rodriguez RA, Joya C, Hines RM. Common ribs of inhibitory synaptic dysfunction in the umbrella of neurodevelopmental disorders. Frontiers in Molecular Neuroscience. 2018 Apr 24;11:132.

Romasko EJ, DeChene ET, Balciuniene J, Akgumus GT, Helbig I, Tarpinian JM, et al. PCDH19-related epilepsy in a male with Klinefelter syndrome: Additional

evidence supporting PCDH19 cellular interference disease mechanism. Epilepsy Research. 2018 Sep 1;145:89–92.

Rudolph U, Knoflach F. Beyond classical benzodiazepines: Novel therapeutic potential of GABAA receptor subtypes. Nature Reviews Drug Discovery [Internet]. 2011 Sep [cited 2021 Dec 14];10(9):685. Available from: /pmc/articles/PMC3375401/

Rudolph U, Möhler H. Analysis of GABAA Receptor Function and Dissection of the Pharmacology of Benzodiazepines and General Anesthetics Through Mouse Genetics. http://dx.doi.org/101146/annurev.pharmtox44101802121429 [Internet]. 2004 Jan 16 [cited 2021 Dec 15];44:475–98. Available from: https://www.annualreviews.org/doi/abs/10.1146/annurev.pharmtox.44.101802.121429

Ryan SG, Chance PF, Zou CH, Spinner NB, Golden JA, Smietana S. Epilepsy and mental retardation limited to females: an X-linked dominant disorder with male sparing. Nature Genetics 1997 17:1 [Internet]. 1997 [cited 2021 Nov 29];17(1):92–5. Available from: https://www.nature.com/articles/ng0997-92

Sano K, Tanihara H, Heimark RL, Obata S, Davidson M, st. John T, et al. Protocadherins: a large family of cadherin-related molecules in central nervous system. The EMBO Journal [Internet]. 1993 Jun 1 [cited 2021 Dec 6];12(6):2249–56. Available from: https://onlinelibrary.wiley.com/doi/full/10.1002/j.1460-2075.1993.tb05878.x

Schaarschuch A, Hertel N. Expression profile of N-cadherin and protocadherin-19 in postnatal mouse limbic structures. The Journal of comparative neurology [Internet]. 2018 Mar 1 [cited 2021 Dec 3];526(4):663–80. Available from: https://pubmed.ncbi.nlm.nih.gov/29159962/

Scheffer IE, Turner SJ, Dibbens LM, Bayly MA, Friend K, Hodgson B, et al. Epilepsy and mental retardation limited to females: an under-recognized disorder. Brain. 2008;131(Pt 4):918–27.

Schwartz-Bloom RD, Sah R. γ-Aminobutyric acidA neurotransmission and cerebral ischemia. Journal of Neurochemistry [Internet]. 2001 Apr 15 [cited 2021 Dec 14];77(2):353–71. Available from: https://onlinelibrary.wiley.com/doi/full/10.1046/j.1471-4159.2001.00274.x

Schwarzer C, Tsunashima K, Wanzenböck C, Fuchs K, Sieghart W, Sperk G. GABA(A) receptor subunits in the rat hippocampus II: altered distribution in

kainic acid-induced temporal lobe epilepsy. Neuroscience. 1997 Aug 11;80(4):1001–17.

Serratto GM, Pizzi E, Murru L, Mazzoleni S, Pelucchi S, Marcello E, et al. The Epilepsy-Related Protein PCDH19 Regulates Tonic Inhibition, GABAAR Kinetics, and the Intrinsic Excitability of Hippocampal Neurons. Molecular Neurobiology. 2020 Dec 1;57(12):5336–51.

Shansky RM, Murphy AZ. Considering sex as a biological variable will require a global shift in science culture. Nature Neuroscience [Internet]. [cited 2021 Dec 11]; Available from: https://doi.org/10.1038/s41593-021-00806-8

Shibata M, Ishii A, Goto A, Hirose S. Comparative characterization of PCDH19 missense and truncating variants in PCDH19-related epilepsy. Journal of Human Genetics 2020 66:6 [Internet]. 2020 Dec 2 [cited 2021 Dec 2];66(6):569–78. Available from: https://www.nature.com/articles/s10038-020-00880-z

Sigel E, Steinmann ME. Structure, Function, and Modulation of GABAA Receptors. The Journal of Biological Chemistry [Internet]. 2012 Nov 23 [cited 2021 Dec 14];287(48):40224. Available from: /pmc/articles/PMC3504738/

Simon, J., Wakimoto, H., Fujita, N., Lalande, M., & Barnard, E. A. (2004). Analysis of the set of GABA(A) receptor genes in the human genome. *The Journal of biological chemistry*, *279*(40), 41422–41435. https://doi.org/10.1074/jbc.M401354200

Smith KR, Kittler JT. The cell biology of synaptic inhibition in health and disease. Current Opinion in Neurobiology. 2010 Oct 1;20(5):550–6.

Smith L, Singhal N, el Achkar CM, Truglio G, Rosen Sheidley B, Sullivan J, et al. PCDH19-related epilepsy is associated with a broad neurodevelopmental spectrum. Epilepsia. 2018 Mar 1;59(3):679–89.

Specchio N, Marini C, Terracciano A, Mei D, Trivisano M, Sicca F, et al. Spectrum of phenotypes in female patients with epilepsy due to protocadherin 19 mutations. Epilepsia. 2011 Jul;52(7):1251–7.

Taglialatela G, Hogan D, Zhang W-R, Dineley KT. Intermediate-and Long-Term Recognition Memory Deficits in Tg2576 Mice Are Reversed with Acute Calcineurin Inhibition.

Tai K, Kubota M, Shiono K, Tokutsu H, Suzuki ST. Adhesion properties and retinofugal expression of chicken protocadherin-19. Brain Research. 2010 Jul 16;1344:13–24.

Takeichi M. The cadherin superfamily in neuronal connections and interactions. Vol. 8, Nature Reviews Neuroscience. 2007. p. 11–20.

Talbot SR, Biernot S, Bleich A, van Dijk RM, Ernst L, Häger C, et al. Defining body-weight reduction as a humane endpoint: a critical appraisal. Laboratory Animals [Internet]. 2020 Feb 1 [cited 2021 Dec 14];54(1):99–110. Available from: https://journals.sagepub.com/doi/full/10.1177/0023677219883319

Tan C, Shard C, Ranieri E, Hynes K, Pham DH, Leach D, et al. Mutations of protocadherin 19 in female epilepsy (PCDH19-FE) lead to allopregnanolone deficiency. Hum Mol Genet. 2015 Apr 9;24(18):5250–9.

Tan Y, Hou M, Ma S, Liu P, Xia S, Wang Y, et al. Chinese cases of early infantile epileptic encephalopathy: A novel mutation in the PCDH19 gene was proved in a mosaic male- case report. BMC Medical Genetics [Internet]. 2018 Jun 4 [cited 2021 Nov 29];19(1):1–8. Available from: https://bmcmedgenet.biomedcentral.com/articles/10.1186/s12881-018-0621-x

Tau GZ, Peterson BS. Normal development of brain circuits. Neuropsychopharmacology [Internet]. 2010;35(1):147–68. Available from: http://dx.doi.org/10.1038/npp.2009.115

Terracciano A, Trivisano M, Cusmai R, de Palma L, Fusco L, Compagnucci C, et al. PCDH19-related epilepsy in two mosaic male patients. Epilepsia. 2016;57(3):e51–5.

Terunuma M. Review Diversity of structure and function of GABA B receptors: a complexity of GABA B-mediated signaling.

Thiffault I, Farrow E, Smith L, Lowry J, Zellmer L, Black B, et al. PCDH19-related epileptic encephalopathy in a male mosaic for a truncating variant. Am J Med Genet A. 2016 Jun 1;170(6):1585–9.

Trivisano M, Pietrafusa N, Terracciano A, Marini C, Mei D, Darra F, et al. Defining the electroclinical phenotype and outcome of PCDH19-related epilepsy: A multicenter study. Epilepsia [Internet]. 2018 Dec 1 [cited 2021 Nov 30];59(12):2260–71. Available from: https://onlinelibrary.wiley.com/doi/full/10.1111/epi.14600

van Harssel JJT, Weckhuysen S, van Kempen MJA, Hardies K, Verbeek NE, de Kovel CGF, et al. Clinical and genetic aspects of PCDH19-related epilepsy syndromes and the possible role of PCDH19 mutations in males with autism spectrum disorders. Neurogenetics. 2013 Feb;14(1):23–34

van Roy F. Beyond E-cadherin: roles of other cadherin superfamily members in cancer. Nature Reviews Cancer 2014 14:2 [Internet]. 2014 Jan 20 [cited 2021 Dec 14];14(2):121–34. Available from: https://www.nature.com/articles/nrc3647

Vanhalst K, Kools P, Staes K, van Roy F, Redies C. δ-Protocadherins: A gene family expressed differentially in the mouse brain. Cellular and Molecular Life Sciences. 2005;62(11):1247–59.

Vlaskamp DRM, Bassett AS, Sullivan JE, Robblee J, Sadleir LG, Scheffer IE, et al. Schizophrenia is a later-onset feature of PCDH19 Girls Clustering Epilepsy. Epilepsia [Internet]. 2019 Mar 1 [cited 2021 Dec 9];60(3):429–40. Available from: https://pubmed.ncbi.nlm.nih.gov/30828795/

Wahlsten D. Mouse Behavioral Testing. Mouse Behavioral Testing [Internet]. 2011 [cited 2021 Dec 14]; Available from: https://www.hoepli.it/libro/mouse-behavioral-testing/9780123756749.html

Watabe-Uchida M, John KA, Janas JA, Newey SE, van Aelst L. The Rac activator DOCK7 regulates neuronal polarity through local phosphorylation of stathmin/Op18. Neuron [Internet]. 2006 Sep 21 [cited 2021 Dec 14];51(6):727–39. Available from: https://pubmed.ncbi.nlm.nih.gov/16982419/

Weiner JA, Jontes J. Protocadherins, not prototypical: A complex tale of their interactions, expression, and functions. Frontiers in Molecular Neuroscience. 2013;6(MARCH 2013):1–10.

Whittington MA, Traub RD, Jefferys JGR. Synchronized oscillations in interneuron networks driven by metabotropic glutamate receptor activation. Nature 1995 373:6515 [Internet]. 1995 Feb 16 [cited 2021 Dec 14];373(6515):612–5. Available from: https://www.nature.com/articles/373612a0

Wolverton T, Lalande M. Identification and Characterization of Three Members of a Novel Subclass of Protocadherins. Genomics. 2001 Aug 1;76(1–3):66–72.

Wong M. Too Much Inhibition Leads to Excitation in Absence Epilepsy. Epilepsy Currents [Internet]. 2010 Sep [cited 2021 Dec 12];10(5):131. Available from: /pmc/articles/PMC2951695/

Wu H, Liu Y, Liu L, Meng Q, Du C, Li K, et al. Decreased expression of the clock gene Bmal1 is involved in the pathogenesis of temporal lobe epilepsy. Molecular Brain [Internet]. 2021 Dec 1 [cited 2021 Dec 14];14(1):113. Available from: /pmc/articles/PMC8281660/

Yang L, Liu J, Su Q, Li Y, Yang X, Xu L, et al. Novel and de novo mutation of PCDH19 in Girls Clustering Epilepsy. Brain and Behavior [Internet]. 2019 Dec 1 [cited 2021 Dec 14];9(12). Available from: /pmc/articles/PMC6908879/

Yang X, Chen J, Zheng BX, Liu X, Cao Z, Wang X. PCDH19-Related Epilepsy in Early Onset of Chinese Male Patient: Case Report and Literature Review. Frontiers in Neurology. 2020 Apr 30;11:311.

Yonezawa S, Shigematsu M, Hirata K, Hayashi K. Loss of γ-tubulin, GCP-WD/NEDD1 and CDK5RAP2 from the Centrosome of Neurons in Developing Mouse Cerebral and Cerebellar Cortex. Acta Histochemica et Cytochemica [Internet]. 2015 Oct 29 [cited 2021 Dec 15];48(5):145. Available from: /pmc/articles/PMC4652029/

Zhang G, Raol YH, Hsu FC, Coulter DA, Brooks-Kayal AR. Effects of status epilepticus on hippocampal gabaa receptors are age-dependent. Neuroscience [Internet]. 2004 [cited 2021 Dec 11];125(2):299. Available from: /pmc/articles/PMC2441871/

Zhang Y, Chen K, Sloan SA, Bennett ML, Scholze AR, O'Keeffe S, et al. An RNA-Sequencing Transcriptome and Splicing Database of Glia, Neurons, and Vascular Cells of the Cerebral Cortex. Journal of Neuroscience [Internet]. 2014 Sep 3 [cited 2021 Dec 14];34(36):11929–47. Available from: https://www.jneurosci.org/content/34/36/11929

LIST OF FIGURES AND TABLES

Figure 2. Exon 3 excision by Cre recombinase prevents Pcdh19 expression in vitro	Figures Table	
Figure 3. Generation of the Pcdh19 cKO mouse model	Figures Table	
Figure 4. Mosaic Pcdh19 expression in Pcdh19 cKO female mice	Figures Table	
Figure 5. Pcdh19 cKO male mice are also characterized by a PCDH19 mosaic expression in their brain	Figures Table	
Figure 6. Pcdh19 cKO female mice are characterized by a transient growth retardation close to the weaning time.	Figures Table	
Figure 7. Pcdh19 cKO female displayed structural and functional synaptic defects in the hippocampus	Figures Table	
Figure 8. PCDH19 negative DGGCs showed an aberrant excitability compared to PCDH19 retaining neurons	Figures Table	
Figure 9. Pcdh19 cKO mice displayed an aberrant surface expression of $GABA_ARs$ $\alpha 1$ subunit	Figures Table	
Figure 10. Pcdh19 cKO mice display ASD and ID behavioral deficits	Figures Table	
Figure 1 Schematic representation of the possible pathological mechanisms characterized by a reduced $GABA_ARs$ inhibition	Discussion and conclusions	Chap. 3
Figure 2 Schematic representation of two possible pathological mechanisms characterized by excessive $GABA_ARs$ inhibition	Discussion and conclusions	Chap. 3

Fig. 3a and Fig. 8a (Chapter Results) were created thank to **BioRender Software** (www.biorender)

DISSEMINATION OF RESULTS

The results here presented were disseminated to the scientific and to the general public by participating to international and national conferences.

Specifically, during my three – year PhD program, I had different opportunities to share my results with the scientific community, by presenting posters (IN – CNR Retreat, 2018; IV Workshop BioMeTra, 2019; Brayn Conference, 2019; VBC PhD Symposium, 2021) and as invited speaker (V Workshop BioMeTra, 2021) while attending conferences.

Soon, all these data will be disseminated and make public through indexed – journal paper publication (Manuscript in preparation).

SHORT LAY SUMMARY

English version

Mutations in the *PCDH19* gene cause a sever genetic disorder, called Developmental and Epileptic Encephalopathy 9 (DEE9). DEE9 affected patients are characterized by epilepsy with an early onset, autism, and intellectual disability. *PCDH19* is localized on the X chromosome, and it encodes for a cell – cell adhesion molecule (PCDH19), predominantly localized in the brain. The main role of PCDH19 is to promote neuronal interaction to favour a correct brain development and function. However, DEE9 is still an unknown disease, since the mechanisms responsible for the disorder are still unknown. In our laboratory, we generated a new mouse model to study DEE9 pathological mechanisms. We used a genetic tool which allowed to remove PCDH19 specifically from neurons. The aim of my PhD was to characterize molecularly, functionally, and behaviourally this new mouse model for PCDH19.

Italian version

Mutazioni nel gene *PCDH19* causano una severa malattia genetica, chiamata Encefalopatia Epilettica e dello Sviluppo di tipo 9 (DEE9). I pazienti affetti da questa malattia sono caratterizzati da epilessia con esordio precoce, autismo e ritardo mentale. Il gene *PCDH19* è localizzato sul cromosoma X e codifica per una proteina di adesione cellulare (PCDH19), localizzata prevalentemente nel cervello. Il ruolo principale di PCDH19 è quella di promuovere l'interazione tra neuroni per favorire un corretto sviluppo e una corretta funzione del cervello. Però, ad oggi, DEE9 è ancora una malattia sconosciuta, poiché non si conoscono i meccanismi responsabili dei sintomi.

Nel nostro laboratorio, abbiamo generato un nuovo modello di topo per studiare i meccanismi patologici di DEE9. Abbiamo sfruttato una metodica genetica per rimuovere PCDH19 specificatamente dai neuroni. Lo scopo del mio progetto di dottorato è stato quello di caratterizzare a livello molecolare, funzionale e comportamentale questo nuovo modello animale per PCDH19.